ANISOTROPIC NANOSTRUCTURES AND THEIR APPLICATIONS IN SURFACE ENHANCED SPECTROSCOPY

THESIS SUBMITTED TO
THE UNIVERSITY OF KERALA
FOR THE AWARD OF THE DEGREE OF
DOCTOR OF PHILOSOPHY
IN CHEMISTRY UNDER THE FACULTY OF SCIENCE

By

JATISHKUMAR

UNDER THE SUPERVISION OF
Prof. K. GEORGE THOMAS

PHOTOSCIENCES AND PHOTONICS SECTION
CHEMICAL SCIENCES AND TECHNOLOGY DIVISION
CSIR-NATIONAL INSTITUTE FOR INTERDISCIPLINARY SCIENCE AND TECHNOLOGY
TRIVANDRUM - 695019
KERALA, INDIA

2012

Dedicated to my beloved Parents,

Teachers and Friends

DECLARATION

I hereby declare that the Ph.D. thesis entitled "**ANISOTROPIC NANOSTRUCTURES AND THEIR APPLICATIONS IN SURFACE ENHANCED SPECTROSCOPY**" is an independent work carried out by me at the Photosciences and Photonics Section, Chemical Sciences and Technology Division, CSIR-National Institute for Interdisciplinary Science and Technology (NIIST), Trivandrum, under the supervision of Prof. K. George Thomas and the same has not been submitted elsewhere for any other degree, diploma or title.

In keeping with the general practice of reporting the scientific observations, due acknowledgement has been made wherever the work described is based on the findings of other investigators.

Jatishkumar

Trivandrum

INDIAN INSTITUTE OF SCIENCE EDUCATION AND RESEARCH
THIRUVANANTHAPURAM
[An Autonomous Institution under MHRD, Government of India]

Prof. K. George Thomas
Dean, Academics and Administration &
Professor, School of Chemistry
Tel: 0091-471-2597425
Fax: 0091-471-2597427
E-mail: kgt@iisertvm.ac.in

IISER
THIRUVANANTHAPURAM

CET CAMPUS
THIRUVANANTHAPURAM-695 016
KERALA, INDIA
www.iisertvm.ac.in

October 03, 2012

CERTIFICATE

This is to certify that the work embodied in the thesis entitled: " **ANISOTROPIC NANOSTRUCTURES AND THEIR APPLICATIONS IN SURFACE ENHANCED SPECTROSCOPY** " has been carried out by Mr. Jatishkumar under my supervision and guidance at the Photosciences and Photonics Section, Chemical Sciences and Technology Division, CSIR-National Institute for Interdisciplinary Science and Technology (NIIST), Trivandrum and the same has not been submitted elsewhere for a degree.

K. George Thomas

(Thesis Supervisor)

ii

ACKNOWLEDGEMENTS

CONTENTS

Chapter 3: Nanorod Dimer Junction for Raman Signal Enhancement

Chapter 4: Lateral Assembly of Au Nanorods and Creation of Quartet for Raman Signal Enhancement

Chapter 5: Single Particle Optical Investigations of Gold Nanorod Assemblies

List of Tables Page

List of Figures Page

List of Schemes   **Page**

List of Abbreviations

AuNPs   Gold Nanoparticles

AuNRs   Gold Nanorods

bipy-DT   5,5'-bis(mercaptomethyl)-2,2'-bipyridine

bipy-MT	5-mercaptomethyl-5'-methyl-2,2'-bipyridine
bz-DT	phenylenedimethanethiol
bz-MT	benzyl mercaptan
CARS	Coherent Antistokes Raman Scattering
C6DT	1,6-hexanedithiol
CCD	Charge-coupled device
CE	Chemical enhancement
CTAB	Cetyltrimethylammonium bromide
DFM	Dark-field microscopy
DNA	Deoxyribonucleic acid
DTTC	Diethylthiatricarbocyanine
DTTCI	3,3'-Diethylthiatricarbocyanine iodide
EDTA	Ethylenediaminetetraacetic acid
EF	Enhancement Factor
EGFR	Epidermal Growth Factor Receptors
EME	Electromagnetic Enhancement
FDTD	Finite Difference Time Domain
FEM	Finite Element Method
FIB	Focused ion beam
ITC	Isothermal Titration Calorimetry
ITO	Indium tin oxide
LSP	Localized surface plasmons

LUMO	Lowest Unoccupied Molecular Orbital
MPS	(3-mercaptopropyl)trimethoxysilane
PDT	1,4-phenylenedimethanethiol
PEG	Polyethylene glycol
PSP	Propagating surface plasmons
RNA	Ribonucleic acid
RRS	Resonance Raman Scattering
SEM	Scanning electron microscopy
SERS	Surface Enhanced Raman Scattering
ScFv	single-chain variable fragment
SMSERS	Single Molecule Surface Enhanced Raman Scattering
TDAB	Tetradecylammonium bromide
TEM	Transmission Electron Microscope
TOAB	Tetraoctylammonium bromide
TEGU	Tetra(ethylene glycol)undecanethiol

PREFACE

There is a growing interest on the development of newer spectroscopic techniques for the enhancement of molecular signals, particularly for the detection and identification of chemically and biologically important molecules. Among the various techniques, surface-enhanced Raman spectroscopy (SERS) has emerged as one of the most powerful tools due to the unique ability of the nanoparticles to interact with light. Interactions of light with metal nanoparticles results in the coherent oscillation of electrons on the surface of nanoparticle (surface plasmons) giving rise to a region of increased electric field around the vicinity of the particle. A Raman-active molecule when placed in the vicinity of the nanoparticle's surface give rise to enhancement in signal intensity due to (i) high electric field prevailing on the metal surface (electromagnetic enhancement) and (ii) a charge-transfer interaction between the metal nanoparticle and the molecular system (chemical enhancement). The overall objective of thesis is to fabricate efficient SERS substrates and create hotspots which are capable of producing large signal enhancements of various molecules.

Detailed literature review regarding Raman Spectroscopy with special reference to Surface Enhanced Raman Spectroscopy (SERS) is presented in the first chapter of the thesis. Different approaches adopted for the enhancement in Raman signal intensity are also presented in this chapter.

Chapter two of the thesis, probes the Surface Enhanced Raman Spectroscopic investigations of isolated Au nanorods, having various aspect ratios, with analyte molecules. Electrostatic interactions of analyte molecules onto the surface of Au nanorods were investigated by following isothermal titration calorimetric (ITC) studies. A comparative investigation on the SERS efficiency of spherical Au nanoparticles and 1D Au nanorods were carried out. Au nanorods were found to be better substrates for SERS investigations and the enhancement factor was found to increases with the aspect ratio of the nanorods. The high electric field concentrated at the edges of nanorods contributes primarily towards the enhancement in signal intensity.

A new methodology have been developed for enhancing the Raman signals of analyte molecules by placing them (i) at the edges of Au nanorods, using monothiol derivatives and (ii) at the junctions of two Au nanorods using dithiol derivatives. These aspects are presented in Chapter three. Edges of Au nanorods are regions of high electric field and when two Au nanorods are brought together in a linear fashion, through dithiol linkages, their longitudinal plasmon oscillations couple each other, creating regions of enhanced electric field (hot spots) at the junctions. An enhancement of Raman signals was observed when these molecules are placed at the edges and junctions of Au nanorods. The enhancement factors were estimated as 1.2×10^4 for isolated Au nanorods and 1.5×10^5 for dimeric systems. (*J. Phys. Chem. Lett.* **2010**, *1*, 610-615).

Fabrication of Au nanorod quartets and their use as SERS substrate is described in the fourth chapter. The lateral assembly was achieved by using a thiol derivative which possesses hydrophobic and hydrophilic moieties. The extinction spectral changes were monitored as function of time and aspect ratio of Au nanorods. It was observed that the side-by-side assembly proceeds through dimers, trimers and tetramers to larger aggregates and can be controlled by varying the concentration of the thiol derivative. It was also found that the extent of lateral coupling increases with increase in the aspect ratio of nanorod. Further, the lateral and longitudinal assembly processes were combined for the fabrication of nanorod quartets and higher order assemblies. When four nanorods are brought close together to form the quartet junctions, their plasmons couple each other, to form a region of enhanced electric field and molecules placed at the junction show enhanced signal intensity. The methodology developed can be further extended for the detection of biologically important molecules such as amino acids and proteins.

Chapter 5 describes the single particle investigations on the Au nanorods assembled (i) in a linear fashion utilizing the covalent interaction of dithiols and (ii) in a lateral fashion through electrostatic interaction. The scattering properties of the various assemblies were investigated at the single particle level by adopting a correlation method involving high resolution scanning electron microscopy and dark-field spectroscopy. The scattering wavelength and intensity of the peaks were highly

dependent on the number of nanorods and their orientation in the assembly. Au nanorods assembled in a linear fashion showed a gradual bathochromic shift in the longitudinally coupled plasmon band with increase in the number of rods in a chain. Laterally assembled Au nanorods showed a gradual hypsochromic shift in the longitudinally coupled plasmon band and bathochromic shift in the transverse coupled band. The effect of orientation on the optical properties of linearly assembled Au nanorod dimers was investigated. It is observed that the position and intensity of the coupled plasmon resonance largely depends on the angle between the dimers. All the assembled nanostructures exhibited polarization dependent scattering and the energy levels involved in various modes of excitation were calculated from theoretical studies using Field Element Method and plasmon hybridization models.

Surface Enhanced Raman Spectroscopy: An Overview
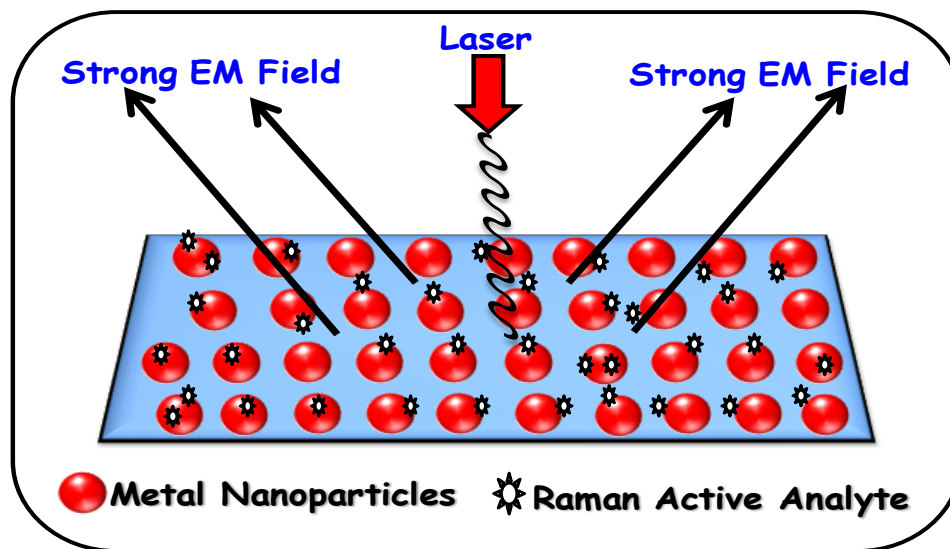
1.1. History of Raman Spectroscopy

In 1928, five years after the discovery of Compton Effect [Compton 1923], the Indian physicist Chandrasekhar Venkata Raman and his student Kariamanikam Srinivasa Krishnan discovered another effect involving a change in wavelength of scattered monochromatic visible light [Raman 1928]. Both of them, in a series of experiments tried to focus sunlight onto samples of purified liquids or gases. In the initial experiments, they used sunlight as source, a narrow band photographic filter to create monochromatic light, and a crossed filter to block this monochromatic light. He found that a small amount of light changed frequency and passed through the crossed filter (Scheme 1.1). The experiment was repeated with about sixty common liquids and found that the results were the same, with

varying degrees of the effect. They could observe a frequency shift in the scattering of the light. This resulted in the discovery of a "new type of secondary radiation" that has since then known as Raman scattering [Raman 1928]. The principle of Raman effect or the inelastic scattering of light was actually predicted by the Austrian scientist Adolf Smekal (1923) some five years earlier [Smekal 1923], and the same effect was also observed by Landsberg and Mandelstam (Soviet Union) at about the same time as Raman's discovery [[a]Landsberg 1928 and [b]Landsberg 1928]. However, Raman's papers represented the more thorough and conclusive investigations for which he was awarded the Nobel Prize for physics in the year 1930 [Raman 1928]. Due to its generality, scientists around the world at that time stated the discovery of the phenomena of light scattering, as one of the most convincing proofs of the quantum theory of light. The theory of the Raman Effect was developed by George Placzek (Czechoslovakia) in early 1930s [Placzek 1934].
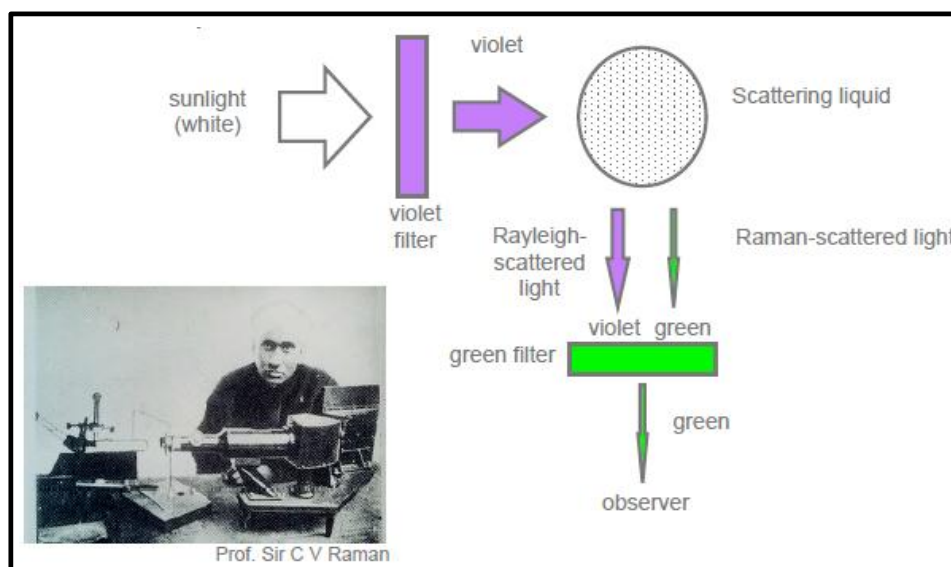
Scheme 1.1. *Schematic illustration of the experiment carried out by Prof. Sir C. V. Raman [Colthup 1990 and Long 2002].*

1.1. Introduction to Raman Spectroscopy

Raman spectroscopy is a spectroscopic technique that results from the inelastic scattering of monochromatic light and is used to study the vibrational, rotational and other low-frequency modes in a molecular system. Raman spectroscopy arises due to a change in frequency when light is scattered by molecules or atoms with which it interacts. When a photon collides with a scattering molecule, the collision can be considered either elastic or inelastic. In the former case, there is no change in the frequency of scattered light. In contrary, there is a small probability that the inelastic collision can cause a change in the frequency of the scattered light. When a photon of frequency v_0 collides with a scattering molecule, most of the light scattered has the same frequency as that of the incident light and the phenomenon is termed as Rayleigh scattering (case 1, Figure 1.1) [Weber 1979 and Ball 2001]. The Rayleigh lines are the most intense lines and in an ordinary Raman spectrometer these lines are eliminated using a notch filter. However, a small component of the scattered light has a frequency v_r which is different from that of the incident light and the difference $(v_r - v_0 = \Delta v)$, is referred to as the Raman frequency [Woodward 1967, Ball 2001 and Long 2002]. A particular molecule may have a characteristic range of Raman frequencies and is collectively referred to as the Raman spectrum of the molecule. During the transition, if the molecule relaxes to a higher energy state, then the corresponding shift in frequency, Δv, will be negative (case 2, Figure 1.1). The resulting Raman scattered photon possesses a lower energy, hv_r, than that of the incident photon. The difference in energies of the incident and scattered photons can be represented as $h\Delta v$ which gives rise to the Stokes lines in Raman spectrum. On the other hand, if a molecule in the excited state relaxes to a lower energy level, then the scattered photon may possess greater energy than incident photon energy

(case 3, Figure 1.1). In such a situation, the difference in energy, Δv is positive, which give rise to anti-Stokes lines in Raman spectrum. Thus, while observing Raman scattering, there will be at least three possibilities: spectral lines due to (i) the corresponding incident light frequency v_0 (Rayleigh scattering), (ii) one having lower energy of $v_r = v_0 - \Delta v$ (Stokes lines), and (iii) the other one at higher energy $v_r = v_0 + \Delta v$ (anti-stokes lines). The Stokes lines are usually more intense than the anti-Stokes lines, since the number of molecules excited from the higher energy level of the ground state is generally small at room temperature (case 2, Figure 1.1). By comparing the ratio of the heights of the Stokes and anti-Stokes lines, Raman spectroscopy can be used as a sensitive temperature probe. The shift in frequency is independent of the frequency of the incident photon and is rather a characteristic of the vibrational energy levels of the scattering molecule. Thus, Raman spectroscopy provides fingerprint of the molecule under investigation and can be used for the detection and identification of a variety of molecular systems.
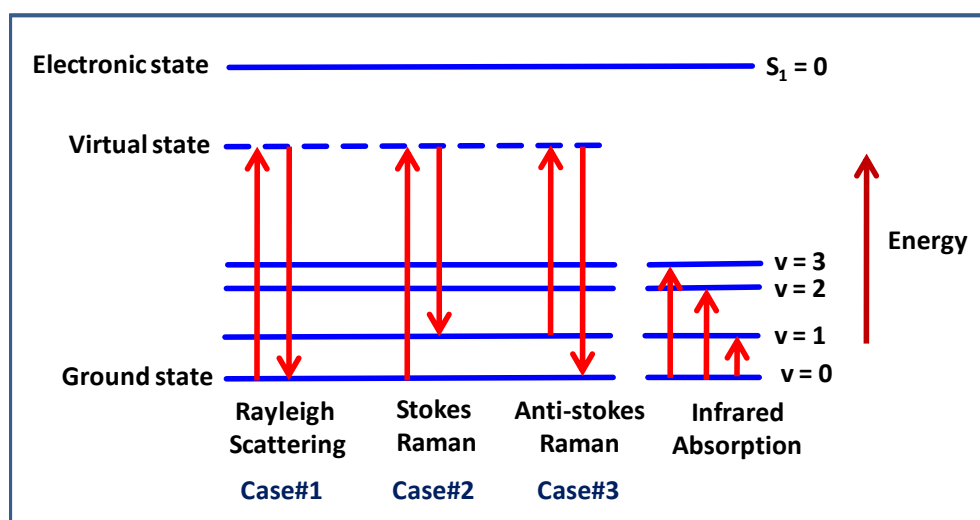
Figure 1.1. *Energy level diagram showing the states involved in Raman scattering and Infrared absorption [Woodward 1967 and Long 2002].*

The principle of Raman scattering resembles with that of fluorescence in many aspects, but closer analysis reveals that the two processes are completely different. Sir C. V. Raman in his original paper [Raman 1928] stated that the observed shift in frequencies were too small to be due to fluorescence. He also found that unlike fluorescence, which tends to emit depolarized light, Raman scattering gives rise to strongly polarized light depending upon the polarization of the incident light [Raman 1928]. The major difference between the two techniques is that fluorescence is associated with the possibility of quenching. In contrast, quenching is not observed in the process of Raman scattering. This is due to the fact that the molecule does not absorb the photon, and there is no transition to a higher intermediate excited state, upon collision with the incident photon. Instead the molecule is perturbed, and the photon is immediately scattered. Since the molecule was not excited to an intermediate state, there is no possibility of the molecule to transfer electron or energy to another molecule ruling out the possibility of quenching in Raman scattering [Woodward 1967]. Another feature that distinguishes the Raman effect from fluorescence is the presence of anti-Stokes lines, which are absent in fluorescence spectrum since the molecules always lose some energy before emitting the photons from the singlet excited state through vibrational relaxation (case 2, Figure 1.2). The major difference is that, unlike fluorescence which requires specific wavelength of excitation, Raman effect is observed for incident light of any frequency. Therefore in contrast to the fluorescence effect, the Raman Effect is not a resonant effect [Tian 2004].
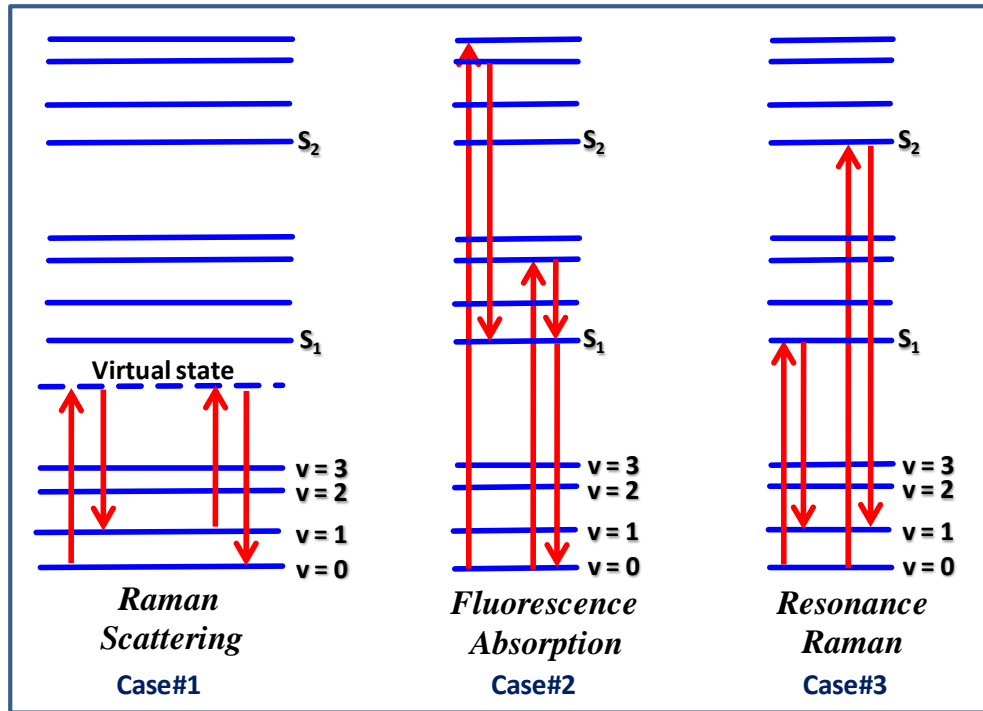
Figure 1.2. Energy level diagram showing the difference between the energy states involved in Raman Scattering, Fluorescence and Resonance Raman Scattering [Tian 2004].

1.2.   Principle of Raman Scattering

We know that the intensity of Raman spectrum depends on the ability of sample to scatter light. Then an important question arises: what causes the scattering of a photon? It has been observed that the main property of a molecule to scatter a photon is its polarizability. The polarizability, α, represents the ability of an applied electric field, E, to induce a dipole moment, $\mu_{induced}$, in an atom or a molecule:

$$I_{Raman} = \mu_{induced} = \alpha. \, E \tag{1.1}$$

where I_{Raman} is the intensity of Raman spectrum, $\mu_{induced}$ is the induced dipole moment, α is the polarizability and E is the applied electric field. Polarizability of atoms is isotropic, whereas polarizability of molecules may be anisotropic depending on its symmetry of the molecule [Ball 2001]. Certain rotational or vibrational changes in a molecule induce

polarization. Thus, the oscillating electric field associated with the electromagnetic radiation can distort the electron cloud of the molecule thereby creating an induced electric dipole moment. This oscillating induced dipole moment in turn emits or scatters electromagnetic radiation, giving rise to Raman spectrum. Thus the selection rule states that Raman transition from one state to another is activated optically only in the presence of non-zero polarizability derivative with respect to the normal coordinate or

$$\delta\alpha/ \delta Q \neq 0$$

where $\delta\alpha$ is the change in polarizability and δQ is the change in position with respect to normal coordinates. This condition may be physically interpreted to mean that the vibrational displacement of atoms corresponding to a particular vibrational mode results in a change in the polarizability.
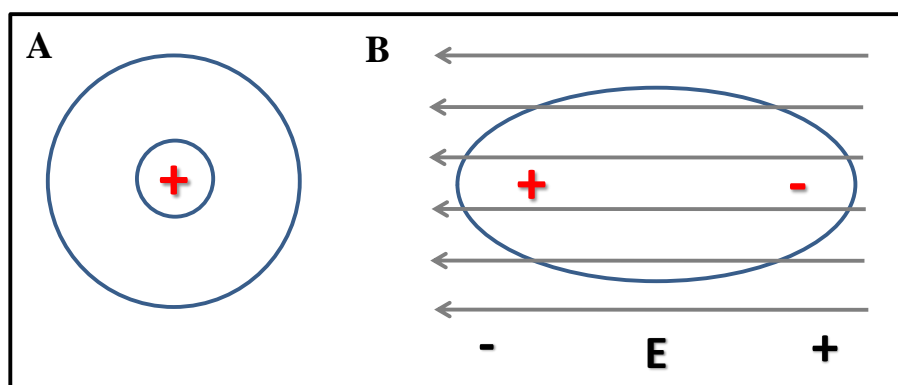
Figure 1.3. *A molecule (A) in the absence of electric field and (B) in the presence of electric field that distorts the molecular orbitals.*

The major advantage of Raman spectroscopy over other spectroscopic techniques is that it provides the fingerprint of the molecule under investigation. Due to this unique feature, the technique is found to be extremely important in almost all the branches of science. However, the low intensity of signals limits the use of Raman spectroscopy. This is due to the fact that the Raman scattering cross section is extremely small compared to other

spectroscopic techniques such as infrared and fluorescence [Tian 2004]. Attempts have been made to improve the number density of molecules absorbed upon irradiation and thereby enhancing the Raman scattering cross section. With the advent of newer laser sources, substantial improvement has been achieved in enhancing the Raman scattering cross section. This has opened up a new field of coherent or stimulated Raman spectroscopy wherein molecular vibrations are coherently excited. Various other enhanced Raman spectroscopic techniques developed in recent years include Resonance Raman Scattering (RRS), Surface Enhanced Raman Scattering (SERS) and Coherent Antistokes Raman Scattering (CARS). The studies in this thesis mainly focus on SERS and brief description on the underlying principles is given below.

1.4.   Surface Enhanced Raman Spectroscopy

One of the breakthroughs in the field of Raman spectroscopy came in 1970s, largely through the experiments carried out by three different groups. Substantial enhancement in Raman signals, of about a million times greater than expected, were observed when molecules are adsorbed onto a specially prepared silver surface. Intense Raman scattering was first observed by Fleischmann et al. in 1974 from aqueous solution of pyridine adsorbed onto a roughened silver electrode surface [Fleishmann 1974]. In late 1970s, two different groups, Jeanmaire and Van Duyne from Northwestern University [Jeanmaire 1977], and Albrecht and Creighton from University of Kent [Albrecht 1977], independently tried to explain the mechanism of large Raman signal enhancement. They recognized that the large intensities observed may not be due to the increase in the number of scattering molecules. Two different mechanisms were proposed: Jeanmaire and Van Duyne suggested an electric field enhancement mechanism whereas Albrecht and Creight on put forward a charge-

transfer effect due to the broadening of molecular electronic states through their interaction with the metal surface. Thus, the discovery of this new technique, which was termed as "Surface Enhanced Raman Spectroscopy", led to a revolution in the field of Raman spectroscopy, since it could overcome the inherent problem associated with low signal to noise ratio.

It is further interesting to compare the spectrum obtained through SERS and normal Raman spectroscopy (Scheme 1.2). While the spectra obtained in most SERS experiments are similar to the non-surface enhanced spectra, with an enhancement in signal intensity, there are often differences in the number of modes present [Campion 1998 and Kneipp 1999]. Certain modes which are not found in the ordinary Raman spectrum may appear in SERS spectrum, while certain other modes observed in Raman spectrum may disappear. The different modes observed in a spectroscopic experiment are governed by the symmetry of the molecules and these are usually summarized by selection rules. The mutual exclusion principle states that "in molecules with a center of symmetry, the vibrational modes that are Raman active are infrared inactive and vice versa". Interestingly, modified selection rules are applicable for SERS since many molecules lose their center of symmetry when adsorbed onto a surface. The loss of a center of symmetry eliminates the requirements of the mutual exclusion rule, which states that modes can only be either Raman or Infrared active. Thus modes that would normally appear only in the infrared spectrum of the free molecule and (not in the normal Raman spectrum) can appear in the SERS. The intensities of the bands observed in SERS generally fall off with increasing vibrational frequency; C–H stretches, for example, tend to be relatively weak in SERS. The spectra tend to be depolarized, in contrast to those taken from molecules adsorbed on atomically smooth surfaces. Excitation

profile largely depends on the electrode potential in electrochemical experiments and varies for different vibrational modes. Depending on the substrate morphology, the enhancement may be long ranged, extending tens of nanometers from the surface.
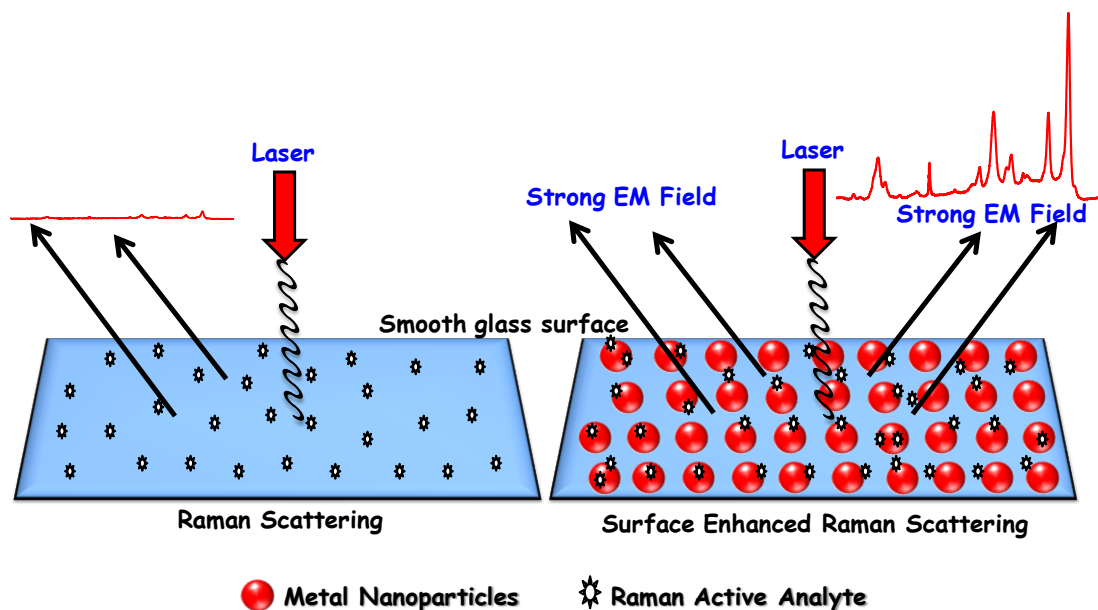
Scheme 1.2. *Schematic representation comparing the Raman scattering and SERS. In SERS, analyte molecules adsorbed on to metal nanoparticles generate high electric field on illumination with light of appropriate wavelength, giving rise to enhanced Raman signal intensities.*

Surface Enhanced Raman Spectroscopy provides greatly enhanced signals from Raman-active analyte molecules when adsorbed onto certain specially prepared metal or metal nanoparticle surfaces [Campion 1998 and Kneipp 1999]. An increase in the intensity of signal on the order of 10^4-10^6 has been regularly observed and can be as high as 10^8 and 10^{14} for some specially designed systems. SERS is both surfaces selective and sensitive. Even though many of the transition metals can be used, metal nanoparticles such of silver, gold and copper show large enhancements. It is also observed that metal nanoparticles in the size range of 20-300 nm show large enhancement. In general smooth surfaces are not Raman

active compared with rough surfaces, and have a long-range effect ranging to about tens of nanometers. In case of multilayer substrates, molecules adsorbed on the first layer on the surface show largest enhancements. Enhancement of Raman signal operates through two mechanisms namely an electromagnetic enhancement (EME) [Schatz 1984 and Moskovits 2005] and chemical enhancement (CE) [Otto 1992 and Otto 2005] mechanisms. The electromagnetic effect is dominant compared to the chemical effects, contributing substantially to the enhancement factor. The electromagnetic enhancement is dependent on the roughness of the metal surface, while the chemical enhancement involves changes in the electronic states of the adsorbate due to chemisorptions of the analyte onto the surface.

1.5.   Enhancement Mechanisms

As mentioned in the previous section, electromagnetic enhancement mechanism is a direct consequence of the presence of metal roughness features at the metal surface and contributes substantially towards the enhancement mechanism. The Raman scattering intensity is proportional to the induced dipole moment (μ_{ind}) in the molecule, which in turn is proportional to the molecular polarizability (α) and the electric field strength (E) as given by the Equation 1

$$I_{Raman} = \mu_{ind} = \alpha.\ E \tag{1}$$

High electric field is generated in the vicinity of metal surface on interaction with a highly directional and focused laser beam, compensating the inherent weakness associated with Raman scattering.

The metal nanoparticle absorbs electromagnetic radiation of appropriate wavelength when the frequency of incident light is in resonance with the free electrons on the surface of nanoparticle. A brief description on the metal nanomaterials and the plasmon resonance is

given in section 1.5. The nanoparticle absorbs light when the frequency of laser is in resonance with the plasmon oscillation of the nanoparticle, leading to the concentration of large amount of energy at the surface (Figure 1.4A). The nanoparticle reemits a portion of this energy by Mie scattering, resulting in the creation of a region of high electric field on the surface with very high energy density (Figure 1.4A). In electrostatics, the scattered field intensity (E_{surf}) is given by

$$E_{surf}{}^2 = 4\ E_0{}^2\ g^2 \tag{2}$$

where g is related to the complex dielectric function of metal given by

$$g = \varepsilon - \varepsilon_m\ /\ \varepsilon + 2\varepsilon_m \tag{3}$$

where $\varepsilon = \varepsilon_1 + i\ \varepsilon_2$ and ε_m is the medium's dielectric constant at optical frequency.

The field on the nanoparticle surface [Eq. (3)] interacts with adsorbate (Raman active molecule) and causes an induced dipole in the molecule, which radiates at a Raman-shifted optical frequency. In addition, there is also enhanced emission from the induced dipole; this enhancement is determined by an expression similar to Equation (3); hence, the SERS intensity is the product of the squares of the incoming field and the outgoing field. An approximation gives rise to the well-known fourth-power dependence of SERS signals on the electric field [Eq. (5)]:

$$I_{SERS}\ \alpha\ \ 16\ E_0{}^4\ g^4 \tag{4}$$

Therefore, it is observed that the intensity of Raman signals in SERS is proportional to the forth power of electric field. Thus, according to the electromagnetic SERS mechanism, the amplification of both the incident laser field and the scattered Raman field occurs on interaction of electromagnetic radiation with nanoparticles under the resonance conditions of surface plasmon excitation.
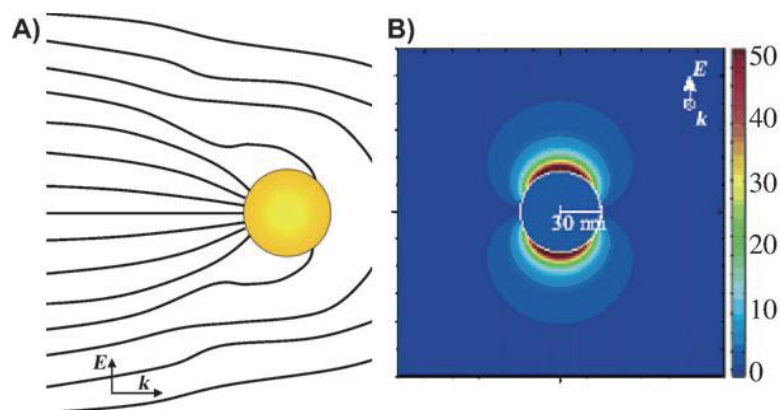
Figure 1.4. *A) Electromagnetic energy concentrated by an Ag nanoparticle when its surface plasmon is resonantly excited. The particle's extinction cross section is much larger than its geometrical cross section. B) Calculated near-field distribution of Mie scattering [Schatz 2002].*

Apart from the EME, other factor that contributes to the SERS enhancement mechanism is the chemical enhancement. Raman active molecule can undergo electronic coupling with metal nanoparticles forming charge-transfer intermediates with higher Raman scattering cross-sections. Chemical enhancement mechanism can also be explained as follows: the molecular orbitals of the adsorbate broaden in to the conducting electrons of the metal, altering the energy levels of the analyte. The exact mechanism involved in the charge transfer process is still not understood. The proposed steps in the chemical enhancement mechanism are (i) excitation of an electron into a hot electron state and its transfer to the LUMO of the molecule (ii) transfer of the hot electron from the LUMO to the metal and (iii) Return of the electron to its initial state and stokes photon creation.
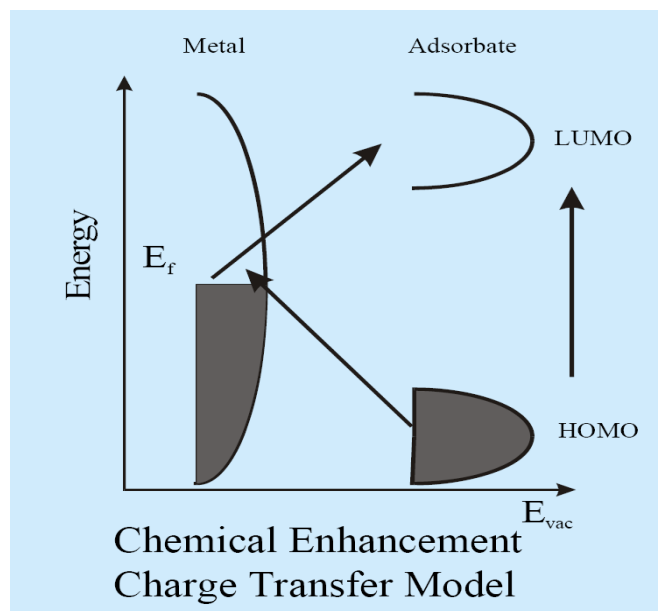
Figure. 1.5. *Typical energy level diagram for a molecule adsorbed on a metal surface. The occupied and unoccupied molecular orbitals are broadened into resonances by their interaction with the metal states; orbital occupancy is determined by the Fermi energy. Possible charge transfer excitations are shown [Campion 1998].*

Interestingly, the charge transfer mechanism influences the scattering cross-section: the chemical nature of the analyte undergoes variation as a result of the interaction with the metal. In contrast, the scattering cross section is not influenced by the electromagnetic effect; however, it influences the intensity of those analyte molecules which scatter electromagnetic radiation. For systems in which both electromagnetic and chemical mechanisms operate simultaneously, the effects are multiplicative and it is difficult to obtain the contribution of induced components.

1.6.   Brief Introduction to Nanomaterials

Nanoscience and nanotechnology pertain to the synthesis, characterization, exploration of their properties and utilization of materials, which possess at least one of its dimensions in the nanometer size regime (~1-100 nm). A comparison of the size domains of

various naturally existing systems is presented in Figure 1.6. Nanomaterials incorporate collections of atoms or molecules, whose properties are distinctly different from those of isolated atoms/molecules or bulk systems [Kreibig 1995, El-Sayed 2001, Katz 2003 and Thomas 2007]. Thus, nanostructured materials can act as a bridge between single atoms/molecules and bulk systems. The difference in properties at the nanoscale arises mainly due to the confinement of electrons that do not scale linearly with size. The interesting property of materials having nanoscale dimension is that they show fascinating size and shape dependent properties and these properties are least dependent on their chemical composition [Kelly 2003, Shenhar 2003, Thomas 2003, Daniel 2004 and Burda 2005]. Some of the examples of nanostructured materials include metal and semiconductor nanoparticles and carbon based nanostructured systems such as fullerenes, carbon nanotubes and graphene. A unique feature associated with these materials is their large surface to volume ratio which makes them a suitable candidate in catalytic applications. Another attractive property of noble metal nanoparticles is that they possess strong optical absorption arising from the surface plasmon resonance (yellow, red and blue color for Ag, Au and Cu, respectively). Theoretical description on surface plasmon resonance of metal nanoparticle is presented below.
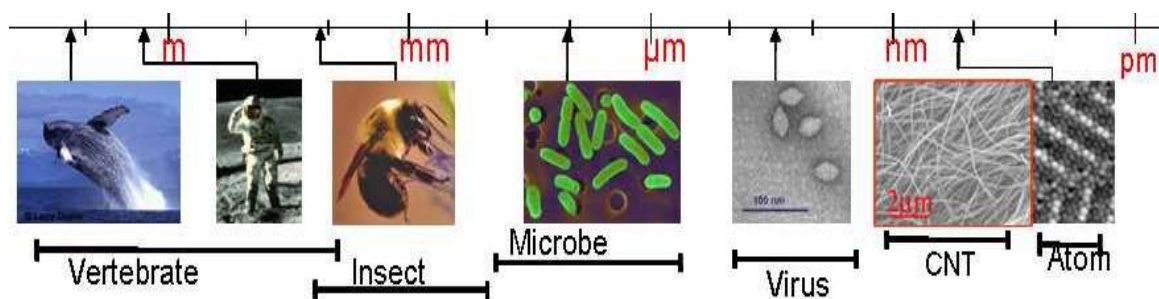
Figure 1.6. *Comparison of size domains of naturally existing systems.*

Interaction of light with metal nanoparticles and nanostructured films results in the collective oscillation of free electrons on the surface, giving rise to hybrid surface waves known as surface plasmons. An interesting property of surface plasmons is that it can trap light at the metal/dielectric interface resulting in the enhancement of field at the metal surface. According to the Drude-Lorentz model, metal can be treated as plasma consisting of an equal number of positive ions and conduction electrons. In the presence of electromagnetic radiation, the electric vector displaces the free electrons in the metal, whereas the columbic attraction between the electron cloud and nuclei acts as the restoring force. The oscillating nature of the electric field of light induces coherent oscillation of the electron cloud over the nanoparticle surface, with a resonance frequency which is dependent on the size and nature of the material. The surface plasmons can be broadly classified as Propagating Surface Plasmons (PSP) and Localized Surface Plasmons (LSP). Propagating surface plasmons are associated with smooth, thin metallic films where the plasmon feels a boundary due to the planar surface. These surface plasmons have a combined electromagnetic wave as well as surface charge character and are highly bound to the surface (Figure 1.7A). The surface plasmon in such a metal/dielectric interface is highly bound to the surface. As a result, an enhanced field is observed near the surface in the perpendicular direction, the amplitude of which decays exponentially with distance from the surface [Barnes 2003]. Localized surface plasmons (LSPs) originate from the collective oscillation of free electrons on the surface of a nanoparticle, when excited with electromagnetic radiation [Kelly 2003]. In contrast to the propagating surface plasmons, localized surface plasmons are confined in a finite volume on the surface, depending upon the size and shape of the nanoparticle. When a metal nanoparticle is irradiated by light, the oscillating electric

field causes the conduction electron to oscillate coherently (Figure 1.7B). The absorption

occurs when the incident photon frequency is in resonance with the collective oscillation of

the conduction electrons, resulting in unique optical properties. For Ag, Au and Cu

nanoparticles, the frequency of the oscillating electron cloud matches with that of the visible

radiation and hence the surface plasmon resonance absorption is usually in the spectral range

of 400-800 nm depending on the size and shape. The presence of surface plasmons gives rise

to regions of high electric field on the nanoparticles' surface and the use of this field for

sensing application is discussed in this thesis.
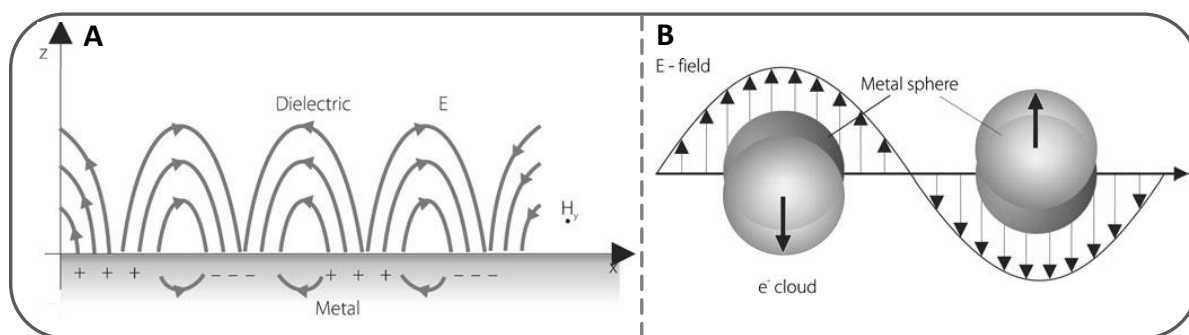
Figure 1.7. *(A) Surface plasmons at the interface between a metal and a dielectric material having a combined electromagnetic wave and surface charge character [Barnes 2003] (B) Schematic of plasmon oscillation for a sphere, showing the displacement of the conduction electron charge cloud relative to the nuclei [Kelly 2003].*

1.7. **Au Nanorods and Edge Effect**

Electron density distribution on the surface of metal nanoparticle and the electric

field around them is mainly dependent on their size and shape. Most of the early

investigations on the electric field distribution around the metal nanostructures are mainly

focused on spherical nanoparticles. Attempts have been made to use the electric field around

spherical Au nanoparticle for sensing application. However, the major drawback associated

with spherical particle is that they undergo random aggregation on binding with analyte due to their isotropic nature.

Gold nanorods are one dimensional system having promising optical properties. More recently these systems are extensively utilized for sensing applications. Various approaches have been reported for the synthesis of Au nanorods. The most common one are (i) hard and (ii) soft template mediated synthesis. In the former case, the metal ions are reduced inside the cylindrical pores of oxide or polymeric membranes, usually called 'hard template synthesis' [Brumlik 1991 and Martin 1996]. In the latter method, neutral or charged surfactants are used for growing nanorods, usually known as 'soft template syntheses by adopting electrochemical, photochemical or seed mediated methods [Yu 1997, Link 1999, Jana 2001 and Busbee 2003]. Electrochemical synthesis of Au nanorods involves the reduction of $HAuCl_4$ in the presence of 'shape-inducing' cationic surfactants and other additives [Yu 1997]. These cationic surfactants were found to favor rod formation and act as both the supporting electrolyte and stabilizer. Electrochemical synthesis is carried out in the presence of a cationic surfactant, namely, cetyltrimethylammonium bromide (CTAB) and a hydrophobic surfactant such as tetradecylammonium bromide (TDAB). The ratio between the surfactants controls the average aspect ratio of the Au nanorods.

The seed mediated method developed by Murphy and coworkers for the synthesis of Au nanorods has excellent control over the aspect ratio [Jana 2001 and Busbee 2003]. Chloroauric acid ($HAuCl_4$) was reduced using a mild reducing agent namely, ascorbic acid in the presence of Au nanoparticle as seed and CTAB as the capping agent. Au nanorods having different aspect ratios were synthesized by varying the volume of the seed solution added. Later, this method was modified by El-Sayed and coworkers, which improved the

yield of nanorods [Link 1999]. A photochemical method was developed for the synthesis of Au nanorods by Yang and coworkers which involved the reduction of $HAuCl_4$ in the presence CTAB as surfactant and tetraoctylammonium bromide (TOAB) as the co-surfactant [Kim 2002]. Photographs of nanorod solutions of various aspect ratio and the corresponding extinction spectrum are shown in Figure 1.8. In this case, the aspect ratio of nanorods was conveniently varied by varying the concentration of $AgNO_3$ added.
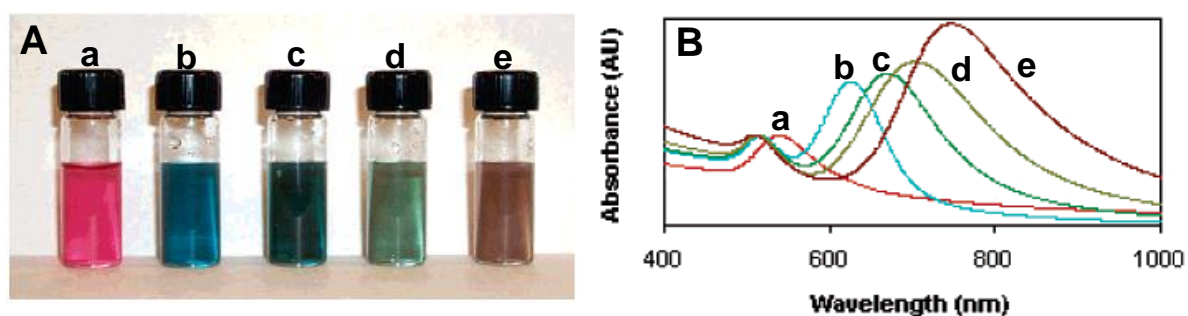
Figure 1.8. *(a) Photographs of photochemically prepared gold nanorods solution and (b) the corresponding UV-vis spectrum. The solution 'a' was prepared in the absence of silver ions and spherical Au nanoparticles were obtained. The other solutions (b-e) were prepared by adding 15.8, 31.5, 23.7, and 31.5 µL of silver nitrate solution, respectively. The middle solution was prepared with longer irradiation time (54 h) compared to that for all other solutions (30 h), and the transformation into shorter rods can be observed [Kim 2002].*

1.8.   Hot spots in SERS

Fabricating efficient and reproducible nanoparticle assemblies that can produce large enhancement in Raman signals is one of the major challenges in the field of Surface Enhanced Raman Spectroscopy (SERS). Creating regions on the surface of the substrates which can produce large enhancement in signal intensities are called "hot spots". Various methods have been reported in the literature for the creation of such hot spots which can produce enhancement factors of the order of 10^5-10^8 and values as high as 10^{14} has been

reported for single molecule detection. Different methodologies have been adopted for increasing the scattering cross section and enhancing molecular signals in Raman spectroscopy. Various methods include (i) exciting at the plasmon resonance of the nanomaterial, (ii) using sharp edged nanostructures wherein their fields are concentrated at the edges and (ii) use of coupled plasmons which arises when two or more nanoparticles are brought in close proximity. The design and fabrication of substrates possessing a combination of these properties can result in higher enhancement factor values.

Ensemble-averaged SERS enhancement factors (EF) from isolated colloidal nanoclusters have been reported by Chen and coworkers using Au@Ag core-shell nanoparticles as substrates [[a]Chen 2010]. Uniform sized Au@Ag core-shell nanoparticles were synthesized by reducing $AgNO_3$ using ascorbic acid in presence of Au nanoparticles as the seed and sodium citrate as capping agent (Figure 1.9). The extinction peak of the Au@Ag core-shell system (400 nm) was similar to that of 20 nm silver nanoparticles, suggesting that the Au cores did not contribute to the plasmon resonance of the core-shell system. Monolayer coverage of the SERS analytes, namely 2-naphthalenethiol over the nanoparticle system was achieved by incubation. Sodium Chloride was then added to induce aggregation of nanoparticles which was further encapsulated in a polymer, namely polystyrene-block-poly-(acrylic acid) (PSPAA). Resulting nanoclusters were separated by differential centrifugation method leading to the enrichment of one type of aggregate (dimers as well as trimers). The uniform polymer coating over the nanoparticle surface and the formation of monomers and trimers were confirmed with the help of TEM images (Figure 1.9 e-g). SERS studies of these systems gave an ensemble averaged EF of 1.3×10^3 for the monomers (Figure 1.11a) and in the range of 10^5-10^7 at the hotspots of the dimers and trimers (Figures 1.9c and 1.9c).
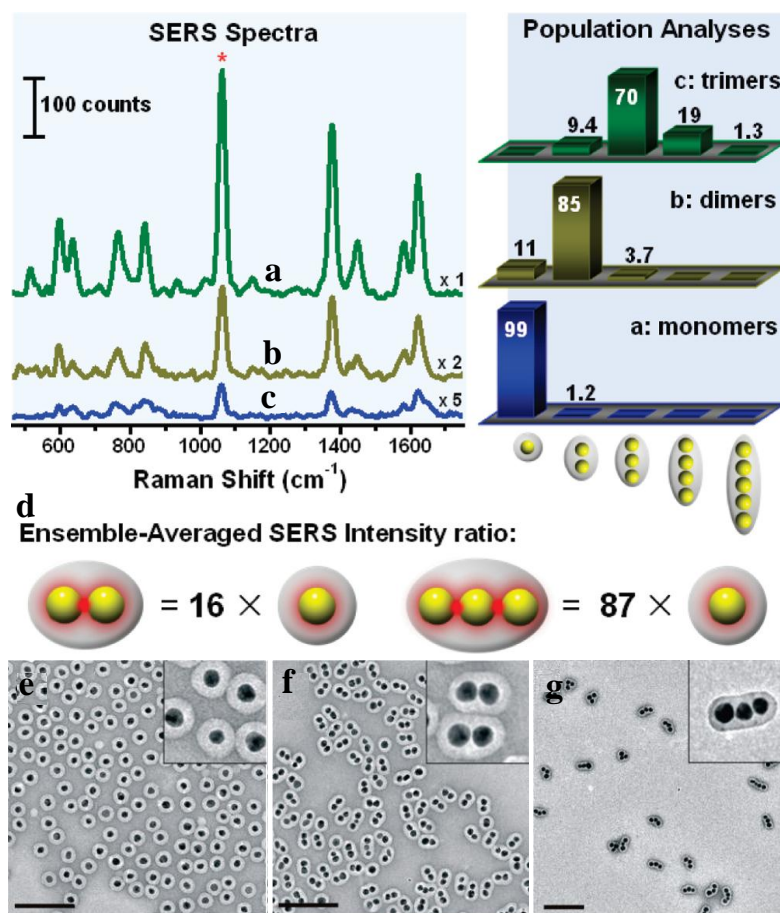
Figure 1.9. *SERS spectra of (a) monomers and samples enriched with (b) dimers and (c) trimers of Au@Ag nanoparticles of diameter 20 nm; excitation: 785 nm at 290 mW; (insets: the histograms of these samples).(d) The schematics in the lower panel show the SERS intensity ratio of the nanoclusters. (e-g) TEM images of (e) monomers of Au@Ag nanoparticles and the samples enriched with Au@Ag, (f) dimers, and (g) trimers; inset shows the corresponding magnified images [[a]Chen 2010].*

A detailed investigation on the specific nanoparticle structures that give rise to Single Molecule Surface Enhanced Raman Scattering (SMSERS) was carried out by Van Duyne and coworkers [Camden 2008]. Citrate reduced silver nanoparticles were treated with a mixture of Rhodamine 6G and were aggregated by the addition of NaCl for the fabrication of SERS active substrates. Even though a variety of structures giving rise to large

enhancements were observed, dimers consisting of two Ag nanocrystals form the basic model of the organized assembly (Figure 1.10A). The Raman spectrum and the Rayleigh scattering spectrum from a nanoparticle assembly are collected by utilizing the correlation method involving TEM and dark field microscopy (Figures 2.10C and 2.10D). The electrodynamics calculations suggested that the enhancement factor in SMSERS is consistent with a combination of molecular resonance enhancement and electromagnetic enhancement (Figure 1.10B).
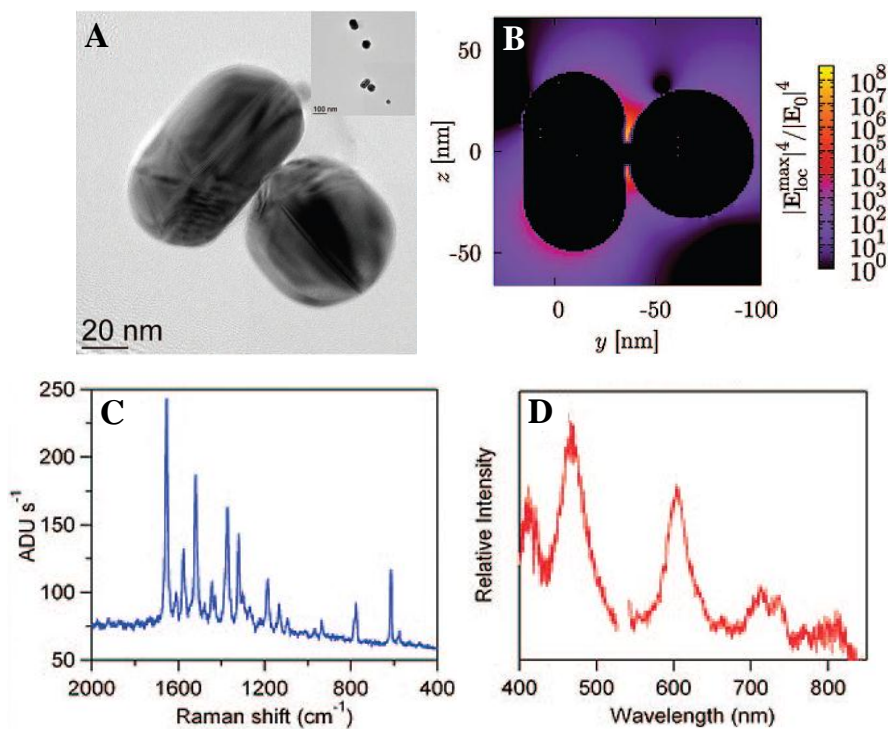
Figure 1.10. *(A) TEM image and (B) contour plot of maximum SERS enhancement at 532 nm (where the maximum value of enhancement factor is 3.9 × 10^{8}) of the single-molecule SERS active dimer. (C) Raman spectra of Rhodamine 6G molecule trapped at the dimer junction (excitation wavelength = 532 nm). (D) Dark-field scattering spectrum of a single-molecule SERS active structure [Camden 2008].*

High electric field and preferential reactivity at the edges of the gold nanorods make them promising SERS substrates compared to spherical nanoparticles. The preferential

binding of the thiol molecules on the {111} facets, at the edges of Au nanorod allows their one dimensional organization. Detailed mechanistic investigations on the end-to-end assembly of Au nanorods using α,ω-dithiols showed that the nanochain formation proceeds through three distinct steps: (i) incubation, (ii) dimerization and subsequent (iii) oligomerization.

Another factor that influences the SERS signal intensity is the orientation of molecules on the surface of metal nanoparticles. Recently, Chen and coworkers studied the changes in SERS fingerprints of the molecules trapped at the hot spots [[b]Chen 2010]. Hot spots were created by the salt-induced assembly of Au nanorods as linear chains by blocking their lateral sides with polymers (Figure 1.11j). The TEM images of the polymer coated Au nanorods and the nanorod assemblies formed through the salt induced aggregation are shown in Figures 1.11f and 1.11g respectively. Molecules such as 4-mercaptobenzoic acid were incorporated at the hot spots and large enhancement in the molecular signals corresponding to the analyte was observed during the assembly process (Figure 1.11c). Transformation in the position and intensity of SERS signals corresponding to the analyte molecules were observed during the assembly of nanorods. The variation in the SERS signals were attributed to the formation of hot spots and detailed spectral analysis showed that the reorientation of analyte molecules from nearly upright to parallel/tilted conformation at the nanorod junctions was the reason for these variations in signals (Figures 1.11h and 1.11i). The aggregation of Au nanorods exerts physical stress on the molecules at the nanorod junctions resulting in the molecular reorientation during the linear assembly of nanorods.
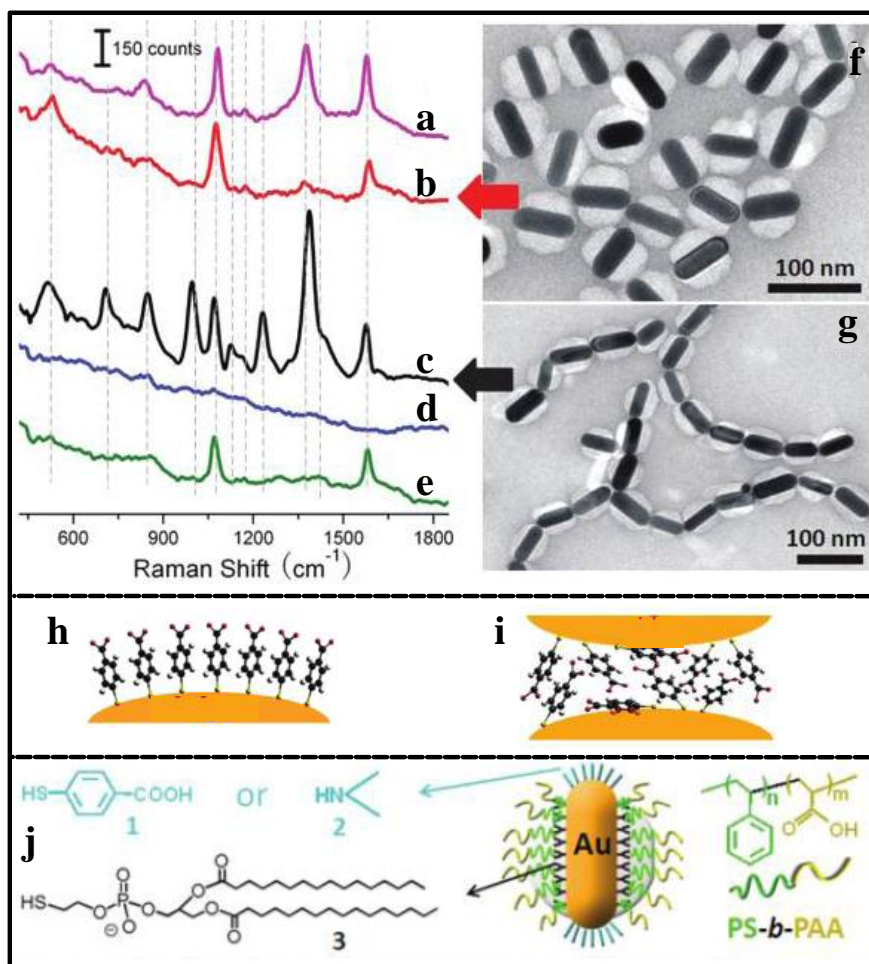
Figure 1.11. *(a) Raman spectrum of 50 mM 4-mercaptobenzoic acid in 5 M aq NaOH; (b) SERS spectrum of 4-mercaptobenzoic acid adsorbed onto the edges of polymer capped isolated Au nanorods; (c) SERS spectrum of sample b after the salt-induced linear aggregation (d) absence of SERS of dimethylamine trapped at the junctions of in linearly aggregated Au nanorods;(e) SERS spectrum of sample d after incubation with 4-mercaptobenzoic acid at 60 °C for 24 h; (f and g) TEM images of polymer encapsulated (f) isolated Au nanorods and (g) their linear aggregates; (h) Schematic illustrations of the surface ligands adsorbed onto isolated rod   and (i) at the junctions of two rods. (j) Structure of Raman reporter molecules (**1** and **2**), polymer used for encapsulating the lateral surface of nanorods (**3**) and the schematics showing the nanorod wrapped with polymer and Raman reporter molecules [[b]Chen 2010].*

Interestingly, the detection limit of SERS has been achieved at single molecular level using various methods. Two different groups independently reported the single molecule detection of analyte using SERS for the first time in late 1990s. Single molecule detection of cresyl violet adsorbed on aggregated silver clusters was reported by Kneipp et al. They used near-infrared excitation, non-resonant without any intramolecular optical transitions of the dye but exciting the plasmon of the fractal aggregate [Kneipp 1997]. On the other hand, Nie and Emory combined surface plasmon and resonance enhancement (SERRS) to produce the required sensitivity for the detection of single dye molecule adsorbed on a single silver particle [Nie 1997].

Using standard citrate reduction method, Nie and Emory synthesized a collection of isolated silver nanoparticles having various sizes and shapes [Nie 1997]. Interestingly, only a small number of particles gave high enhancement in signals ('hot' particles). Combined optical and AFM measurements showed that for large enhancements observed, most of the particles were isolated having a size of ~100 nm and shapes ranging from spherical to rod-like (Figure 1.12 A-D). Samples were prepared with less than one adsorbed molecule per particle on average, by using appropriately dilute solutions. Highly intense scattering was observed when the laser polarization was aligned along the long axis of an ellipsoidal particle. Also, large enhancement was observed for particles having their plasmon in resonance with the excitation wavelength, emphasizing the role of electromagnetic theory of enhancement. For single rhodamine 6G molecules adsorbed on the selected nanoparticles, the intrinsic Raman enhancement factors were on the order of 10^{14} to 10^{15}, much larger than the ensemble-averaged values. Hence, Raman scattering cross sections on the order of 10^{-15} cm^2 per molecule is obtained which is comparable with that of the optical cross sections of single-chromophoric fluorescent dyes. This enormous enhancement leads to vibrational

Raman signals that are more intense and stable than single-molecule fluorescence. It was estimated that only one out of a hundred or a thousand particles is 'hot' and, in addition, that only about one in ten thousand surface sites leads to efficient enhancement. Support for this conclusion comes from the rapid saturation of the effect with surface coverage. Further, polarization dependent Raman measurements were carried out at the single-particle level. Excitation polarization data obtained for two different silver nanoparticles under identical conditions showed that, intense signals can be observed with either s- or p-polarized light (parallel or perpendicular to the plane of incidence), depending on the orientation of the particle relative to the polarization axis. When one is maximally excited along the s polarization, the other is minimally excited, and vice versa, indicating that the two nanoparticles should have orthogonal orientations.
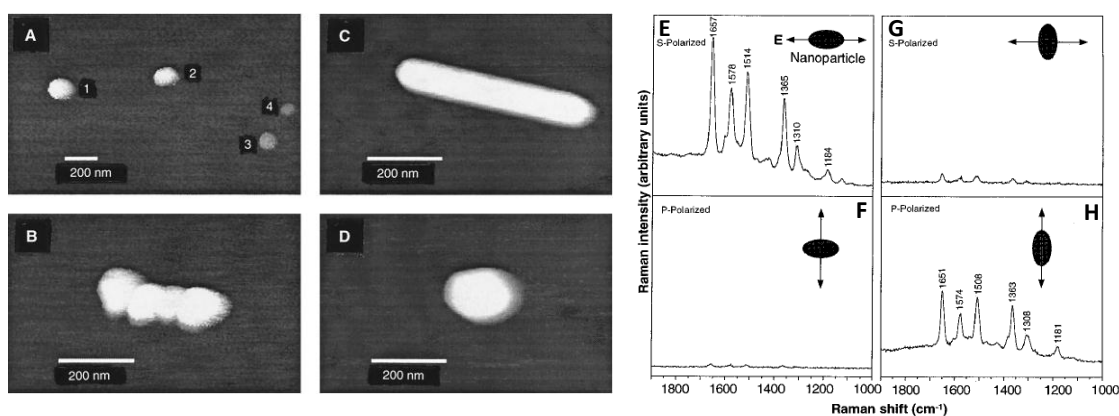
Figure 1.12. *(A-D) Tapping-mode AFM images of screened Ag nanoparticles. (A) Large area image showing four single nanoparticles. Particles 1 and 2 were highly efficient for Raman enhancement, but particles 3 and 4 (smaller size) were not. (B) Hot aggregate containing four linearly arranged particles, (C) rod-shaped hot particle and (D) faceted hot particle. (E-H) SERS spectra of Rhodamine 6G (2 x 10^{-11}M) adsorbed onto two different silver nanoparticles obtained with a linearly polarized laser beam. The direction of laser polarization and the expected particle orientation are shown schematically for each spectrum. Wavelength of laser beam used is 514.5 nm with a laser power of 250 nW. Laser focal radius is 250 nm and integration time is 30 s [Nie 1997].*

There are several reports on the use of nanoparticle assemblies as hot spots in SERS. Hybridized plasmons originate when two nanoparticles are brought in close proximity which generate regions of enhanced electric field near the surface of the particle leading to the creation of hot spots. Raman-active molecules when trapped at the hotspots give rise to enhancement of SERS signals upon illumination with light of appropriate wavelength. Various approaches adopted in the literature for the design of nanoparticle assemblies with hot spots include various lithographic methods, salt-induced aggregation methods and DNA based assembling using various chemical methods.

1.9. Applications of SERS

Raman spectroscopy provides useful information about various molecular vibrations and provides fingerprint of the molecular systems. Raman spectroscopy offers various advantages over conventional microscopic analysis. A small volume of sample (1 μM in volume) is sufficient and spectra obtained can provide useful information about the identity of molecular systems present. One of the major advantage is that water does not generally interfere in Raman spectra analysis and hence SERS is suitable for the microscopic investigations of a wide range of systems such as inorganic materials (minerals and ceramics), polymeric materials, biological materials (cells, proteins, nucleic acids, lipids) and forensic trace materials. The technique is widely used for the (i) rapid detection of explosives and landmines, (ii) identification of adulterated medicine, (iii) detection and structural identification of molecules and (iv) following chemical and biological reactions. One of the recent studies indicate that the SERS is useful in the *in vivo* detection of cancer cells and details are given below.

The use of biocompatible and nontoxic nanoparticles for *in vivo* tumor targeting and detection, based on surface enhanced Raman scattering have been reported by Nie and coworkers [Qian 2008]. A Raman reporter molecule, namely malachite green was attached onto Au nanoparticle and this was covered by a layer of polyethylene glycol (PEG). These PEGylated SERS nanoparticles were found to be brighter with emission in the near infrared window, compared to that of semiconductor quantum dots. These nanoparticles were modified with tumor-targeting antibodies (single-chain variable fragment, ScFv) and specifically targeted to the tumor biomarkers such as epidermal growth factor receptors (EGFR) on human cancer cells and in xenograft tumor models (Figure 1.13 A). The SERS spectra were obtained by incubating the ScFv-conjugated gold nanoparticles with human carcinoma cells and are shown in Figure 1.13 b. The human head-and-neck carcinoma cells (Tu686) were EGFR positive, and were detected by strong SERS signals. In contrast, the human non-small cell lung carcinoma (NCI-H520) which did not express EGFR, showed little or no SERS signals. For control cancer cells (EGFR negative) and control nanoparticles (plain PEG-coated nanotags and PEG-nanotags functionalized with a nonspecific antibody), the spectra showed a weak but reproducible background (Figure 1.13 b). This may be due to the presence of residual SERS nanoparticles in the mixing solution that were not completely removed during cell isolation. Also, substantial differences were observed in signal intensities for the targeted and nontargeted nanoparticles in the tumor, whereas the SERS signals from nonspecific liver uptake were similar. This result indicates that the ScFv-conjugated gold nanoparticles were able to target EGFR-positive tumors and *in vivo* detection could be achieved using SERS (Figure 1.13 C).
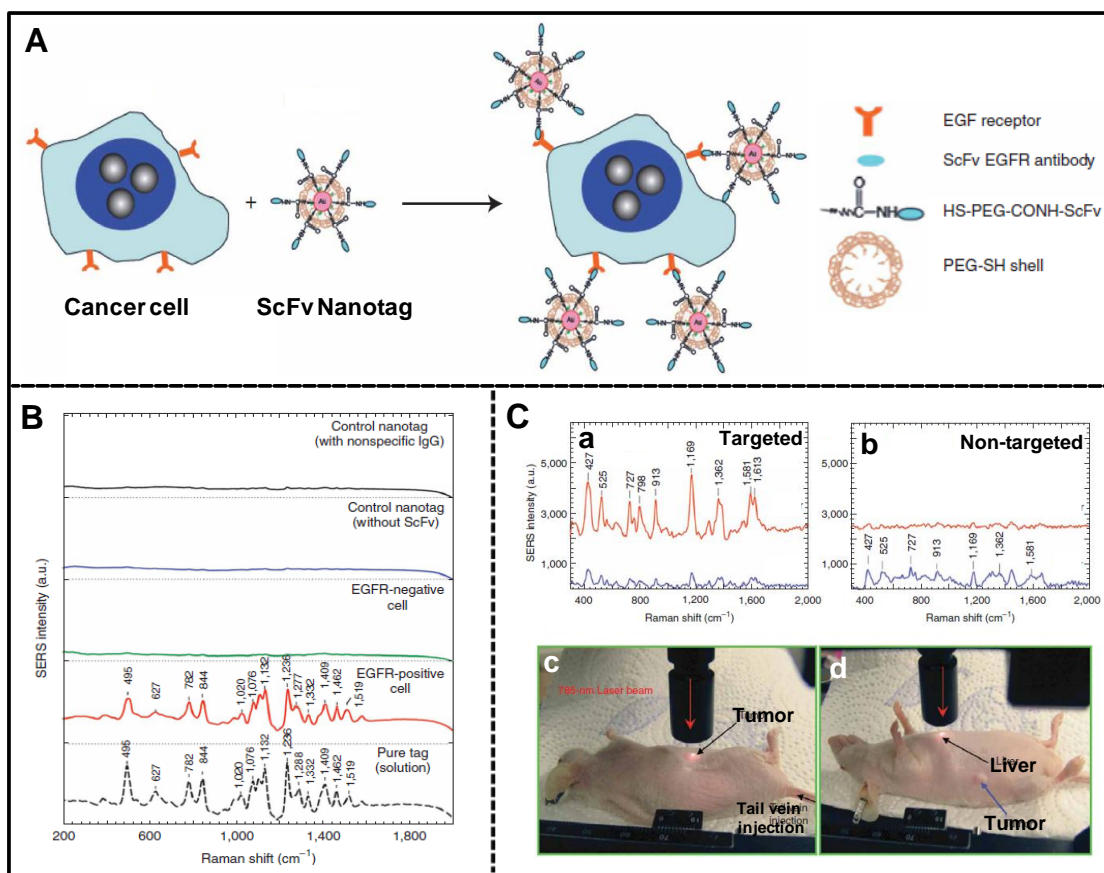
Figure 1.13. *(A) Schematic representation of cancer cell targeting and spectroscopic detection by using antibody-conjugated SERS nanoparticles. (B) SERS spectra were obtained from EGFR-positive cancer cells (Tu686) and EGFR negative cancer cells (human non-small cell lung carcinoma NCI-H520), together with control data and the standard tag spectrum. (C) SERS spectra obtained from the tumor and the liver locations by using targeted (a) and non-targeted (b) nanoparticles. Photographs showing a laser beam focusing on the (c) tumor site or on the (d) anatomical location of liver. The Raman reporter molecule is malachite green [Qian 2008].*

1.10. Objectives of the present work

The objective of the thesis is to design plasmonic assemblies for Surface Enhanced Raman Spectroscopy (SERS) and investigate the optical properties of single nanoparticle assemblies. A comparative investigation on the SERS efficiency of Au nanoparticles and Au nanorods is presented in the second chapter. The Raman spectroscopic investigations of various analyte molecules, when bound on the surface of isolated Au nanorods having different aspect ratios were also probed. The mode of analyte-substrate interactions were investigated in detail, in the second part of the chapter, using Isothermal Titration Calorimetry (ITC). Raman signal enhancement of analyte molecules when bound at the (i) edges of Au nanorods, using monothiol derivatives and (ii) junctions of two Au nanorods using dithiol derivatives is discussed in the third chapter. The details of the new methodology developed for the organization of Au nanorods in lateral fashion and Au nanorod quartets, through the combination of lateral and longitudinal assembly, are presented in the fourth chapter. The use of Au nanorod quartets as substrates for enhancing the Raman spectroscopic signal is also discussed. The optical properties of various single nanorod assemblies are discussed in chapter 5. The scattering spectra of nanorod assemblies were investigated by combining the dark-field spectroscopy with high resolution scanning electron microscopy. The energy levels involved in the excitation of various modes are deduced with the help of polarization dependent studies and from the plasmon hybridization model.

Gold Nanorods as Substrates for Surface Enhanced Raman Spectroscopy
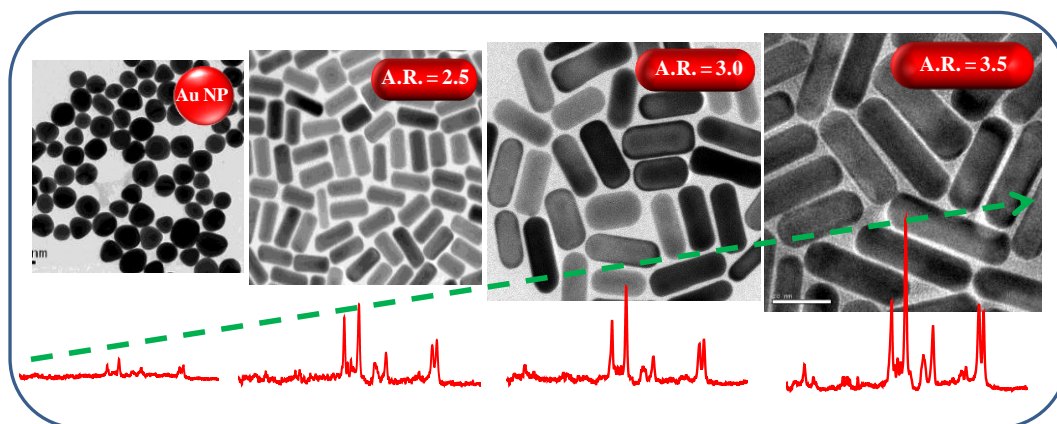
2.1. Abstract

The main objective of the present investigation is to probe the Raman signal intensity of various analyte molecules when bound onto isolated Au nanorods, having various aspect ratios. Analyte molecules can bind to the surface of Au nanorods through various interactions (for example, electrostatic, hydrogen bonding and covalent) and these aspects were investigated by following Isothermal Titration Calorimetric (ITC) studies. The enhancement of Raman signal of analyte molecules bound onto spherical Au nanoparticles and Au nanorods were compared. Au nanorods were found to be a more efficient substrate for Surface Enhanced Raman Spectroscopy (SERS), compared to Au nanoparticles and the enhancement factor was found to increase with the aspect ratio of nanorods. The analyte molecules can preferentially bind onto the {111} facets at the edges of Au nanorods and the high electric field concentrated at the edges are primarily responsible for the enhancement of Raman signal intensity through electromagnetic enhancement mechanism.

2.2. Introduction

Raman spectroscopy, discovered in 1928 by Sir C. V. Raman [Raman 1928] did not gain much attention in early years, compared to other spectroscopic techniques, mainly due to the low scattering cross section. The Raman scattering cross section is 10^{13}-10^{16} times lower when compared to other spectroscopic techniques such as infrared and fluorescence [Tian 2004]. This inherent problem associated with Raman scattering was resolved with the advent of lasers and various surface enhanced techniques. Among various surface enhanced techniques, surface enhanced Raman spectroscopy (SERS), which uses metal surfaces or metal nanoparticles as substrates, has gained much attention [Moskovits 1985 and Kneipp 1999]. In recent years, efforts have been focused on fabricating efficient SERS substrates using a variety of nanostructured materials [Campion 1998]. It is theoretically proposed and experimentally demonstrated that the size, shape and composition of the material plays a dominant role in the enhancement of signals [Margueritat 2011 and Zhu 2011]. It is also observed that the way in which nanomaterials organize can influence the enhancement of signals of analyte molecules [Camden 2008]. In this Chapter, efforts are directed towards optimizing the size and shape of Au nanoparticles as substrates in SERS.

The chemical and physical properties of materials at the nanoscale depend on the size and shape of the material which can be well explained by quantum confinement effect [Kelly 2003]. The shape of the nanoparticle plays a crucial role in the distribution of the surface electron density and hence the electric field around the nanoparticles [Hao 2004]. The way in which the surface electrons are distributed has a dramatic influence on the oscillation of electrons in the presence of electromagnetic field which contribute to different properties such as absorption and scattering. For example, spherical Au nanoparticles (Figure 2.1A)

having smaller size possess identical oscillation of electrons along the three directions resulting in only one band in the extinction spectrum (Figures 2.1B and 2.1D). On the other hand, Au nanorods (Figure 2.1C) split the dipolar resonance into two surface plasmon bands wherein the induced dipole oscillates along the transverse and longitudinal axes (Figures 2.1B and 2.1E) [Link 2005]. The position of longitudinal surface plasmon band shifts to longer wavelengths with increase in aspect ratio, while the transverse surface plasmon band remains more or less unaffected. These results indicate that the dimensionality plays a crucial role in determining the plasmon resonance of metal nanoparticles [Templeton 2000].
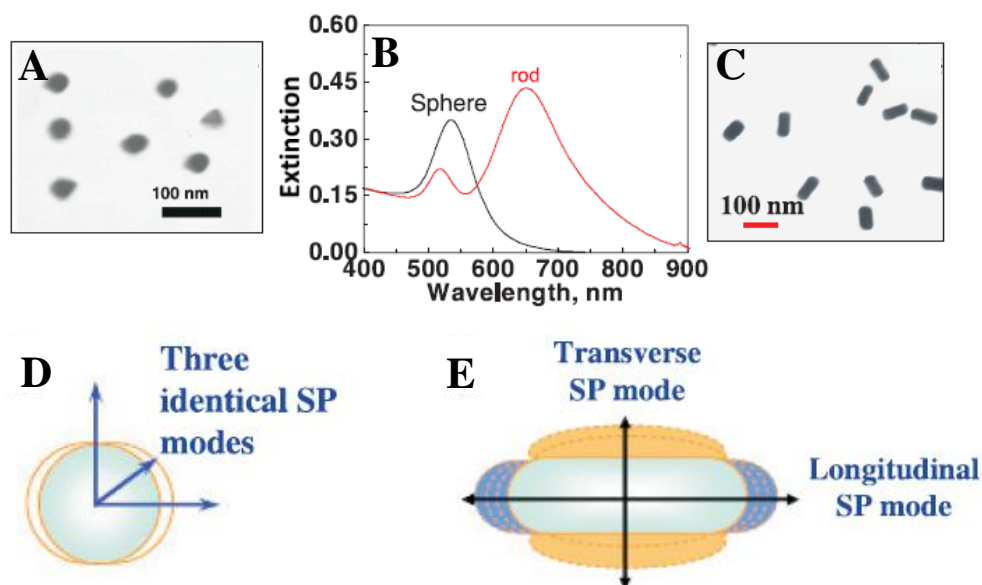
Figure 2.1. *(A) TEM images of gold nanoparticles; (B) extinction spectrum of Au nanoparticles and nanorods; (C) TEM images of gold nanorods; (D) identical surface plasmon oscillation of spherical gold nanoparticles and (E) the surface plasmon oscillation of gold nanorods in the transverse and longitudinal axes [Thomas 2009].*

2.2.1. High Edge Reactivity of Au Nanorods

It has been proved from the electron diffraction analysis and HRTEM studies that the end facets of Au nanorods are dominated by {111} planes and the lateral facets by {100} and

{110} planes [Wang 1999, Wang 2000, Gao 2003, Johnson 2002 and Murphy 2005]. The surface of nanorods is protected using suitable capping agents such as surfactants and polymers [Nikoobakht 2001]. A surfactant-directed nanorod growth mechanism proposed by Murphy and coworkers involves the differential blocking of {100} or {110} crystallographic facets of Au nanorod by CTAB, promoting the anisotropic growth along the {111} edges (Figure 2.2A) [Gao 2003]. The specific interaction of thiols to the {111} planes of Au nanorods facilitates their 1D organization in an end-to-end fashion [Thomas 2004, Chang 2005, Sudeep 2005 and Joseph 2006].

Several theories have been proposed for the growth of nanomaterials in one dimension. One of the well accepted mechanisms for Au nanorod growth is based on the presence of high electric field at the edges. According to the mechanism proposed by Mulvaney and coworkers, the reduction of Au (III) ions to Au (I) ions occurs in presence of a suitable reducing agent, which further complexes with CTAB micelle [Pérez-Juste 2004]. Electric potential around the spherical seed remains uniform. The change in morphology leads to the concentration of field at points of higher curvature. With the beginning of nanorod formation, preferential reduction at any site will increase the curvature at that point, leading to the faster deposition of ions. The slow collision frequency and the enhanced electric field at the tips allow the reduction of Au (I) almost exclusively at the termini leading to their growth in one dimension (Figure 2.2B).
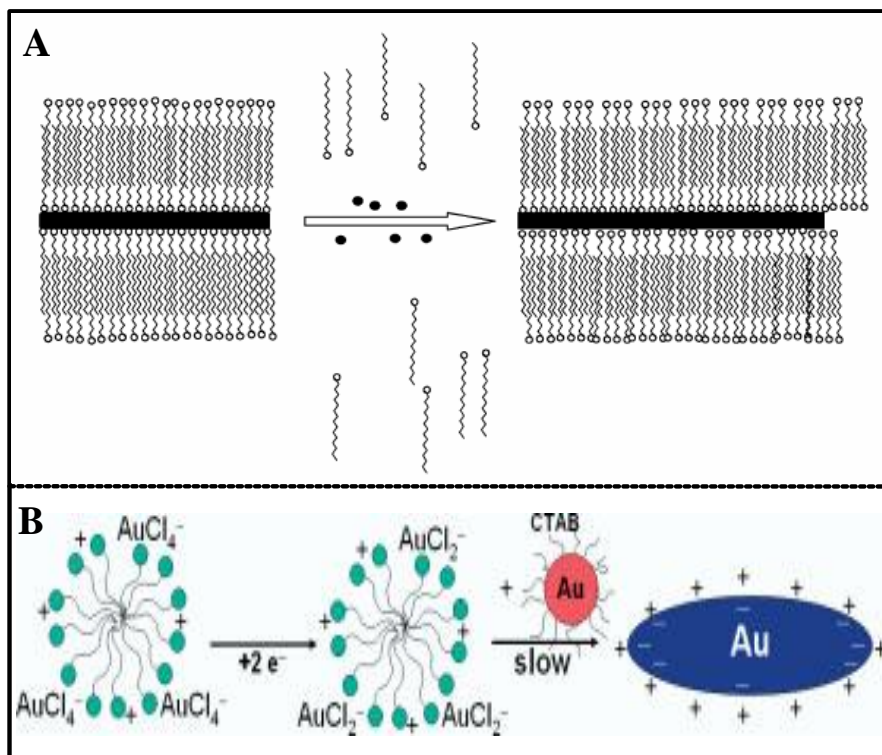
Figure 2.2. *(A) Cartoon illustrating the formation of the bilayer of CTAB molecules on the surface of Au nanorod (black rectangle) that may assist nanorod formation as more gold ions (black dots) are introduced [Gao 2003]. (B) Mechanism for gold nanorod formation proposed by Mulvaney and coworkers. AuCl₄⁻ ions are bound to cationic CTAB micelles, displacing Br⁻ ions [Pérez-Juste 2004].*

Due to these unique properties, Au nanorods are considered as ideal substrates for SERS. However, most of the studies reported in the literature on the Au based systems are related to spherical nanoparticles (Cao 2002 and Yang 2009). There are only a few reports related to the SERS using Au nanorods [Chen 2010, Doherty 2010 and Pedano 2010]. Murphy and coworkers investigated the effect of excitation wavelength on the enhancement using silver and gold nanorods having aspect ratios varying from 1 to 16 [Orendorff 2006]. Different degrees of overlap between the nanorod longitudinal plasmon band and excitation source was obtained by varying the aspect ratio of nanorods. A factor of $10\text{-}10^2$ greater

enhancements for substrates having plasmon band overlap with the excitation source was observed in comparison with that for substrates whose plasmon bands do not possess any overlap. In general, silver nanorods having aspect ratio 10 and gold nanorods having aspect ratio 1.7, with their longitudinal band at excitation wavelength, give ten to hundred times greater SERS enhancements than nanorods of other aspect ratios having their surface plasmon bands away from wavelength of excitation (Figure 2.3). Larger SERS enhancements observed in the case of substrates having plasmon resonance with the excitation source are attributed to greater contributions from the electromagnetic enhancement mechanism.
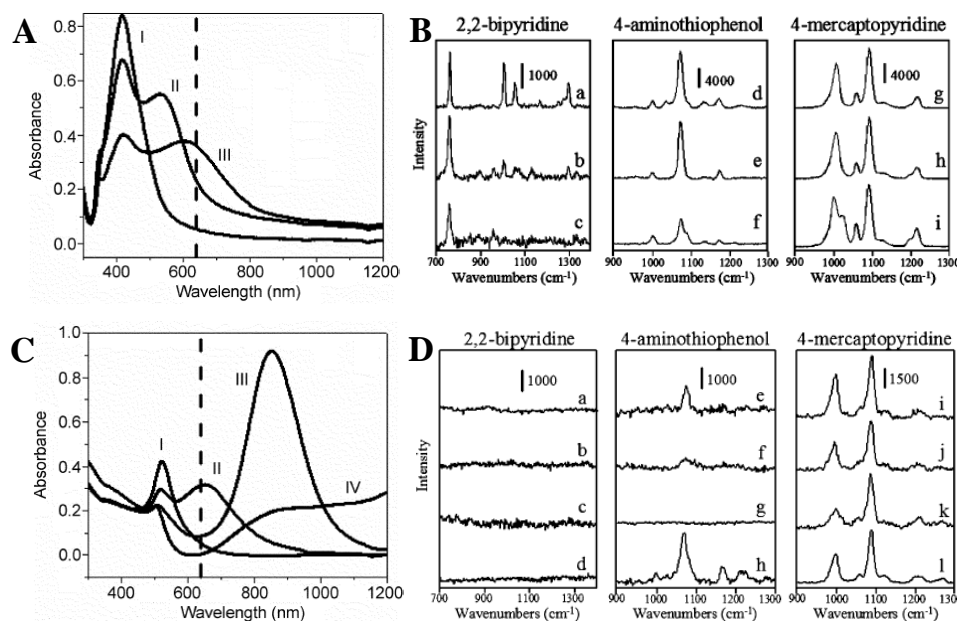
Figure 2.3. Absorption spectra of (A) silver nanorods with aspect ratios 1(trace I), 3.5 (trace II), and 10 (trace III) and (C) gold nanorods with aspect ratios 1 (trace I), 1.7 (trace II), 4.5 (trace III), and 16 (trace IV). Surface enhanced Raman spectra of 2,2'-bipyridine, 4-aminothiophenol and 4-mercaptopyridine at 10^{-6} M using (B) silver nanorods with aspect ratios 10 (a, d and g), 3.5 (b, e and h), and 1 (c, f and i) and (D) using gold nanorods with aspect ratios 1.7 (a, e and i), 4.5 (b, f and j), 16 (c, g, and k) and 1 (d, h and l) [Orendorff 2006].

2.2.2. Stability of Au Nanorods

Detailed study on the stability of Au nanorods in varying solvent compositions was obtained from zeta potential (ζ) studies. It has been observed that CTAB-stabilized Au nanorods are stable in water and in CH_3CN/H_2O mixtures containing more than 70% acetonitrile [Pramod 2008]. It is found that Au nanorods readily precipitate in a mixture (1:4) of CH_3CN and H_2O, irrespective of the aspect ratio. In water, Au nanorods possess positive ζ values which decreases with increase in CH_3CN content and approaches zero in a mixture (1:4) of CH_3CN and H_2O. With further increase in acetonitrile content, Au nanorods attain a negative ζ value and its magnitude increases with increase in aspect ratio. Thus, the stability of Au nanorods in water and acetonitrile-rich solvents may be attributed to the large positive and negative ζ values. As the magnitude of the zeta potential increases, the nanoparticle experiences greater interparticle repulsion and remains isolated in solution; the higher the magnitude of zeta potential, the greater the stability of nanoparticle system. Au Nanorods with larger aspect ratios are found to be more stable in water than those having short aspect ratios due to an increase in positive surface charge. Since the nanorods are stable in water and acetonitrile-rich solvents, all the studies are carried out with nanorods in water and in a mixture (1:4) of water and acetonitrile.

2.2.3. Isothermal Titration Calorimetry

Currently there is a large interest in fabrication of hybrid organic-inorganic nanostructured systems for various applications in material science and biomedical field. Understanding the nature of interactions between organic molecules and metal nanoparticles is an important step in this direction. Isothermal titration calorimetry (ITC) is a unique technique that can directly measure the binding energetics of different chemical and

biological processes, including metal-ion binding, host-guest interactions, protein-ligand binding, DNA-protein binding, protein-lipid binding and antigen-antibody binding [Burrows 1994, Lovatt 1996, Zhang 1998 and Baier 2011]. This technique can precisely determine the Gibbs energy, enthalpy, entropy and heat capacity changes associated with binding [Matulis 2000 and Lang 2010]. The instrument operates based on the principle of dynamic power compensation, i.e., it measures the amount of power required to maintain a constant temperature difference between the sample and the reference cell [Campoy 2004]. A small power is continuously applied to the sample cell by the feedback system, to determine the baseline level. Each injection of the syringe solution triggers the binding reaction; depending on the binding affinity and the concentration of reactants in the cell, a certain amount of complex is formed. The formation of complex is accompanied either by the release of heat (exothermic reaction) or by the absorption of heat (endothermic reaction) which causes a difference in temperature between the sample and the reference cell. Depending on the nature of reaction, the feedback system either lowers or raises the thermal power applied in order to compensate the temperature difference. After each injection, the system reaches equilibrium and the temperature balance is restored. Therefore, the recorded signal shows a typical deflection pattern in the form of a peak (Figure 2.4). The amount of heat associated with the injection is obtained by integrating the area under the peak, assuming the baseline as reference. As the reactant in the cell becomes saturated, the signal due to heat change diminishes and only the background heat due to ligand dilution or liquid friction is observed. The technique has been extensively used in recent years to investigate the binding energetics in various chemical and biological processes [Nair 2009 and Krishnan 2011].
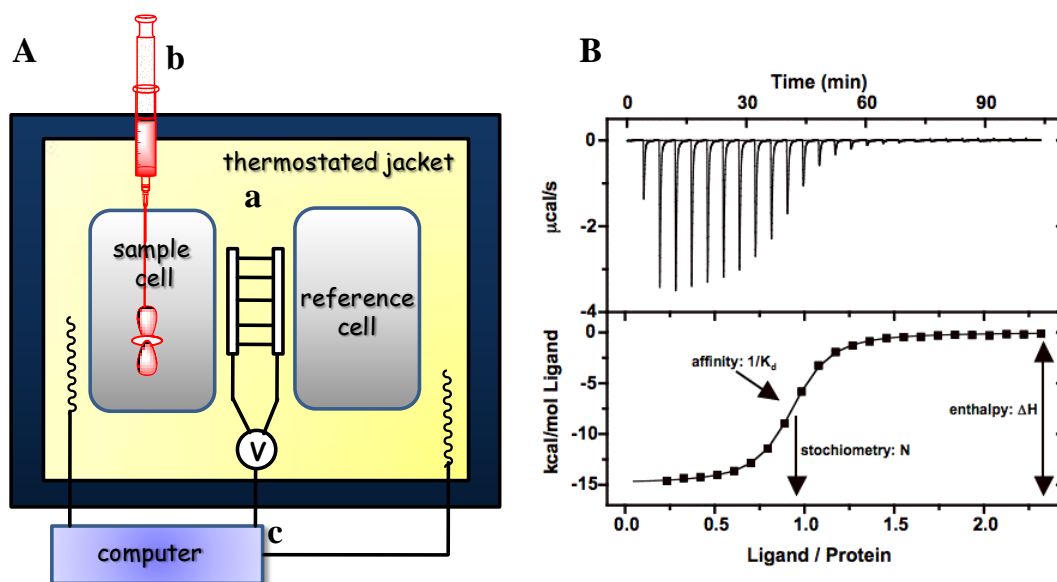
Figure 2.4. *(A) Schematic illustration of the ITC instrument, showing (i) the two cells (sample and reference) surrounded by the thermostated jacket, (ii) the injection syringe that also works as stirring device and (iii) the computer-controlled thermostatic and feedback systems. (B) Illustration of a typical ITC experiment. The top panel shows the sequence of peaks, corresponding to individual injection of solution and the integrated heat plot in the bottom panel. The area under each peak was calculated and normalized per mol of ligand in individual injection and plotted against the molar ratio [Campoy 2004].*

ITC has been used by different groups to probe strong interactions of ligands with gold nanoparticles (AuNP) [Cedervall 2007, De 2007, Klein 2007, Varghese 2008 and You 2008]. Sastry and coworkers have showed that ITC can be used to directly observe the energetics of interaction of DNA bases as well as the corresponding PNA base monomers with Au nanoparticles [Gourishankar 2004]. The strength of interaction of the nucleobases and PNA analogues with Au nanoparticles were evaluated on the basis of the exothermicity during the initial stages of interaction when the surface of nanoparticle is bare. The exothermicity of the interaction of the PNA base monomers during titration with Au nanoparticles (Figure 2.5 E-G) is much higher than for the corresponding DNA bases

(Figure 2.5 A-D) and a concentration 10 times smaller than that of the DNA bases could saturate the gold nanoparticle surface. The strength of interaction of the nucleobases/PNA analogues decreases in the order cytosine (C) > guanine (G) > adenine (A) > thymine (T). It has been shown that amine groups have strong binding affinity with aqueous Au nanoparticles and the weak interaction of thymine with the nanoparticles is due to the absence of an exocyclic amino group in this nucleobase (Figure 2.5 D and 2.5H).
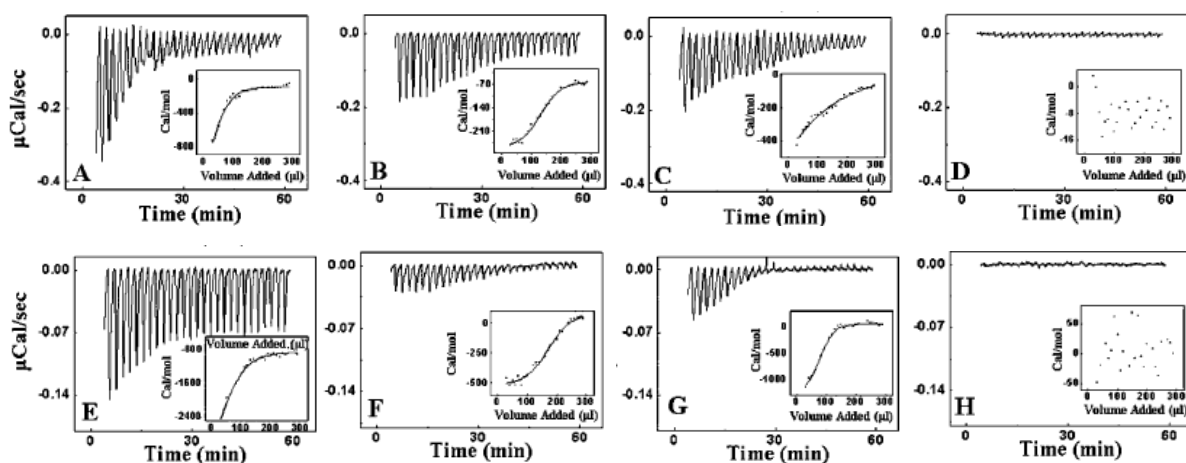
Figure 2.5. AuNP-DNA base interactions and AuNP-PNA monomer interaction investigated using ITC. Curves A-D correspond to AuNP interactions with C, A, G, and T, respectively. Curves E-H corresponds to AuNP interaction with PNA-C, PNA-A, PNA-G, and PNA-T, respectively. ITC experiments were carried out by injection of 300 µL of 2.5 mM aqueous solution of DNA bases and 0.25 mM aqueous solution of PNA monomers in equal steps of 10 µL into 1.47 mL of dialyzed borohydride-reduced gold hydrosol (Gourishankar 2004).

2.3. Results and Discussion

2.3.1. Au Nanoparticles and Au Nanorods as SERS Substrates

In the present study, a comparison of the SERS efficiency of spherical Au nanoparticles and 1D Au nanorods was carried out using 4-mercaptopyridine as the analyte. CTAB capped Au nanoparticles and nanorods were synthesized by following a

photochemical method. Au nanoparticles possess an average diameter of 30 nm with its plasmon band at 530 nm (Figure 2.7 A) and Au nanorods having an aspect ratio of 2.7 with the longitudinal plasmon band at 670 nm (Figure 2.7 D) were selected. The zeta potential (ζ) values of CTAB capped Au nanoparticles as well as Au nanorods are influenced by solvent polarity. In aqueous medium, both the systems possess a high positive ζ value (~ 30 mV) which shifts to a negative ζ value on increasing the acetonitrile content (for example, -29.7 mV for Au nanoparticles and -39.9 mV for Au nanorods). A plot of variation in zeta potential of spherical Au nanoparticles and 1D Au nanorods on varying the solvent composition is shown in Figure 2.6. Both nanoparticles and nanorods are found to be stable in water and solvent systems containing acetonitrile (> 70%) due to high positive and negative zeta potential values, respectively. In the intermediate solvent compositions, the zeta potential values approaches zero and the particles undergo aggregation and precipitates out of the solution. Thus, in our present chapter we have focused our studies on Au nanoparticles and nanorods in either water or in a mixture (1:4) of water and acetonitrile wherein the nanomaterials are stable for hours.
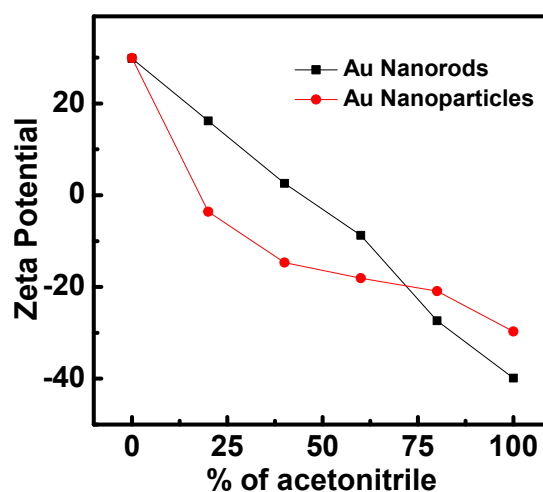
Figure 2.6. *Zeta potential changes of Au nanorods (black trace) and spherical Au nanoparticles (red trace) on addition of varying amount of CH₃CN to water.*

The intensity of Raman peaks of 4-mercaptopyridine on adding varying concentrations (0.0-0.5 µM), to an aqueous solution of Au nanoparticles and nanorods were investigated. The nanoparticle/nanorod solutions were kept for 10 min after the addition of 4-mercaptopyridine and the Raman as well as absorption spectra were recorded. No appreciable changes were observed in the absorption spectral features of either Au nanoparticles or Au nanorods (Figures 2.7A and 2.7D). These results clearly indicate that the Au nanoparticles/nanorods do not undergo any aggregation during the course of experiment, which was further confirmed by following TEM studies (Figures 2.7C and 2.7F). The nanoparticle/nanorod solutions were drop-casted onto a TEM grid at the end of the addition and images were recorded. Au nanoparticles/nanorods remain isolated ruling out the possibility of any aggregation. Interestingly, SERS spectrum showed peaks corresponding to various vibrational modes of 4-mercaptopyridine, the intensity of the peaks were found to be dependent on the size and shape of the nanomaterials (Figures 2.7B and 2.7E). One of the factors which may influence the enhancement factor (EF) is the orientation of molecules on the surface; however, it is difficult to quantify this. Hence, variations due to orientation of molecules are not accounted during the estimation of enhancement factor [Ru 2007]. The EF on addition of 4-mercaptopyridine was estimated using the Equation (1)

$$EF = (I_{SERS} \times N_{bulk}) / (I_{bulk} \times N_{ads}) \tag{1}$$

where I_{bulk} and I_{SERS} are the intensities of the ring deformation band of 4-mercaptopyridine in the absence and in the presence of nanoparticles/nanorods. Raman signals were observed only at a very high concentration of 4-mercaptopyridine (10 µM). The EF was calculated to be 1.1×10^4 for spherical Au nanoparticles and 3.0×10^4 for Au nanorods. From these studies it is concluded that Au nanorods are better SERS substrates compared to spherical Au nanoparticles.
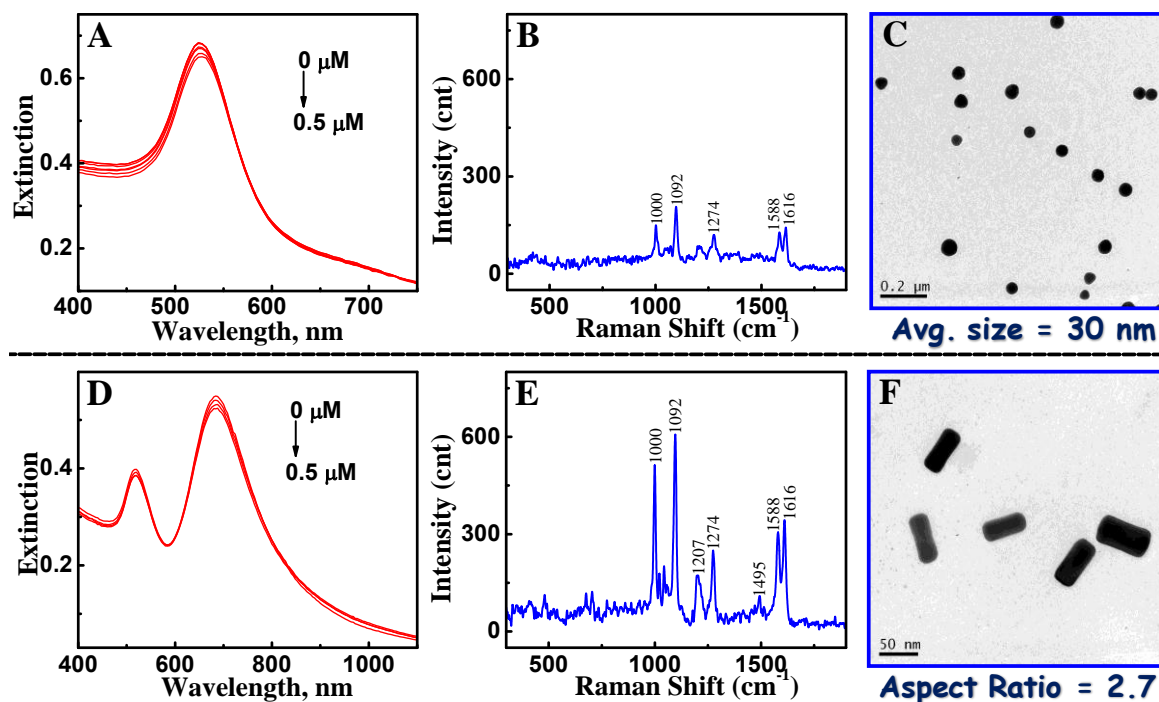
Figure 2.7. *Extinction spectral changes of (A) spherical Au nanoparticles and (D) Au nanorods on addition of varying amounts of 4-mercaptopyridine in water. The Raman spectra of 4-mercaptopyridine (0.5 µM) attached onto (B) spherical Au nanoparticles and (E) Au nanorods. (C,F) The corresponding TEM images are also provided.*

The larger enhancement in Raman signal intensities observed in the case of nanorods can be explained both experimentally and theoretically based on edge effect. The electric field around a spherical Au nanoparticle is uniformly distributed whereas, for nanorods the field gets concentrated at the edges. It is reported that the edges of Au nanorods are dominated by {111} facets and the thiol derivatives preferentially bind onto these {111} planes of the Au nanorods [Gao 2003, Wang 1999 and Johnson 2002]. This specific interaction leads to the localization of analyte molecules at the edges. Thus a thiol functionalized molecule when added to a solution of Au nanorods, results in the preferential binding of molecules at the nanorod edges giving rise to enhanced signal intensities through both chemical as well as electromagnetic enhancement mechanisms. It is assumed that both

mechanisms contribute towards enhancement in signal intensities, with the electromagnetic enhancement being the major contributor. However, it is difficult to separate the contributions of each component. The higher enhancement observed in the case of 1D nanorods may be attributed to the higher contribution from the electromagnetic enhancement arising from the edge effect in anisotropic materials (localization of electric field at the edges).

2.3.2. Edge Effect in Anisotropic Materials

The divergence of the electric field and charge accumulation at the edges and corners of a conductor at a fixed potential is termed as "edge effect". It is well known that the surface charge density as well as the external electric field is high at sharp points and edges. The edge effect of metallic rods has been widely used for the accumulation of charges and utilized for protecting buildings from damage due to lightening. The lightning rod has a sharp end and the lightning bolts pass through a conducting path in air to the rod, protecting the nearby structures from damage. Enhancement in the electric field intensity at the edges of nanomaterials has been successfully demonstrated by various theoretical methods. The enhancement in electric field intensity, calculated using finite difference time domain (FDTD) for nanomaterials of various shapes are shown in Figure 2.8 [Kou 2007]. From these images, it is clear that in the case of anisotropic nanomaterials the electric fields are more concentrated on the edges and corners. The enhancement of field intensity of nanorods is found to be about one sixth of that of the bipyramid, indicating that the shape of the nanoparticles play a dominant role. In a recent report, Swathy and coworkers have theoretically demonstrated that for longitudinal polarization at the resonance and off-resonance conditions, magnitudes of the electric field enhancements for nanorods is an order

of magnitude higher compared to spherical nanoparticles [Thomas 2012]. This is due to the fact that the charges tend to accumulate at the rounded corners (longitudinal edges) of these anisotropic structures, leading to high enhancements of the field which are usually referred to as the "lightning rod effect" or the "edge effect". The higher charge density at the edges of Au nanorods has been experimentally demonstrated by our group through the electrostatic interaction of oppositely charged Au nanoparticles [Pramod 2007]. Thus, when a molecule is localized at the edges, the higher electric field prevailing at the edges of nanorods contributes towards enhancement in Raman signals through elctromagnetic enhancement mechanism.
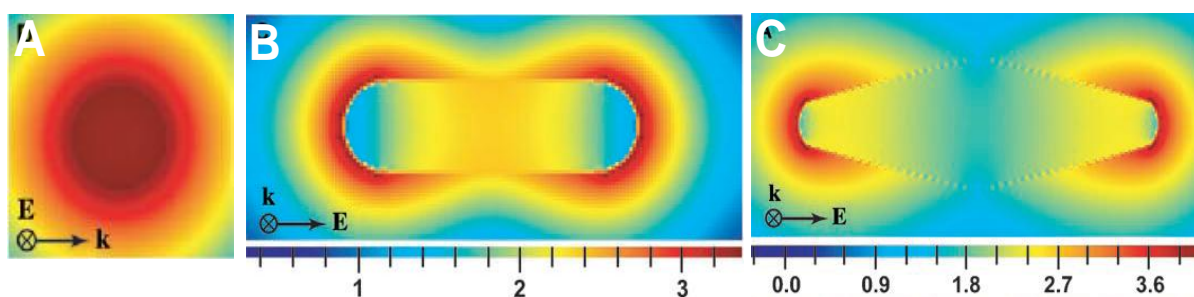
Figure 2.8. Electric field intensity enhancement contours along the longitudinal direction for a (A) nanosphere, (B) nanorod and (C) nanobipyramid obtained from FDTD calculation [Kou 2007].

2.3.3. Dependence of Aspect ratio on Raman Signal Enhancement

Further, we have investigated the variations in Raman signal intensities by varying the aspect ratio of Au nanorods. Au nanorods having aspect ratios 2.7, 3.0 and 3.3 with their longitudinal plasmon bands centered at 660 nm, 700 nm and 730 nm respectively were synthesized by following a photochemical method [Kim 2002]. The analyte molecule was added to the Au nanorod solution in water and was incubated for 10 min. The extinction and SERS spectra were monitored simultaneously. The SERS spectra were monitored by

exciting the solution using 632 nm laser on exposure for 10 sec. The nanorods with their longitudinal plasmon band having no overlap with the excitation wavelength were used, ruling out the contribution from the direct plasmon excitation towards SERS intensity in all the three sets of nanorods. The extiction spectra showed no appreciable changes after the addition of 4-mercaptopyridine, confirming that the nanorods remained isolated without undergoing any aggregation (Figure 2.9A-C). This rule out the contribution of coupled plasmon towards SERS intensity. On addition of 0.3 µM of 4-mercaptopyridine to Au nanorod solution in water, we observed an increase in intensity of the Raman peaks with increasing aspect ratio of the rod (Figure 2.9D-F). For nanorods having aspect ratio of 2.5, peaks of lower intensity were observed, whereas nanorods with aspect ratio 3.5 showed peaks with higher intensity. The enhancement factor values calculated for the nanorods having aspect ratios 2.7, 3.0 and 3.3 were found to be 2.6×10^4, 3.7×10^4 and 7.0×10^4, respectively. It has been experimentally demonstrated by our group that the edges have high electric field and the strength of this field increases with increase in aspect ratio (Pramod 2007). Swathy and coworkers have theoretically demonstrated that, under the longitudinal polarization, the magnitude of the dipolar resonance created in the rods increases with the increase in the aspect ratio of the nanorod [Thomas 2012]. The increased electric field at the edges contributes towards enhancement in SERS signal intensity through electromagnetic mechanism. Thus, the use of anisotropic materials like nanorods can lead to huge enhancements in the electromagnetic field resulting in enhanced spectroscopic signals.
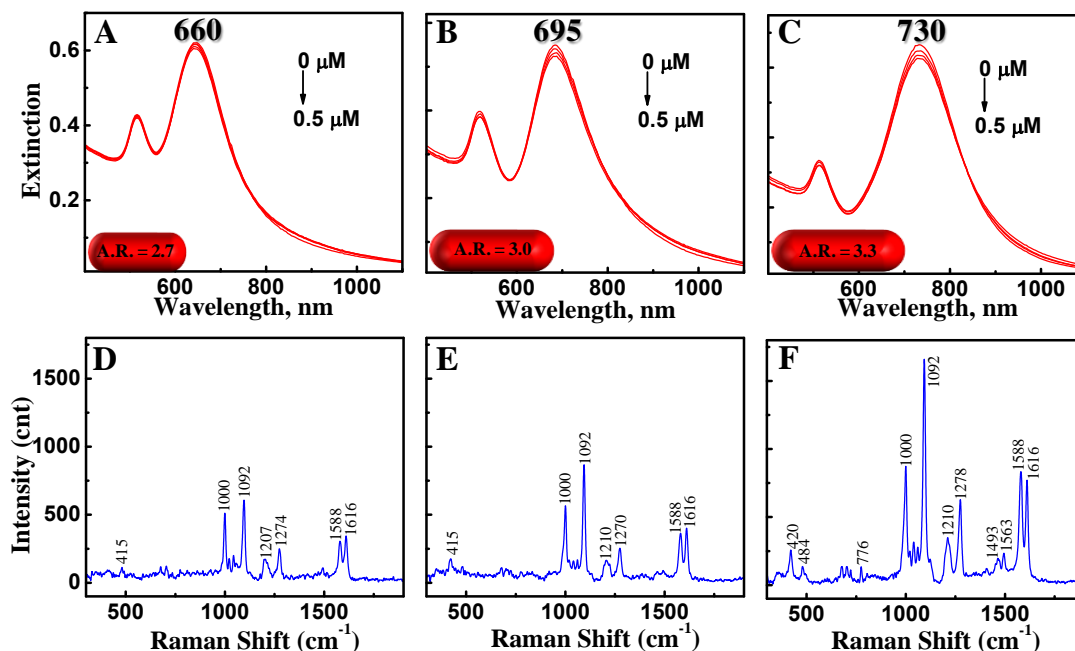
Figure 2.9. *Extiction spectral changes of Au nanorods of aspect ratio (A) 2.7, (B) 3.0 and (C) 3.3 on addition of varying amounts of 4-mercaptopyridine (0.0 – 0.5 μM) in water. (D,E,F) The corresponding SERS spectra obtained on addition of 0.3 μM of 4-mercaptopyridine to the nanorod solution in water.*

2.3.4. Probing the interactions between analytes and SERS substrates

The interaction between analyte molecule and SERS substrates can play a significant role in the enhancement of Raman signals. We have further investigated the strength of interaction between the analyte molecules and Au nanorods by following Isothermal Titration Calorimetry (ITC). Various types of interactions can operate between the analyte molecule and the SERS substrates including covalent bond formation, hydrogen bonding, electrostatic interactions, van der Waals interaction and π stacking. The covalent bond formation between a thiol bearing molecule, namely, 4-mercaptopyridine and Au nanorod surface was investigated using ITC titrations. Electrostatic interactions with the surface of Au nanorods (note: surface charge depends on the solvent composition) was probed using a positively charged molecule, namely, methyl viologen. Au nanorods having an aspect ratio

of 2.5 were synthesized by following photochemical method [Kim 2002] and excess capping agents were removed through centrifugation (experimental section for details). ITC experiments were carried out in two solvent systems: aqueous solution and a mixture of (1:4) of water and acetonitrile. All ITC experiments were carried out at room temperature (25 ± 1°C). Interaction between 4-mercaptopyridine and Au nanorods in aqueous medium was investigated as follows: An aqueous solution (40 µL) of 4-mercaptopyridine (10 µM) was injected in equal steps of 2µL to an aqueous solution of Au nanorods (200 µL; 0.12 nM particle concentration) taken in a cell. Experiments carried out in aqueous medium showed negligible heat change and the results are presented in Figures 2.10A, 2.10C and 2.10E. In contrast, large heat change was observed when the experiments were carried out in a mixture (1:4) of water and acetonitrile (Figures 2.10B, 2.10D and 2.10F). The positive peaks shown in the heat signal curve (Figure 2.10D) indicate that the process is exothermic. The traces presented in Figure 2.10D corresponds to raw calorimetric data obtained during titration and the lower plot represents integrated heat response obtained from the raw data plotted against the volume of the solution added to the reaction vessel containing the aqueous Au nanorods (Figure 2.10F). While investigating the interaction of two species in solution (e.g. protein-substrate reaction), the binding isotherm can be directly plotted against the molar ratio of reactants in solution. However, in the present case, the lack of information on the exact surface area of the nanoparticles (i.e., number of moles of surface gold atoms) restricts us from plotting the binding isotherms against molar ratio involving the analyte and gold nanorod. In the present case, the binding isotherms were plotted against the total volume of the analyte molecule added to the reaction cell (Figures 2.10E and 2.10F). This was used to identify the trends in the binding behavior. From the data presented, it is clear that in

acetonitrile-rich solvents, the reaction is endothermic. From the plot of binding isotherm against the volume of analyte, it is clear that the analyte molecule interacts strongly onto the surface of nanorods. In contrast, under similar conditions in aqueous medium, the analyte-substrate interactions were found to be weak and the heat changes are negligible. This clearly shows that the analyte molecules bind effectively onto the surface of nanorods in acetonitrile-rich solvents; however the interactions are weak in aqueous medium.
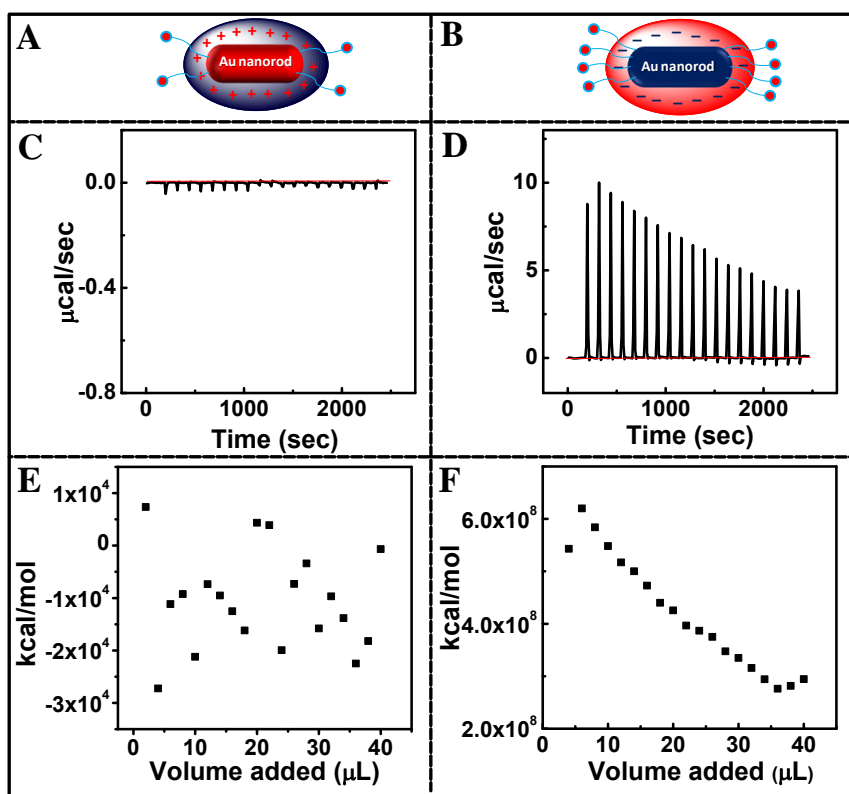
Figure 2.10. *ITC titration illustrating the binding of 4-mercaptopyridine onto gold nanorods with aspect ratio 2.5. Panels A and B show the schematic representation of the interaction of 4-mercaptopyridine with the surface of Au nanorods in (A) water and (B) mixture (1:4) of water and acetonitrile (●═ = 4-mercaptopyridine). Panels C and D shows the raw calorimetric data obtained during injection of 4-mercaptopyridine (10 μM) into the calorimetric cell (200 μL; particle concentration of 0.12 nM) (C) in water and (D) mixture of (1:4) water and CH₃CN. Panels E and F show the integrated data of the curves in panels C and D respectively, plotted as a function of total volume of the 4-mercaptopyridine added to the reaction cell.*

The interactions between the analyte and the Au nanorods were further probed by following SERS studies. Raman spectra were recorded using a confocal Raman spectrometer by exciting at 633 nm (He-Ne laser). The Au nanorod solutions were kept for 10 min after the addition of 4-mercaptopyridine, and the Raman and extinction spectra were recorded. It is reported that the thiol derivatives preferentially bind onto the {111} planes of the Au nanorods resulting in the localization of molecules at the edges [Gao 2003]. CTAB-capped Au nanorods suspended in both water and a mixture (1:4) of water and acetonitrile showed Raman signals corresponding to the solvent molecules; however, no spectroscopic signals corresponding to the CTAB molecules were observed. Au nanorods were found to be stable in both the solvent media even after the addition of higher concentrations of the analyte molecules. It may be noted that Raman signals of 4-mercaptopyridine were not observed in the absence of Au nanorods even in the concentration range of 5 mM of the solution. The Raman spectra obtained on addition of 4-mercaptopyridine (0.5 μM) to an aqueous solution of Au nanorods (particle concentration of 0.12 nM) showed peaks corresponding to the various molecular vibrational modes of 4-mercaptopyridine (Figure 2.11 C); however, the intensity of the peaks were low. Under similar conditions, intense Raman signals corresponding to the molecular vibrations of 4-mercaptopyridine was observed in a mixture containing (1:4) of water and CH_3CN (Figure 2.11 D). The difference in the peak intensities on changing the solvent composition is again a clear indication that the interactions are strong in water-acetonitrile mixture compared to that in aqueous medium. The spectral data and the vibrational assignment of various peaks of 4-mercaptopyridine are listed in Table 2.1. The information on the interaction of analytes on the surface of Au nanorods obtained from ITC measurements and Raman spectral studies are in good agreement.
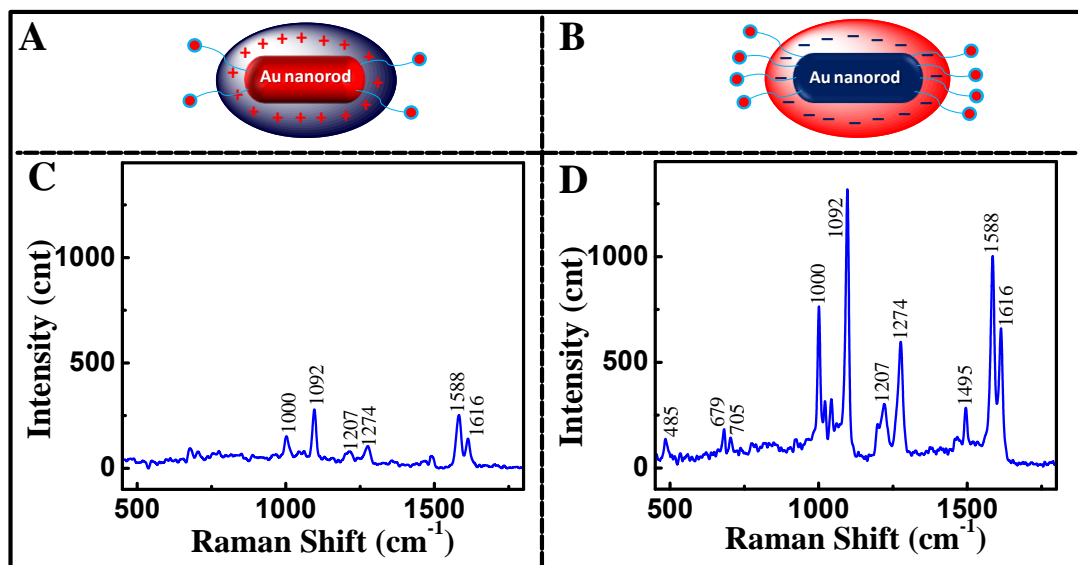
Figure 2.11. *Panels A and B shows the schematic representation of the interaction of 4-mercaptopyridine with the surface of Au nanorods (A) in water and (B) in a mixture (1:4) of water and CH_3CN (━━● = 4-mercaptopyridine). Panels C and D corresponds to the Raman spectra obtained on addition of 4-mercaptopyrine (0.5 µM) to Au nanorods (particle concentration of 0.12 nM) (C) in water and (D) in a mixture (1:4) of water and CH_3CN.*

Table 2.1. Spectral data and vibrational assignment of 4-mercaptopyridine [Chao 2007]

SERS peaks (cm^{-1})	Assignment
485	δ(C-S)/γ(CCC) Ring breathing
679, 705	δ(C-C)/ν(C-S)
1000	ν(ring breathing)
1092,1207, 1274	β(C-H)
1495	ν(C=C/C=N)
1588	ν(C-C)
1616	ν(C-C) Ring stretching

The obvious question is why the interaction of analyte molecules on the surface of Au nanorods is influenced by varying the composition? It is reported that Au nanorods suspended in water are covered by a bilayer of cetyltrimethylammonium bromide (CTAB) molecules, as illustrated in Scheme 2.1. The excess positive charge originates from the polar head groups of CTAB molecules (A in scheme 2.1) and hence the zeta potential (ζ) value increases with aspect ratio in water. Interestingly, with increase in the composition of organic solvent, the bilayer structure collapses to a monolayer, resulting in the loss of CTAB from the surface of the Au nanorods; as a result, a decrease in ζ was observed. In a mixture (1:4) of CH_3CN and water, the negative surface charge on Au nanorods may be neutralized by the positive charge on CTAB molecules and ζ approaches zero (''B'' in Scheme 2.1). Interestingly, a charge reversal from positive ζ to negative ζ was observed with further increase in CH_3CN content. In acetonitrile-rich solvents, the number of CTAB molecules protecting the Au nanorods may be much lower compared to that in a mixture (1:4) of water and CH_3CN and the inherent negative surface on Au nanorods contribute high negative ζ value.
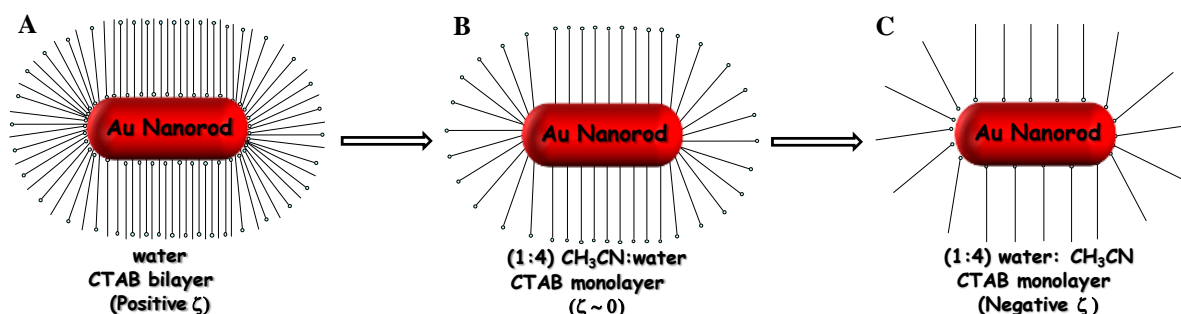
Scheme 2.1. *Schematic representation of charge reversal in Au nanorods as a function of solvent composition.*

The structure presented in the earlier section clearly indicates that in aqueous medium, nanorods are thickly packed by the bilayer of CTAB and the analyte molecules have less interaction with the surface of the nanorods. This results in a weak binding of analyte molecules with Au nanorod surface as evidenced by ITC. On increasing the composition of CH_3CN, the CTAB bilayer breaks into monolayer, exposing the nanorod surface to the solvent environment. In acetonitrile-rich solvents, analyte molecules can easily penetrate through the monolayer of CTAB and interact with the nanorod surface giving rise to intense Raman signals. The variation in the intensity of the ring breathing mode of 4-mercaptopyrine were plotted against varying concentration of the analyte molecule as shown in Figure 2.12. A large increase in Raman signal was observed in acetonitrile-rich solvent compared to that of aqueous medium. The TEM images of Au nanorods in water and a mixture (1:4) of water and acetonitrile after the addition of 1µM of the analyte molecule are presented in Figures 2.12B and 2.12C. These results indicate that Au nanorods are stable and remain isolated; they do not undergo any aggregation.
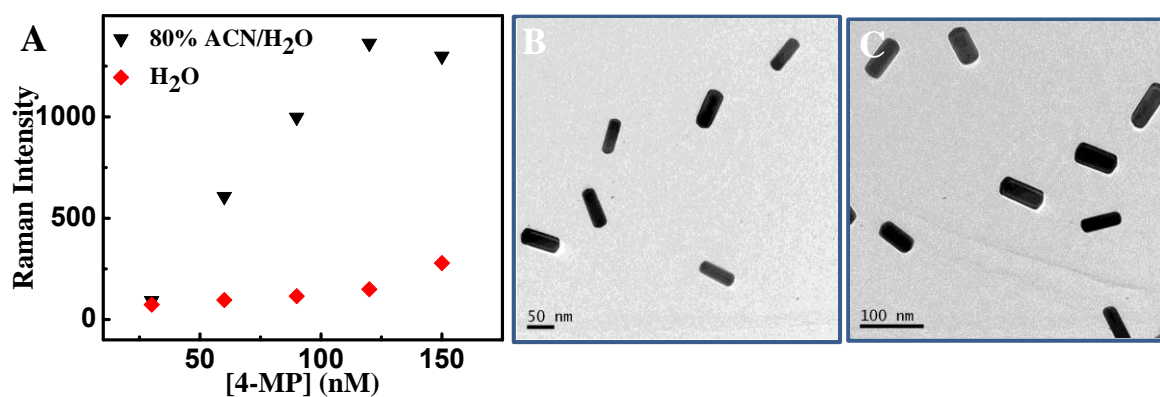
Figure 2.12. (A) Variation in Raman signal intensity of the ring breathing mode of 4-mercaptopyridine on addition of varying concentrations of 4-mercaptopyridine to Au nanorods (particle concentration of 0.12 nM) in water as well as in a mixture (1:4) of water and CH_3CN. TEM images of Au nanorods (B) in water and (C) in a mixture (1:4) of water and CH_3CN after the addition of 4-mercaptopyridine.

Further, the electrostatic interaction between the positively charged molecule, namely, methyl viologen and Au nanorods was probed by following ITC and Raman spectra. The ITC data obtained on addition of methyl viologen in aqueous medium and in a mixture (1:4) of water and CH_3CN are presented in Figure 2.13. In aqueous medium, experiments are carried out as follows: an aqueous solution of methyl viologen (10 µM) was added in 2 µL quantities (20 additions) to Au nanorods (particle concentration of 0.12 nM) in water kept in the cell. The heat changes after each addition was monitored. Experiments carried out in aqueous medium showed negligible heat change, whereas, a large heat change was observed on addition of the methyl viologen to a solution of Au nanorods in a mixture (1:4) of water and CH_3CN (Figure 2.13). The spectrum presented in Figures 2.13C and 2.13D show the raw calorimetric data obtained during analyte-substrate titration. As in the earlier case with 4-mercaptopyridine as analyte, the lack of information on the exact surface area of the nanoparticle restricts us from plotting the binding isotherms against molar ratio involving the analyte and gold nanorods. Integrated heat responses obtained from the raw data are plotted against the volume of the solution added to the reaction vessel containing gold nanorods. These results are presented Figures 2.13E and 2.13F. The positive peaks represent endothermic process (Figure 2.13 D) indicating that heat is absorbed after each injection of the methyl viologen into the gold nanorod solution as a function of time. The heat changes from the ITC clearly indicate that, in acetonitrile-rich solvents, nanorods possess a negative surface charge. The positively charged analyte molecule strongly interacts with the surface of rods. On the other hand, under similar conditions, in aqueous medium where the nanorods possess a positive zeta potential, the analyte-substrate interactions were found to be negligible.
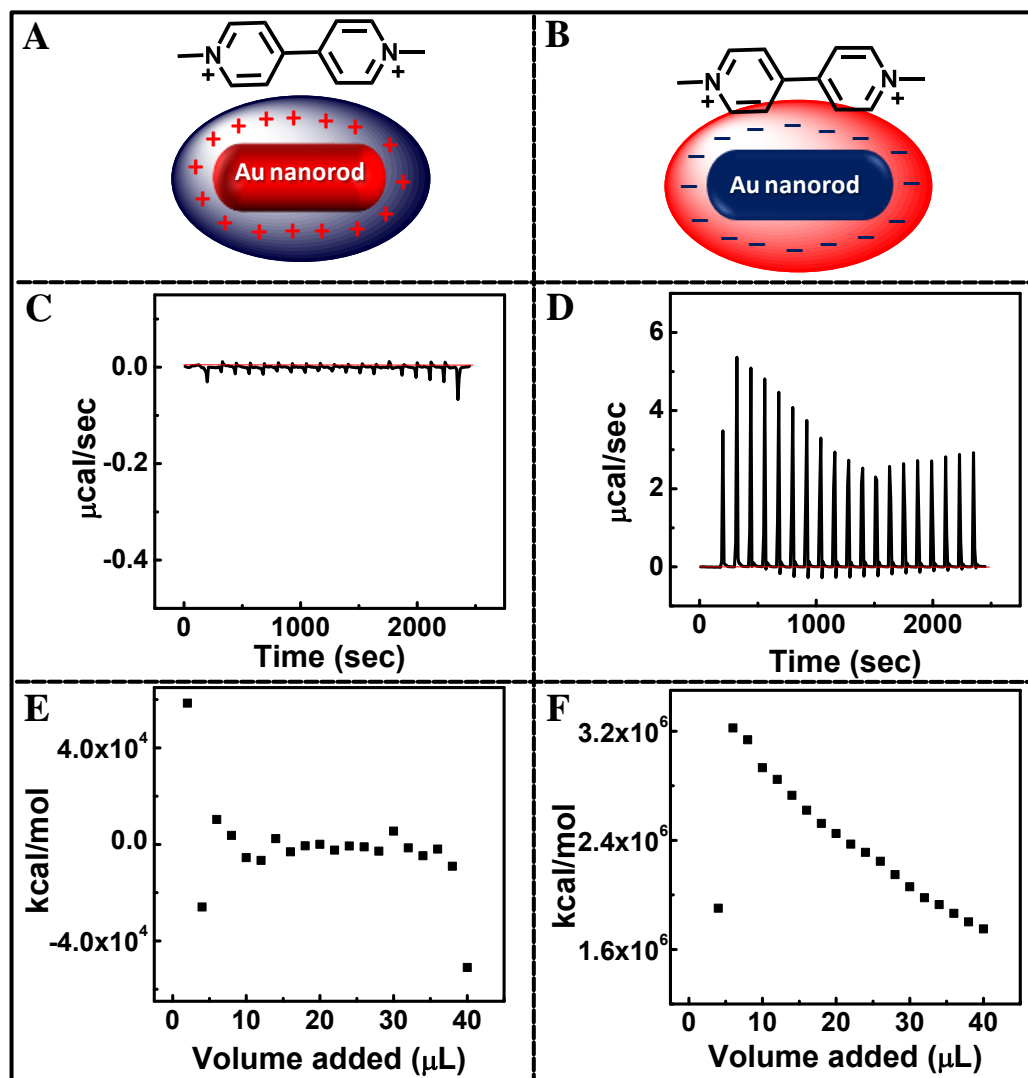
Figure 2.13. *Interaction of methyl viologen with gold nanorods followed by ITC. Panels A and B shows the schematic representation of the interaction of methyl viologen with the surface of Au nanorods (A) in water and (B) in a mixture (1:4) of water and CH_3CN. Panels C and D show the raw calorimetric data obtained during injection of methyl viologen (10 μ M) into the calorimetric cell containing gold nanorods (200 μL; particle concentration of 0.12 nM (C) in water and (D) a mixture (1:4) of water and CH_3CN. Panels E and F shows the integrated data of the curves in panels C and D respectively plotted as a function of total volume of the 4-mercaptopyridine solution added to the reaction cell.*

The electrostatic interactions of analyte molecules with Au nanorods in water and a mixture (1:4) of water and CH_3CN were probed by following Raman spectra. The Raman spectra obtained on addition of methyl viologen to Au nanorod solution are presented in Figure 2.14. On addition of methyl viologen (1 µM) to Au nanorod (particle concentration of 0.12 nM) in water showed Raman peaks of low intensity corresponding to the molecular vibrations of methyl viologen. Under similar conditions, intense peaks were observed when solvent system was varied to a mixture (1:4) of water and CH_3CN. The variation in the peak intensities on changing the solvent composition clearly indicate that the positively charged analyte molecules interact more effectively with the surface of nanorods in a mixture (1:4) of water and CH_3CN compared to that of aqueous medium.
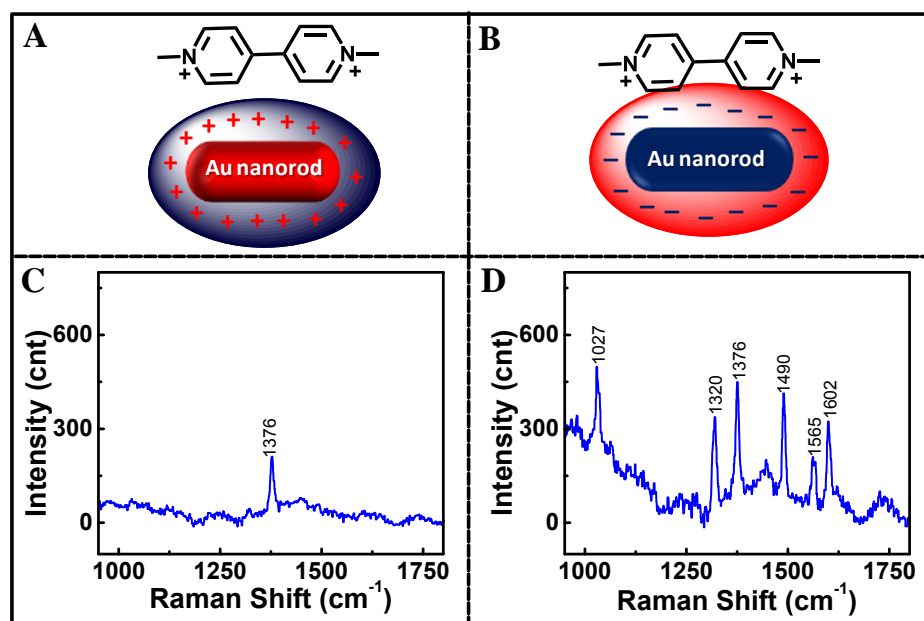
Figure 2.14. Panels A and B shows the schematic representation of the interaction of methyl viologen on to the surface of Au nanorods (A) in water and (B)in a mixture (1:4) of water and CH₃CN. Panels C and D correspond to the SERS spectra obtained on addition of methyl viologen (1 µM) to Au nanorods (particle concentration of 0.12 nM) (C) in water and (D) in a mixture (1:4) of water and CH₃CN.

Table 2.2. Raman spectral data and vibrational assignment of methyl viologen [Zheng 2002 and Feng1990]

SERS peaks (cm^{-1})	Assignment
1027	ν(ring breathing)
1320	interring (C-C), ν(C-C)
1376	ν(N-CH$_3$)
1490	ν(C=C)
1565	ν(C≡N)
1602	ν(C-C), Ring stretching

It has been reported that Au nanorods possess positive ζ value in water and a negative ζ value in acetonitrile-rich solvents. The stability of Au nanorods in H_2O and acetonitrile-rich solvents may be attributed to the large positive and negative ζ values in the respective solvent environments. Au nanorods that possess a positive ζ in water experience a repulsive interaction with positively charged methyl viologen molecules. As a result, the heat change observed is negligible ruling out the possibility of any interaction and weak Raman signals were observed. Under similar conditions, addition of the methyl viologen to Au nanorods in a mixture (1:4) of water and CH_3CN leads to strong electrostatic attraction between the positively charged analyte and the negatively charged SERS substrate. These interactions are endothermic in nature and intense signals are observed in the Raman spectrum.

2.4. Conclusions

In summary, SERS efficiency of spherical Au nanoparticles and Au nanorods were compared. Covalent and electrostatic interactions of analyte molecules on the surface of Au nanorods were followed using ITC. It was observed that analyte molecules interact with the surface of nanorods more effectively in acetonitrile-rich solvents. Detailed investigations on the surface charge of nanorods have revealed that nanorods have a positive zeta potential in water due to the presence of CTAB bilayer. The bilayer structure breaks into monolayer in acetonitrile-rich solvents, resulting in negative surface charge. The positively charged molecule interacts effectively with the negative surface of nanorods in acetonitrile-rich solvents, through electrostatic interaction, giving rise to appreciable heat response in ITC and intense peaks in SERS spectrum. The analyte molecules having thiol groups can preferentially bind onto the edges of nanorods and the high electric field prevailing at the edges contributes primarily towards the enhancement in signal intensity through an electromagnetic enhancement mechanism. Based on SERS investigations, it is concluded that Au nanorods are more efficient substrates, in comparison with spherical particles, and the enhancement factor was found to increases with the aspect ratio of the nanorods.
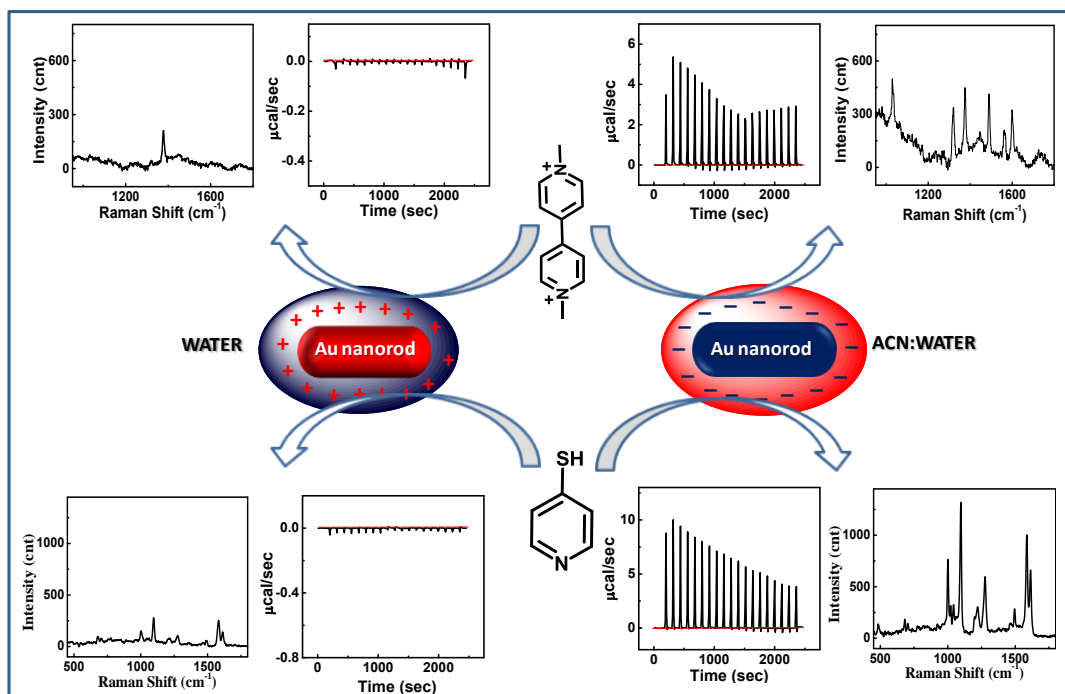
Scheme 2.2. *Schematic representation demonstrating the covalent and electrostatic interactionsbetween analyte and substrate using Isothermal Titration Calorimetry and Surface Enhanced Raman Spectroscopy.*

2.5. Experimental Section

2.5.1. Materials and Instrumental Techniques

Solvents and reagents used were purified and dried by standard methods. Photophysical studies were carried out using spectroscopic grade solvents. The absorption spectral changes, upon the addition of aromatic dithiols, were recorded in a UV-Visible diode array spectrophotometer (Agilent 8453). Stock solutions of 4-mercaptopyridine and methyl viologen were prepared in acetonitrile and water. For HRTEM studies, samples were prepared by drop casting dilute solution from the cuvette on a carbon coated Cu grid and the solvent was allowed to evaporate. The specimens were examined on a FEI-Tecnai 30G^{2}S-Twin or with a 300 kV (JEOL 3010) transmission electron microscope operated at an accelerating voltage of 300 kV. Raman and SERS spectra were recorded using a HR800

LabRAM confocal Raman spectrometer operating at 20 mW laser power using a peltier cooled CCD detector. Raman spectra were collected in a quartz cuvette using a He-Ne laser source having an excitation wavelength of 633 nm and with an acquisition time of 10 seconds using a 5x objective. All the studies were carried out in a mixture (1:4) of water and acetonitrile. The baseline was corrected and the spectra were presented after subtracting the gold nanorod spectra from the original ones. No noticeable absorption spectral changes were observed for the nanorod solution during the measurements, confirming that the nanorods remain stable in solution even after exposure to laser beam. Isothermal titration calorimetry was carried out using a Micorcal VP-ITC instrument. Doubly distilled water and spectroscopic grade acetonitrile was used for all the ITC studies. All experiments were carried out at room temperature.

2.5.2. Synthesis of Au nanorods

A growth solution was prepared by dissolving 440 mg of cetyltrimethylammonium bromide and 4.5 mg of tetraoctylammonium bromide in 15 mL of water in a cylindrical quartz tube (length 15 cm and diameter 2 cm). To this solution, 1.25 mL of 0.024 M $HAuCl_4$ solution was added along with 325 μL of acetone and 225 μL of cyclohexane. It is reported that $AgNO_3$ is essential for synthesizing Au nanorods and controlling their aspect ratio. To the above solution, 325 μL of 0.01 M $AgNO_3$ was added for synthesizing Au rods of aspect ratio 2.2 , 400 μL of 0.01 M $AgNO_3$ was added for synthesizing Au rods of aspect ratio 3.0 and 450 μL of 0.01 M $AgNO_3$ was added for synthesizing Au rods of aspect ratio 3.7. The quartz tube was closed with a rubber stopper through which a glass rod was inserted (15 cm length and 1 cm diameter). The glass rod helps in reducing the effective thickness of the solution and increases the light absorbance. A photochemical reaction was carried out at

300 nm irradiation in a Rayonet photochemical reactor for 18 h. Gold nanoparticles and nanorods prepared by a photochemical method were first purified by centrifugation. The residue obtained after 10 min of centrifugation (7000 rpm) was dispersed in 2 mL of 0.7 M CTAB solution and kept undisturbed for 12 h. The supernatant solution was carefully decanted and the residue was suspended in water. The solution was kept at 5°C for 2 h to remove excess CTAB. Upon cooling, excess CTAB crystallized out which was separated by filtration. The filtrate contains monodisperse Au nanorods that were used directly for various studies.

2.5.3. Synthesis of Au nanoparticles

A growth solution was prepared by dissolving 440 mg of cetyltrimethylammonium bromide and 4.5 mg of tetraoctylammonium bromide in 15 mL of water in a cylindrical quartz tube (length 15 cm and diameter 2 cm). To this solution, 1.25 mL of 0.024 M $HAuCl_4$ solution was added along with 325 μL of acetone and 225 μL of cyclohexane. The quartz tube was closed with a rubber stopper and was irradiated under 300 nm in a Rayonet photochemical reactor for 18 h. Gold nanoparticles prepared by a photochemical method were subjected to repeated centrifugation at 7000 rpm for 20 min. The supernatant solution was carefully decanted and the residue was suspended in water. This solution contains monodisperse Au nanoparticles that were used directly for various studies.

2.5.4. Calculation of Enhancement Factor (EF)

$$EF = [I_{SERS}]/[I_{Raman}] \times [N_{bulk}]/[N_{ads}]$$

I_{bulk} and I_{SERS} correspond to the intensities of the ring deformation band of monothiols/dithiols in the absence and presence on Au nanorod, containing various concentrations of monothiols/dithiols. N_{bulk} and N_{ads} are the number of molecules probed in acetonitrile solution in the absence and presence of Au nanorods.

Au nanorods possess a capsule shape having two hemispherical caps at the two ends of a cylinder and various calculations are carried by following an ealier procedure [Joseph 2006].

Volume of sample probed   (for depth of focus 1.01 mm) = 168 pL

Concentration of Au nanorod = 0.12 nM

Number of nanorods in 3 mL of the solution = ~2.16 x 10^{11}

Number of nanorods in the probed volume = ~1.2 x 10^4

In the absence of nanorods

No. of analyte molecules in the probed volume (10 mM in water), N_{bulk} = 1.01 x 10^{11}

Intensity of the ring deformation band of 4-mercaptopyridine (10 mM in water), I_{bulk} = 79

In the presence of nanorods

No. of thiol molecules at each edge after the addition of 0.3 μM 4-mercaptopyridine = ~1250

{based on rod (0.12 nM) to molecular ratio (0.3 μM)}

Number of thiols in the probed volume (adsorbed on nanorods), N_{ads} = ~3 x 10^7 (value corresponding to 1.2 x 10^4 rods)

Intensity of the ring deformation band of 4-mercaptopyridine (0.3 μM) at the edges of isolated nanorods of aspect ratio 2.7, I_{SERS} = 613

Intensity of the ring deformation band of 4-mercaptopyridine (0.3 μM) at the edges of isolated nanorods of aspect ratio 3.0, I_{SERS} = 876

Intensity of the ring deformation band of 4-mercaptopyridine (0.3 μM) at the edges of isolated nanorods of aspect ratio 3.3, I_{SERS} = 1666

EF (for aspect ratio 2.7) = [I_{SERS}]/ [I_{Raman}] x [N_{bulk}]/ [N_{ads}]

$$= 613 \text{ x } 1.01 \text{ x } 10^{11} / 79 \text{ x } 3 \text{ x } 10^7 = \textbf{2.6 x } 10^4$$

EF (for aspect ratio 3.0) = 876 x 1.01 x 10^{11} / 79 x 3 x 10^7 = **3.7 x 10^5**

EF (for aspect ratio 3.3) = 1666 x 1.01 x 10^{11} / 79 x 3 x 10^7 = **7.0 x 10^5**

Gold Nanorod Dimer Junctions for Raman Signal Enhancement
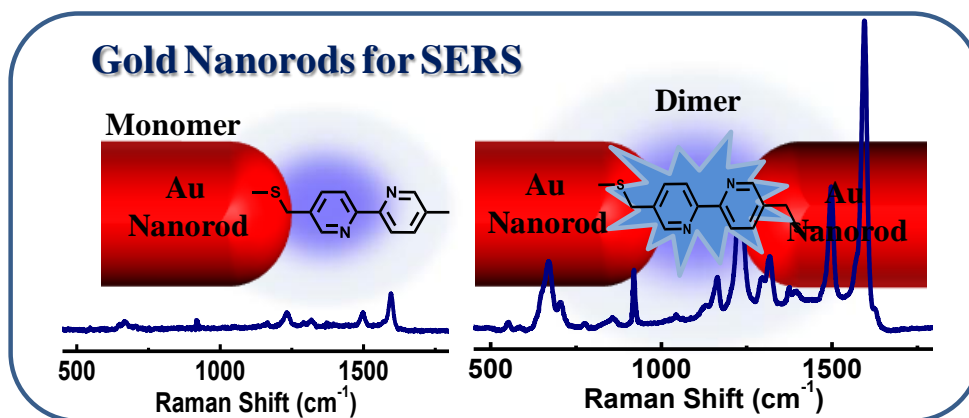
3.1. Abstract

The main objective of the present investigation is to understand the variation in the Raman intensity of a molecule when placed at the (i) edges of an isolated Au nanorod and (ii) junctions of Au nanorod dimers. Monothiol as well as dithiol derivatives of Raman-active molecules have been used to investigate these aspects. The rationale behind this strategy is that the monothiol derivatives specifically bind on the edges of an isolated Au nanorod, whereas the dithiol derivatives bind on the edges of two nanorods, leading to dimerization and subsequently the localization of molecules at the junctions. Edges of Au nanorods are regions of high electric field and when two Au nanorods are brought together in a linear fashion through dithiol linkages, their longitudinal plasmon oscillations couple with each other, creating hot spots (regions of high electric field) at the junctions resulting in enhanced Raman signal intensities.

3.2. Introduction

Surface Enhanced Raman Spectroscopy (SERS) using noble metal nanoparticles as substrates has emerged as one of the most powerful tools for the enhancement of molecular signals, particularly for the detection and identification of chemically and biologically important molecules [Campion 1998 and Kneipp 1999]. Light absorption in spherical metal nanoparticles originates from surface plasmon resonance which may be defined as the coherent oscillation of electrons on the nanoparticle's surface [Thomas 2007]. This results in trapping of light at the metal-dielectric interface leading to an increase in electric field on the surface of the nanoparticle. A Raman active molecule when placed in the vicinity of the nanoparticle's surface can give rise to enhanced signal intensity due to (i) high electric field prevailing on the metal surface (electromagnetic enhancement) [Schatz 1984 and Moskovits 2005] and (ii) charge transfer interactions between metal nanoparticle and the molecular system (chemical enhancement) [Otto 1992 and Otto 2005]. The two other major factors that can contribute to the enhancement of Raman signal intensity are the metal roughness features (or the presence of sharp edges) and the presence of coupled plasmons due to the interaction between neighbouring nanoparticles.

Spherical metal nanoparticles have been widely used as substrates in SERS and the electric field is uniformly distributed around their surface [Kou 2007]. In contrast, the edges of the anisotropic nanomaterials such as spheroids, rods, bipyramids and triangles experience enhanced electric field making them promising candidates for SERS studies [Hao 2004 and Chen 2009]. Theoretical studies using Finite Difference Time Domain (FDTD) method on Au nanorods have shown that the field at the edges of the Au nanorod is three orders of magnitude higher compared to the lateral faces, under resonant conditions, for the

longitudinal polarization of the incident light [Thomas 2012]. Localization of charges at the edges of Au nanorods has been experimentally demonstrated by our group through electrostatic interactions with oppositely charged gold nanoparticles (Scheme 3.1B) [Pramod 2007]. The preferential binding of nanoparticles at the edges of Au nanorods resulted in a spontaneous bathochromic shift in the longitudinal plasmon band (Scheme 3.1A). Site specific interactions of nanoparticles at the edges of nanorods were confirmed through TEM studies (Scheme 3.1C). Further, Murphy and coworkers have reported a large enhancement of Raman signal of the adsorbate molecules on selective excitation of the longitudinal plasmon band of Au nanorods [Orendorff 2006].
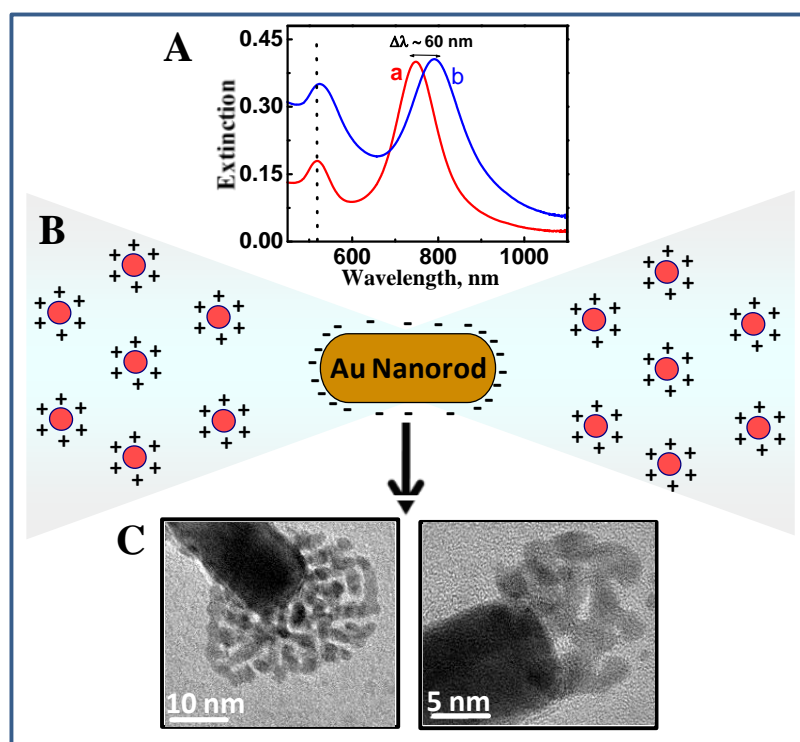
Scheme 3.1. *(A) Extinction spectral changes during the preferential growth of nanoparticles at the edges of Au nanorods. (B) Schematic representation illustrating the enhanced potential at the edges of Au nanorods. (C) TEM image showing the preferential binding of Au nanoparticles onto the edges of Au nanorods [Pramod 2007].*

Another factor that influences the SERS signal intensity of adsorbed molecules is the presence of hybridized plasmon, which arises when metal nanoparticles are brought in close proximity [Alvarez-Puebla 2010]. Hybridized plasmon generates 'hot spots' which are regions of enhanced electric field. Raman active molecules when placed at the junctions of nanoparticles, experience high electric field, which results in an enhancement of SERS signals, on illumination with light of appropriate wavelength [Lal 2008 and Nabika 2010]. Most of chemical methods reported in literature employ spherical nanoparticles as substrate for SERS; however, random aggregation of isotropic structures and poor reproducibility are the limiting factors. Various strategies adopted for generating hotspots using nanostructured materials include: (i) assembling of nanoparticles by chemical methods using dithiols [Braun 2007 and Camden 2008] and DNA molecules [Lim 2010], (ii) salt induced aggregation methods [Talley 2005], (iii) etching of nanocubes [Li 2010] and (iv) various lithographic methods [Qin 2006]. Chloride induced one step method for the fabrication of silver nanoparticle dimers has been reported by Xia and coworkers (Figure 3.1A) [Li 2009]. These dimers junctions have been used for generating hotspots and only those molecules trapped in the hot spot region contribute to signal enhancement. No signal was obtained for isolated particles and for dimers separated by large distances (Figure 3.1B). Using 4-mercaptobenzenethiol as the analyte molecule, the enhancement factor for the hot spot region of a silver nanosphere dimer was estimated to be 1.9×10^7. The SERS signals taken from the hot spot were polarization dependent; maximum enhancement was obtained for laser polarized parallel to the longitudinal axis and the signals disappeared when the polarization was in the perpendicular direction.
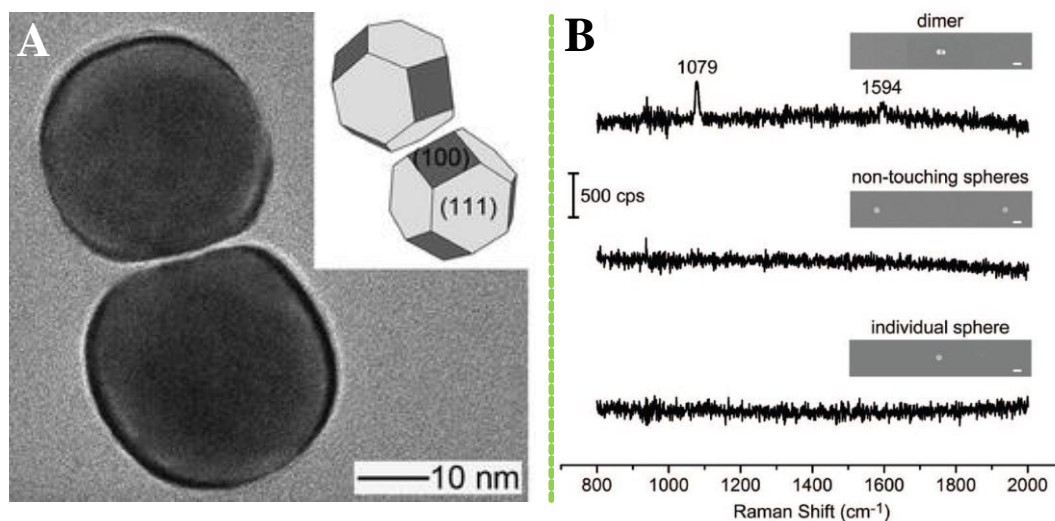
Figure 3.1. *(A) TEM image of silver nanosphere dimer. The inset gives a schematic illustration of the silver nanosphere in the dimer. (B) SERS spectra taken from a dimer of silver nanospheres (top),) two silver nanospheres separated by ~600 nm (middle) and a single silver nanosphere (bottom). The scale bars in the insets correspond to 50 nm [Li 2010].*

The isotropic nature of spherical Au nanoparticles prevents the selective binding of molecules on surfaces, which is a limiting factor for designing linearly assembled nanostructures by chemical functionalization methods. In contrast, the anisotropic features of Au nanorods allow their linear assembly, and several attempts have been made by our group [Thomas 2004, Sudeep 2005 and Joseph 2006] and others [Caswell 2003, Murphy 2005 and Wang 2007] by adopting electrostatic, supramolecular and covalent approaches. It was earlier reported from our group that the plasmon coupling in Au nanorods proceeds through an incubation step, followed by the dimerization and subsequent oligomerization in a preferential end-to-end fashion (Scheme 3.2) [Joseph 2006].
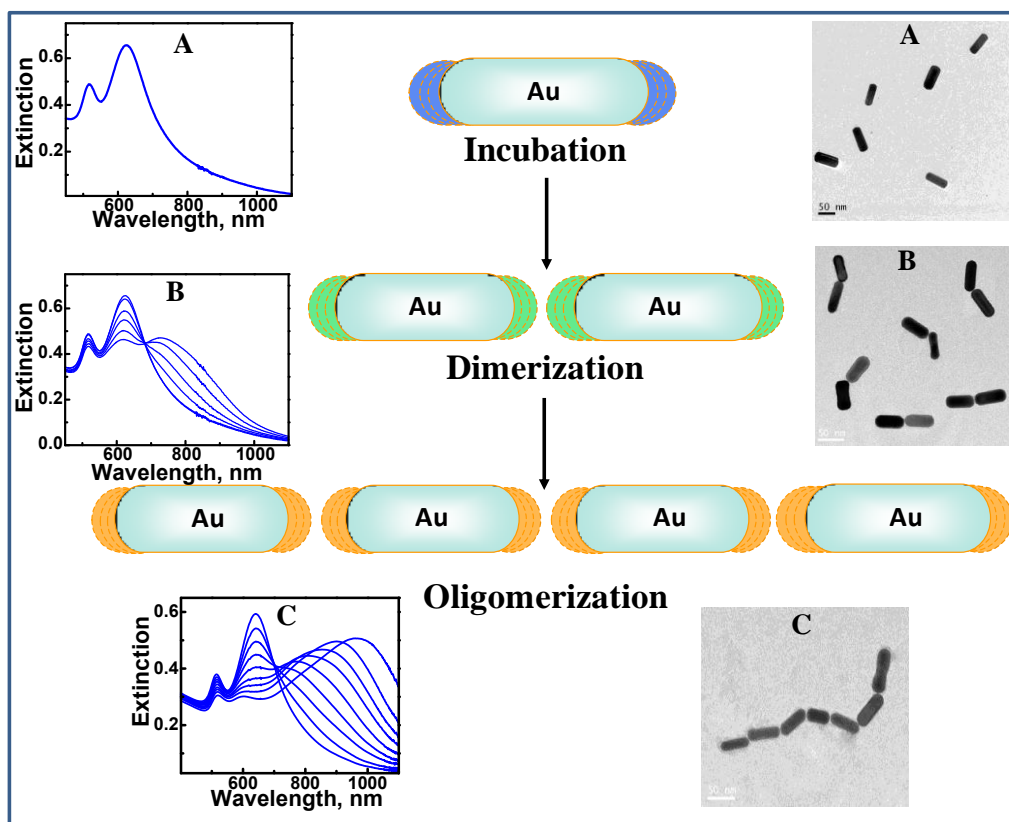
Scheme 3.2. *Schematic representation of various stages of plasmon coupling process and the corresponding extinction spectral changes and TEM images; (A) incubation, (B) dimerization and (C) oligomerization [Joseph 2006].*

The mechanism of dimerization of Au nanorods and nanochain formation has been reported by our group using various bifunctional molecules [Thomas 2004]. The nanorod dimer formation is marked through a gradual decrease in the longitudinal plasmon band with the formation of a new red shifted band through a clear isosbestic point (Scheme 3.2B). The spectral changes observed through a clear isosbestic point indicate the existence of two types of nanorod structures in solution; namely monomers and dimers. The newly formed band originates from the coupling of the longitudinal plasmons of Au nanorods (plasmon hybridization). With increase in time, coupled plasmon band slowly shifts towards longer wavelengths, resulting in the formation of linear assembly of Au nanorods (Scheme 3.2C).

Junctions between the nanorods, created through the linear assembly are regions of high electric field which can serve as promising locations for surface enhanced spectroscopic investigations.

SERS studies have been performed using aggregated Au nanorods as substrates: nanorods were allowed to aggregate randomly by addition of ethanol and Raman signal intensity was found to be more intense for molecules adsorbed on the aggregated nanorods. The observed increase in the SERS intensity was attributed to the enhancement of the electric field between the aggregated nanorods [[a]Nikoobakht 2003]. More recently, enhancement of Raman signals have been demonstrated through salt induced assembly of Au nanorods as linear chains, by blocking their lateral sides with polymers [[b]Chen 2010]. As the number of Au nanorods in a chain increases, several possible orientations exist between the nanorods and such variations can disrupt effective plasmon coupling and enhancement of electric field at the junctions [Gluodenis 2002, Jain 2006, Pramod 2008 and Funston 2009]; hence studies based on dimers may be more suited for SERS. Recently, our group has demonstrated the tuning of plasmon coupling in Au nanorod dimers by varying the distance and orientation [Pramod 2008]. Au nanorod dimers linked through flexible (1,6-hexanedithiol, C6DT) and rigid (1,4-phenylenedimethanethiol, PDT) linker groups were prepared and the plasmon coupling in these systems were investigated as a function of their orientation. The dimers formed using PDT as the linker were more linear (average angle of 146[°]) due to the rigidity induced by the aromatic dithiols (Figure 3.2A), whereas, the flexible linkers gave rise to dimers with bend geometry (average angle of 96[°]) (Figure 3.2B). The plasmon coupling in PDT-linked Au nanorod dimers is found to be more pronounced because of the effective dipolar overlap along their long axes confirming that the orientation

between the nanorods plays a crucial role in plasmon coupling, which can be modulated by varying the nature of the linker group.
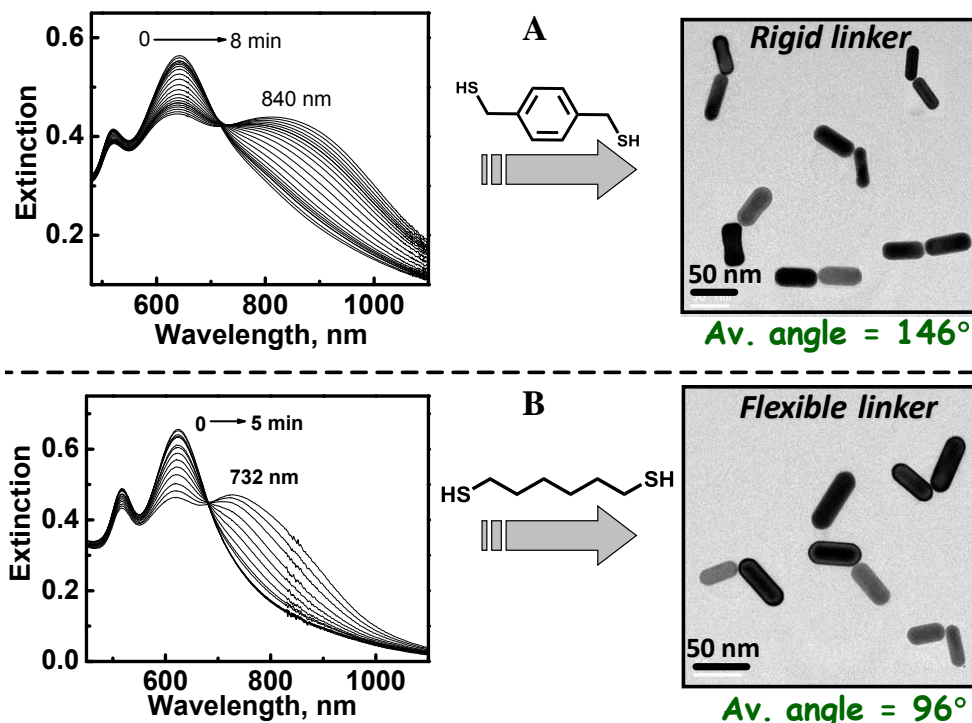
Figure 3.2. *Extinction spectral changes and the corresponding TEM images of Au nanorod dimers formed on addition of 0.8 μM A) PDT and B) C6DT to a solution of Au nanorods (0.12 nM) with an average aspect ratio of 2.7 (8 and 5 min after the addition of PDT and C6DT, respectively, 75 mL of the solution was drop-casted onto the TEM grid) [Pramod 2008].*

There is a growing demand for the development of new SERS substrates capable of producing large enhancement in signal intensities at low concentrations of the analyte molecules. The major problems associated with the fabrication of efficient SERS substrates are the uncontrolled aggregation of nanoparticles and poor reproducibility. Herein, we utilize the anisotropic features of Au nanorods for enhancing the Raman signals of analyte molecules. The enhancement in signal intensity of molecules at the edges (edge effect) is compared with that of the molecules placed at the dimer junctions (hybridized plasmon).

3.3. Results and Discussion

Gold nanorods with an average aspect ratio of ∼2.5 were synthesized by following a photochemical method [Kim 2002] and excess capping agents such as CTAB were removed by centrifugation. Au nanorods possess large positive zeta potential (ζ = 28.5 mV) in water due to the presence of CTAB bilayer and a large negative zeta potential in acetonitrile rich solvents due to the breakdown of the bilayer to monolayer [Pramod 2008]. Raman and absorption spectroscopic studies were carried out in a solvent mixture (1:4) of water and acetonitrile (ζ = -28.8 mV) wherein Au nanorods are stable for several hours. Au nanorods with an aspect ratio of ∼2.5 possess two distinct surface plasmon absorption bands, a short wavelength band at 520 nm corresponding to the transverse mode of plasmon oscillation and a long wavelength band at 635 nm corresponding to the longitudinal mode [Joseph 2006]. Raman spectra were recorded using a confocal Raman spectrometer using a He-Ne laser source having an excitation wavelength of 633 nm and an acquisition time of 10 s. CTAB-capped Au nanorods suspended in a mixture (1:4) of water and acetonitrile showed no spectroscopic signals corresponding to the CTAB molecules; however Raman signals corresponding to the solvent molecules were observed.

The main objective of the present investigation is to understand the variation in Raman intensity of a molecule when placed at the (i) edges of an isolated Au nanorod and (ii) junctions of Au nanorod dimers. Monothiol as well as dithiol derivatives of Raman active molecules have been used for investigating these aspects (Scheme 3.3). The rationale behind this strategy is that the monothiol derivatives (5-mercaptomethyl-5'-methyl-2,2'-bipyridine, **bipy-MT** and benzyl mercaptan, **bz-MT)** specifically bind onto the edges of an isolated Au nanorod (Scheme 3.3A). In contrast, the dithiol derivatives (5,5'-bis(bromomethyl)-2,2'-

bipyridine, **bipy-DT** and phenylenedimethanethiol, **bz-DT**) bind onto edges of two nanorods leading to dimerization and subsequently the localization of molecules at the junctions (Scheme 3.3B). Any variation in orientation between the nanorods can disrupt the effective plasmon coupling [Pramod 2008] and hence rigid molecules were used as linkers in the present study.
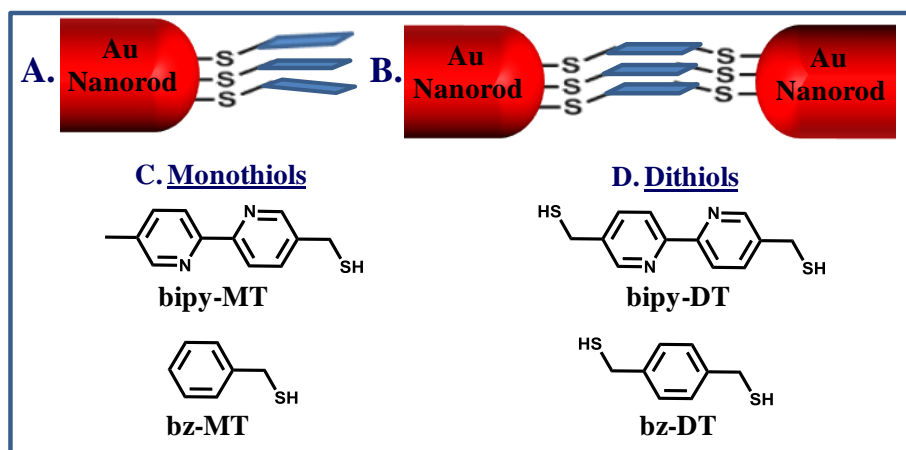
Scheme 3.3. *Schematic representation of Au nanorods with molecules at the edges of (A) an isolated Au nanorod and (B) junctions of Au nanorod dimers. The structures of thiol derivatives used in the present study: (C) monothiols and (D) dithiols.*

3.3.1. SERS at the Au nanorod edges

The Raman intensity of a molecule placed at the edges of an isolated Au nanorod (edge effect) was investigated by adding microlitre quantities of monothiol derivatives (0.5-3.0 µM) to Au nanorods (0.12 nM) in a solvent mixture (1:4) of water and acetonitrile. It is reported that the thiol derivatives preferentially bind onto the {111} planes of the Au nanorods. The edges of Au nanorods are dominated by {111} planes and the specific interaction of thiols with these planes leads to the localization of monothiol molecules more at the edges [Caswell 2003, Gao 2003 and Murphy 2005]. Both the plasmon absorption bands of Au nanorods remain more or less unaffected on increasing the concentration of

monothiols (**bipy-MT** and **bz-MT**) indicating that the nanorods remain stable and isolated in solution (Figure 3.3A,C). These results rule out the possibility of aggregation of nanorods or plasmon coupling between the nanorods. The Raman spectra of molecules bound to the edges of Au nanorods showed a few peaks; however, their intensities were low. The peaks observed at 1600, 1499, 1324, and 1237 cm^{-1} in the case of **bipy-MT** are attributed to the ring stretching (C–C and C–N), in-plane C–H bending, inter-ring stretching and ring deformation modes of **bipy-MT** [Brolo 2003]. Spectral data and assignment of various peaks of the mono and dithiol derivatives are presented in Tables 3.1 and 3.2. Intensities of various peaks were almost doubled upon increasing the concentration of monothiols to 1.0 μM. Raman spectral changes leveled off with further increase in concentration of the analyte molecules (Figure 3.3B) and this may be attributed to the fact that there are no more active sites present at the edges of the nanorods that can produce effective signal enhancement. It is earlier reported that the edges of nanorods are relatively naked compared to lateral face in acetonitrile-rich solvents. The nanorods underwent precipitation upon increasing the concentration of **bipy-MT** above 3.0 μM. Raman and extinction spectral studies were also carried out by varying the concentration of **bz-MT**. Solutions were quite stable at a higher concentration of **bz-MT**, and both the plasmon absorption bands remained unaffected ruling out the possibility of aggregation of nanorods. Raman peaks observed at 1600, 1222, and 655 cm^{-1} for **bz-MT** are attributed to the ring stretching, CH$_2$ wagging, and C–S stretching modes of **bz-MT**, respectively (Figure 3.3D) [Joo 1999]. In both the cases, a gradual increase in the intensity of Raman peaks was observed with the increase in the concentration of monothiols which leveled off at higher concentrations. It is interesting to note that Raman signals corresponding to **bipy-MT**/**bz-MT** were not observed in the absence of Au nanorods,

even upon increasing the concentration by 10^4 fold (5 mM). These results clearly indicate that specific interaction and localization of monothiol molecules at the edges of Au nanorods, which are domains of high electric field, lead to the gradual enhancement in signals.
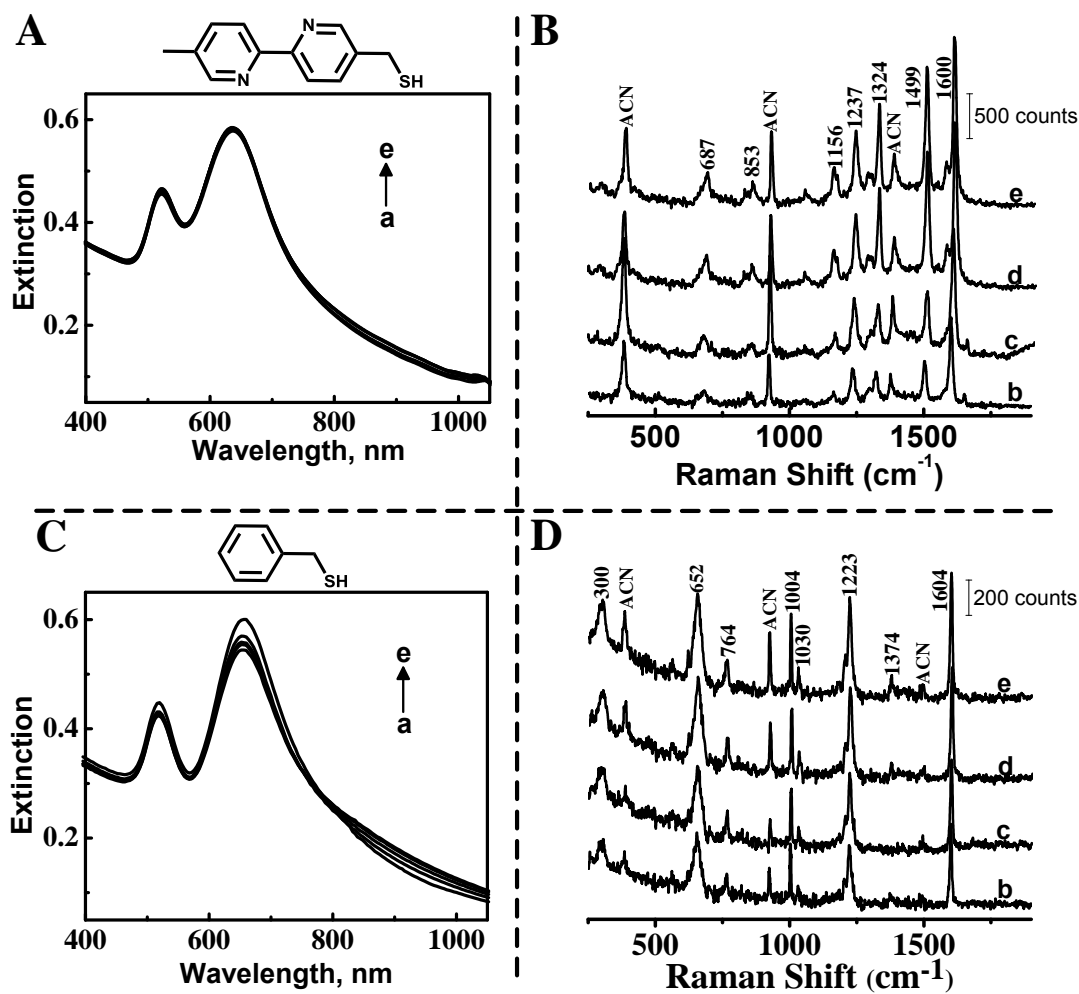
Figure 3.3. *Extinction spectral changes of Au nanorods (a) in the absence of monothiols and (b-e) on addition of varying amounts of **bipy-MT** (A) and **bz-MT** (C) to a mixture (1:4) of water and acetonitrile and the corresponding changes in Raman spectrum (B,D) on excitation with He-Ne laser (633 nm; acquisition time of 10 s). The concentrations of monothiols corresponds to b = 0.5 μM, c = 1 μM, d = 2 μM and e = 3 μM.*

Table 3.1. Spectral data and vibrational assignment of **bipy-MT** and **bipy-DT** [Brolo 2003 and Muniz-Mirandaa 2001]

SERS peaks (cm^{-1})	Assignment
669, 687	Ring i.p. def.
702	Ring breathing
853	CH o.p. bending
1156, 1165	CH i.p. def. + ring str.
1231, 1237	Inter-ring stretch + ring str. + CH i.p. def.
1324	Inter-ring str. + ring str. + CH i.p. def.
1398	CH_2 Wagging
1497, 1499	CH i.p. def. + ring str.
1594, 1600	Ring str.

i.p.: in-plane,   o.p.: out-of-plane,   def.: deformation,   str.: stretching

Table 3.2. Spectral data and vibrational assignment of **bz-MT** and **bz-DT** [Joo 1999 and Venkataramanan 2000]

SERS peaks (cm^{-1})	Assignment
300	δ(C-S)
651, 652	ν (C-S)
738	δ (C-S)
764	δ (CSH)
837	ν (C-H)
1004	ν(ring breathing)
1030, 1177	β C-H
1218, 1223	CH_2 wagging
1604	Ring deformation

3.3.2. SERS at the Au nanorod dimer junctions

For investigating the enhancement in Raman signal intensity during dimerization of Au nanorods, dithiol derivatives (**bipy-DT** and **bz-DT**), were added to Au nanorods in a mixture of water and acetonitrile. Both of the plasmon absorption bands of Au nanorods remain more or less unaffected at lower concentrations (<0.5 μM) of dithiols (trace b in Figures 3.4A and 3.4C). This corresponds to the incubation step in the plasmon coupling process, wherein one of the thiol groups of the dithiol molecule binds to the edges of Au nanorods, leaving the other end free [Joseph 2006]. Peak positions and intensities in the Raman spectra of **bipy-DT** and **bz-DT** (trace b in Figure 3.4B and 3.4D) during the incubation step were almost similar to those observed for the corresponding monothiol derivatives (Figures 3.3B and 3.3D). Dimerization of nanorods proceeds above a critical concentration of dithiols; an increase in the concentration of dithiols (0.8 μM for **bipy-DT** and 1.0 μM for **bz-DT**) leads to a spontaneous decrease in the intensity of the longitudinal surface plasmon band with the concomitant formation of a new band in the near-infrared (NIR) region (traces c-e in Figure 3.4A and 3.4C) through a clear isosbestic point at around 720 nm. The extinction spectral changes clearly indicate that the nanorods are brought together through a dithiol linkage, which results in plasmon hybridization. Interestingly, a spontaneous enhancement in the intensity of Raman signals was observed during the dimerization step and the corresponding time dependent changes in the extinction and Raman spectrum are presented in Figure 3.4. The new band further shifted to longer wavelengths with time (traces f and g in Figure 3.4A and 3.4C), and a deviation from the isosbestic point indicate the formation of oligomers of various chain lengths. Raman signals showed only a slight increase in intensity during the oligomerization, (trace g in Figure 3.4B

and 3.4D) and this may be attributed to the fact that several possible orientations exist between the nanorods in a chain (*vide infra* TEM studies), which can disrupt effective plasmon hybridization and enhancement of the electric field at the junctions.
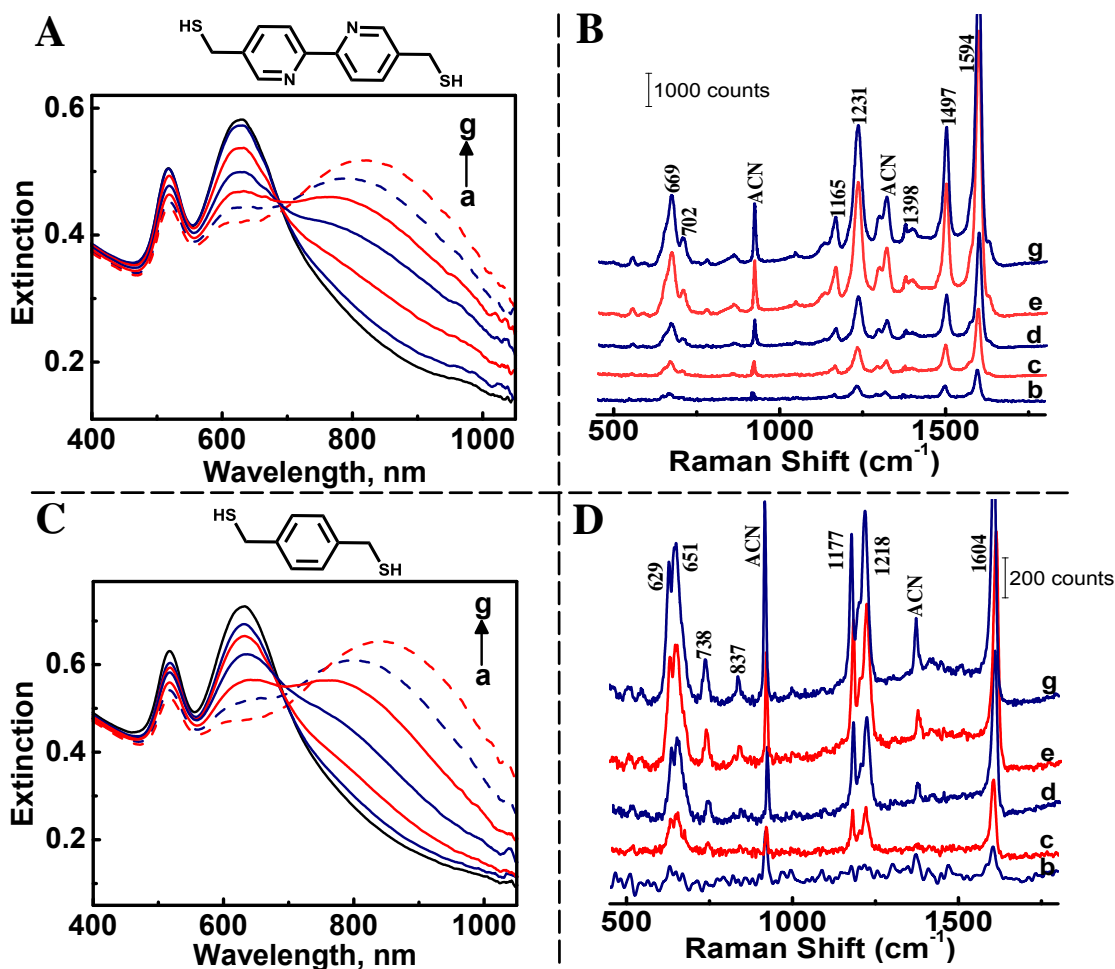
Figure 3.4. *Extinction and Raman spectral changes of Au nanorods (0.12 nM) on addition of dithiols,* ***bipy-DT*** *(A,B) and* ***bz-DT*** *(C,D) in a solvent mixture (1:4) of water and acetonitrile. Plasmon absorption (A,C) of Au nanorods: (a) in the absence of dithiols, (b) at lower concentration of dithiol (0.5 μM for both* ***bipy-DT*** *and* ***bz-DT;*** *no change in spectrum with time), (c-g) at higher concentration of dithiols (0.8 μM of* ***bipy-DT*** *and 1.0 μM of* ***bz-DT****) recorded successively at a time interval of 3 min. The corresponding Raman spectra of* ***bipy-DT*** *(B) and* ***bz-DT*** *(D) on exciting with He-Ne laser (633 nm; acquisition time of 10 s) are presented as traces b-g*.

3.3.3. TEM characterization and SERS enhancement

Nanorod solutions during the incubation, dimerization, and oligomerization steps were drop-casted (75 µL) onto a carbon coated copper grid, and various stages of chain formation of nanorods were confirmed using transmission electron microscopy (TEM). Nanorods were found to be isolated and randomly distributed throughout the grid during the incubation period (Figure 3.5A). The corresponding Raman spectrum of the **bipy-DT** molecules attached to these isolated nanorods showed various peaks; however their intensity was found to be much lower (Figure 3.5D). The Raman signals observed at lower concentrations of the dithiols, in the presence of Au nanorods is attributed to the specific interaction of the thiol molecules onto the {111} planes at the edges of nanorods, which are domains of the enhanced electric field. Upon increasing the concentration of dithiol molecules, a large enhancement in the Raman signals was observed (Figure 3.5B and 3.5E). From the TEM images, it is evident that the rigid dithiol groups link two Au nanorods as dimers in a linear fashion. The effective dipolar overlap between nanorods creates regions of enhanced electric field (hot spots). The molecules at the hotspots, i.e., the Au nanorod dimer junctions experience enhanced electric field, leading to an increase in the intensity of the Raman signal. Dimers of Au nanorods further undergo oligomerization with respect to time and this is marked by a slight increase in the intensity of Raman signal (Figure 3.5C and 3.5F). No enhancement in signal intensity was observed on further keeping the solution for longer time.
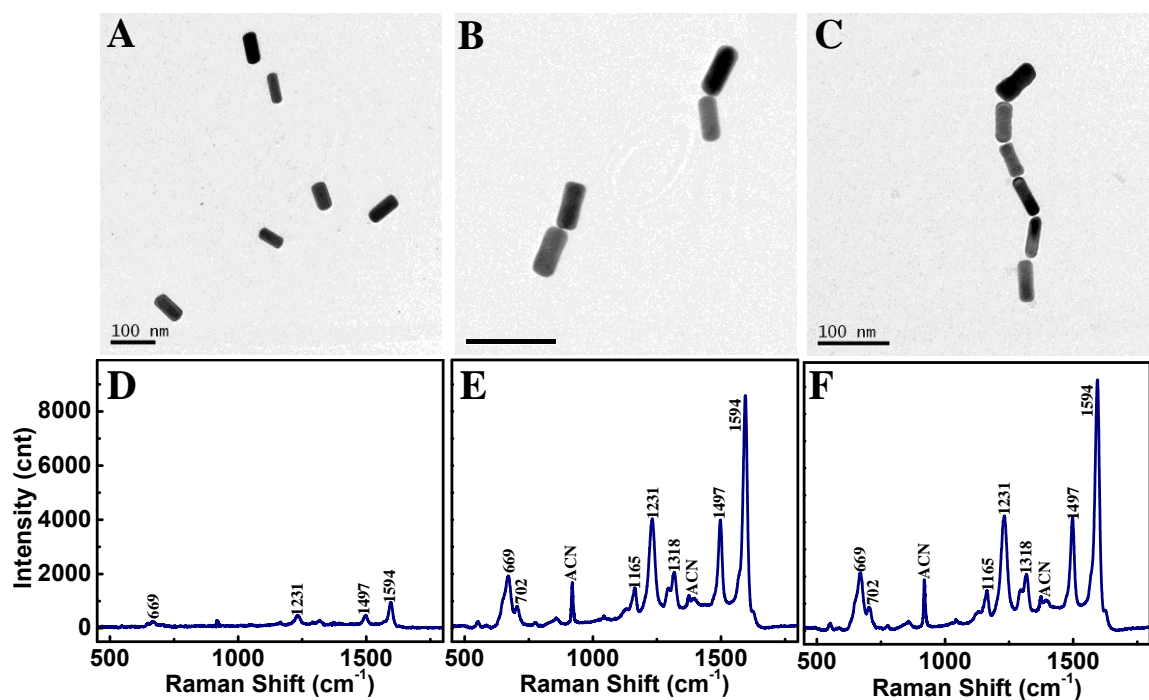
***Figure 3*.5.** *TEM images of gold nanorods (A-C) and Raman spectra of **bipy-DT** (D-F) at various stages of plasmon coupling: incubation (A,D), dimerization (B,E) and oligomerization (C,F) steps.*

The Raman signal enhancement and the TEM images at various stages of chain formation were further confirmed with **bz-DT** as the linker molecule. The same solution used for absorption and Raman spectral studies were drop casted (75µL) at various stages of plasmon coupling onto carbon coated copper grid. The results obtained were similar to that with **bipy-DT** as the linker; nanorods were stable and isolated during the incubation period (Figure 3.6A). Aromatic dithiol molecules are rigid in nature and dimers were found to be linear which further undergo oligomerization (Figures 3.6B and 3.6C). Nanorod chains were found to be distributed throughout the TEM grid (Figure 3.6C). As in the previous case, the intensity of the Raman peaks were found to be less intense during the incubation step (Figure 3.6D). A large enhancement in the Raman signal intensity was observed during the dimerization step (Figure 3.6E) which slightly increased during the oligomerization (Figure

3.6F). Large enhancement in the Raman signal intensity observed during the dimerization is attributed to the high electric field experienced by the molecules at the junctions due to plasmon coupling. However, several possible orientations exist between the nanorods with the increase in number of rods in a chain, and such variations can disrupt effective plasmon coupling. Hence, only a slight increase in Raman intensity was observed during oligomerization.
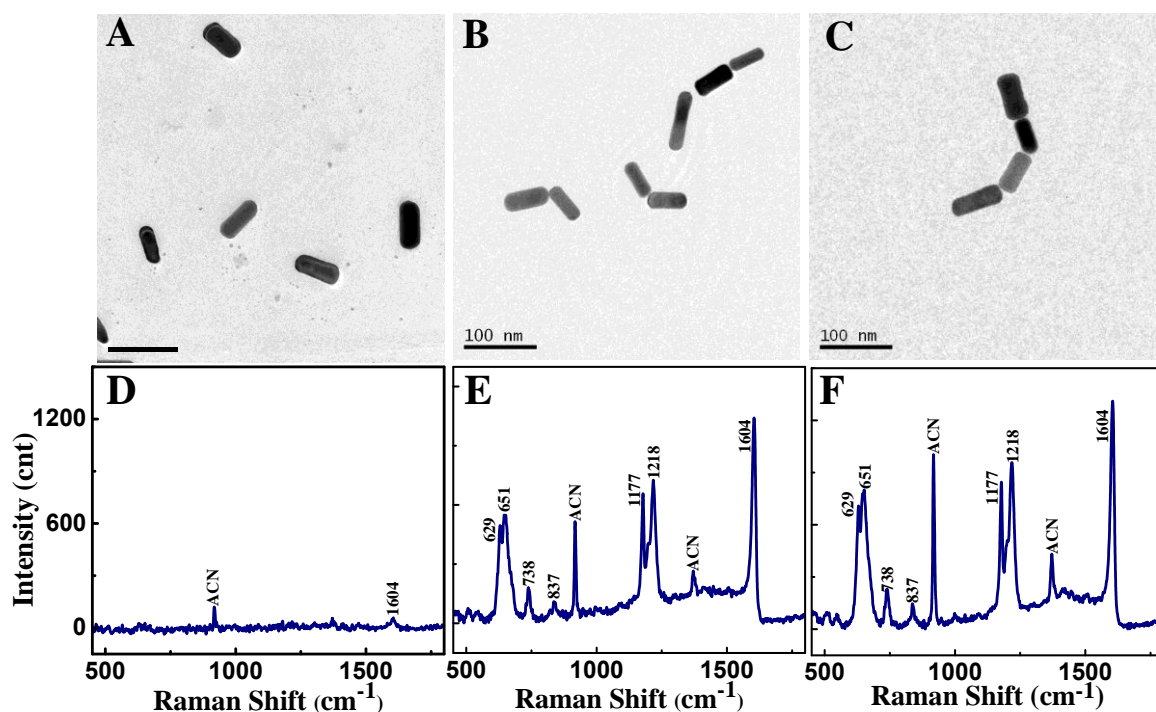
Figure 3.6. TEM images of gold nanorods (A-C) and Raman spectra of bz-DT (D-F) at various stages of plasmon coupling; incubation (A,D), dimerization (B,E) and oligomerization (C,F).

Further evidence for the presence of dithiol molecules at the junctions of Au nanorod dimers was obtained from high resolution TEM imaging. High resolution TEM images clearly showed a gap of ∼1.5 nm between two nanorods when **bipy-DT** is used as linker and ∼1.0 nm when **bz-DT** is used as linker (Figures 3.7C and 3.7D). These distances are in close

agreement with the molecular length of respective linkers confirming the presence of molecules at the dimer junctions. Thus, these molecules effectively glue the nanorods as chain.
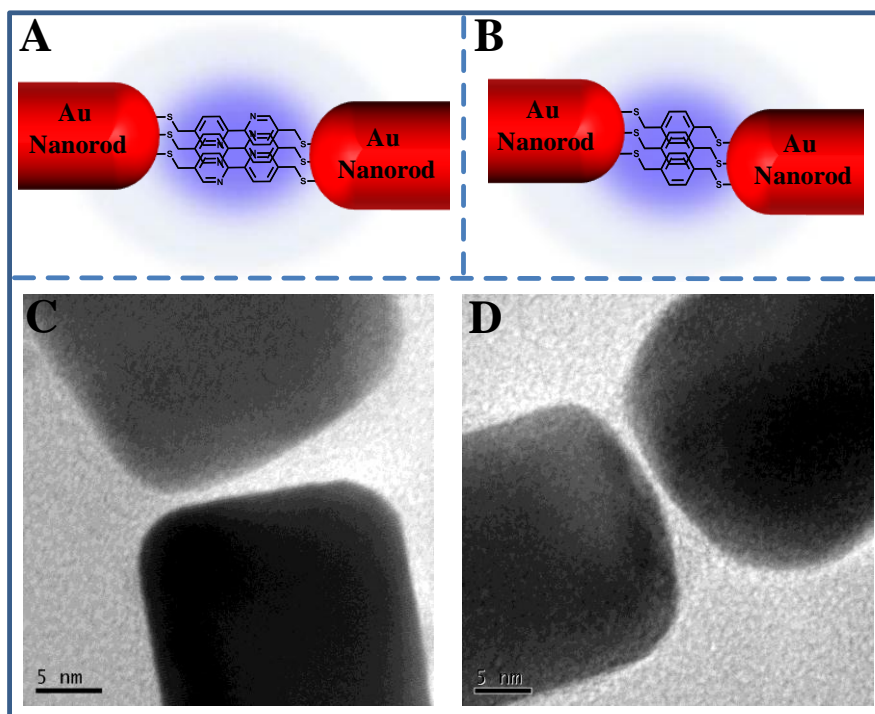
Figure 3.7. *(A,B) Schematic representation of an Au nanorod dimer linked together by (A)* *bipy-DT* *and (B)* *bz-DT*. *(C,D) The corresponding high resolution TEM images showing the molecular gap.*

The variation in intensity of the characteristic ring deformation band of monothiol derivatives (1600 cm^{-1} for **bipy-MT** and **bz-MT**) in the concentration range of 0.5-3.0 μM are presented as a bar graph in Figure 3.8 and the changes observed were found to be gradual. Under identical conditions, higher counts were observed for **bipy-MT** due to the larger Raman scattering cross-section of the bypridine derivatives, compared to that of phenyl systems. However, **bz-MT** molecules showed larger signal enhancement on increasing the concentration: **bz-MT** being a smaller molecule compared to **bipy-MT** can easily penetrate through the capping layer and saturate the edges of the nanorods. The

intensity of the band leveled off at higher concentrations for both the monothiol derivatives due to the saturation of active binding sites on the nanorod surface. Interestingly, the intensity of the ring deformation band of dithiol derivatives (1594 cm^{-1} for **bipy-DT** and 1604 cm^{-1} **bz-DT**) underwent a spontaneous enhancement in signal intensity on increasing the concentration to a critical value (0.8 μM for **bipy-DT** and 1.0 μM for **bz-DT)** which is attributed to the dimerization of the nanorods. Thus, the linker molecules are trapped at the dimer junctions, which are regions of enhanced electric field due to the hybridization of plasmons.
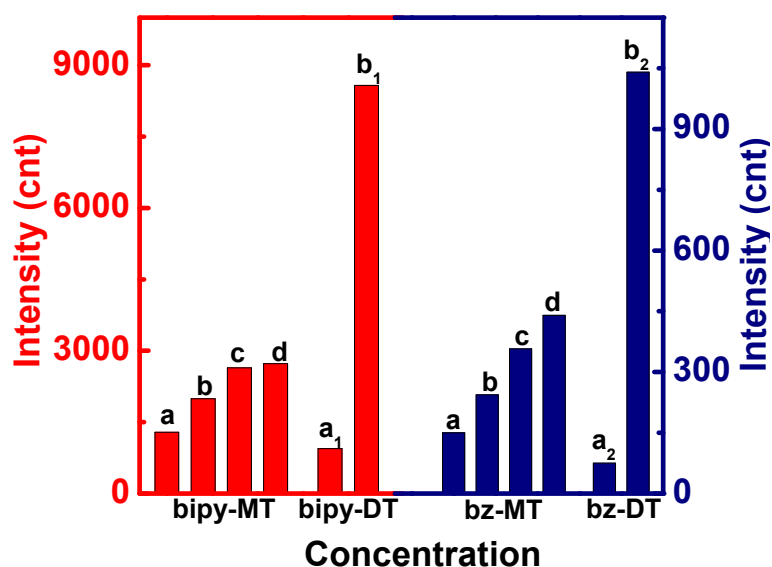
Figure 3.8. Variation in the Raman intensity of the ring deformation band (1600 cm^{-1} for ***bipy-MT*** *and* ***bz-MT***, *1594 cm^{-1} for* ***bipy-DT*** *and 1604 cm^{-1} for* ***bz-DT***) *in Raman spectrum on addition of varying amounts of monothiols and dithiols:* ***bipy-MT*** *and* ***bz-MT*** *($a = 0.5$ μM, $b = 1$ μM, $c = 2$ μM and $d = 3$ μM);* ***bipy-DT*** *($a_1 = 0.5$ μM, $b_1 = 0.8$ μM);* ***bz-DT*** *($a_2 = 0.5$ μM, $b_2 = 1.0$ μM).*

3.3.4. Effect of aspect ratio of the nanorod

The red shift in the longitudinal plasmon band during the end-to-end assembly of nanorods has been theoretically reported earlier by different groups [Gluodenis 2002, Jain

2006 and Funston 2009]. However, experimental investigations on the extent of plasmon coupling by varying the length of the nanorods have not been carried out in a systematic fashion. We have further compared the variation in plasmon coupling and the enhancement in Raman signal intensities as a function of the aspect ratio of the nanorods. Nanorods with aspect ratio 2.7, 3.0 and 3.3 having their longitudinal plasmon band at 650 nm, 670 nm and 700 nm respectively, were used to probe the effect of aspect ratio. In order to avoid the contribution from direct plasmon excitation by laser source, nanorods with longitudinal band having no overlap with the laser excitation wavelength were used. The extinction spectral changes and the corresponding SERS spectrum of nanorods of three different aspect ratios are shown in Figure 3.9.
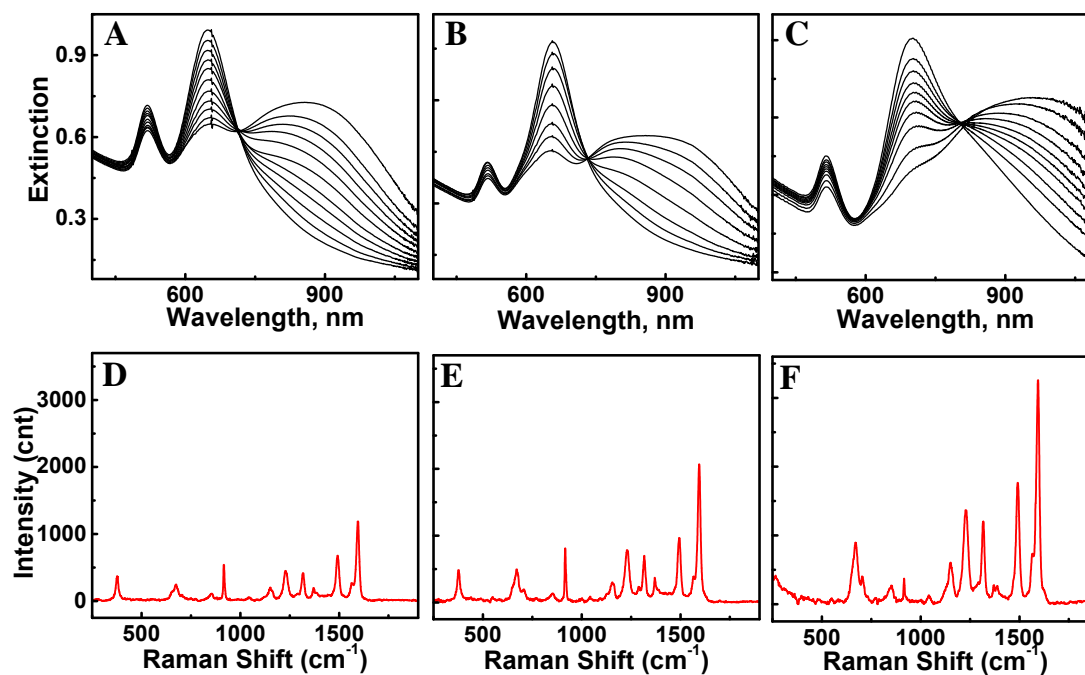
Figure 3.9. *Extinction spectral changes (A,B,C) during the dimerization, step on addition of 0.8 μM **bipy-DT** and the SERS spectrum (D,E,F) recorded 5 min after the addition of dithiols to Au nanorods of aspect ratio 2.7 (A,D), 3.0 (B,E) and 3.3 (C,F) in a mixture of (1:4) of water and acetonitrile.*

The red shift in the longitudinal plasmon band and the increase in Raman signal intensity corresponding to the ring breathing mode (1604 cm^{-1}) of the linker molecule (**bipy-DT**), with the increase in aspect ratio of the rod are shown in Figure 3.10. Nanorods having aspect ratio 2.7 with longitudinal plasmon band at 650 nm shows a 170 nm red shift in the coupled plasmon band, whereas, for nanorods having aspect ratio of 3.3, we observe larger red shift of 270 nm (red bars in Figure 3.10). The increase in red shift of the peak corresponding to dimers is an indication of the effective overlap of the plasmons of the individual rods, resulting in increase in extends of the coupling with increasing aspect ratio. The intensity of different peaks corresponding to various modes of molecular vibrations increases with increasing aspect ratio (blue bars in Figure 3.10). The enhancement in Raman signal intensity may be attributed to the increase in electric field at the junctions with increasing aspect ratio of the rods.
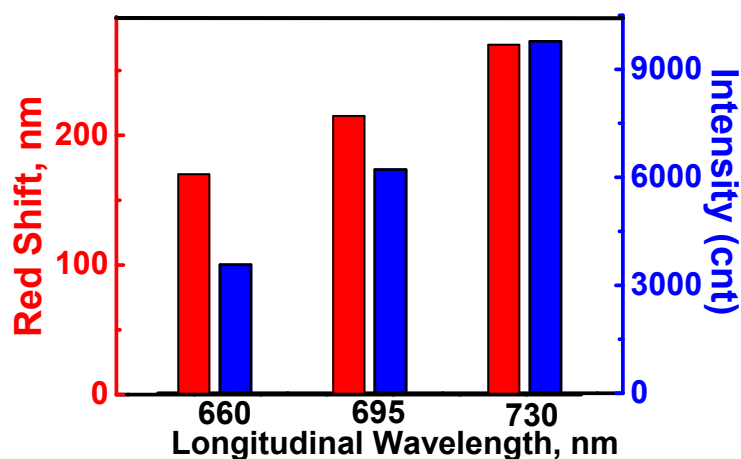
Figure 3.10. Variation in the red shift in longitudinal plasmon band on the formation of dimers (red bars) and the corresponding enhancement in the Raman signal intensity (blue bars) for three different sets of rods having aspect ratio 2.7, 3.0 and 3.3.

The shift in coupled plasmon band and the dependence of dipolar coupling on aspect ratio of nanorods can be explained on the basis of plasmon hybridization model. According to the plasmon hybridization model, organization of Au nanorods into dimers in the longitudinal fashion can give rise to four hybridized plasmon modes; two bonding and two antibonding modes (Scheme 3.4). Two of the modes are optically active (bright modes; dipoles add up), and the other two are optically inactive (dark modes; dipoles cancel each other). For a linear dimer, the transverse antibonding and longitudinal bonding modes are optically active. However, we observe only one red-shifed peak corresponding to longitudinal bonding mode for nanorods assembled in a longitudinal fashion (Schemes 3.4A). In principle, a blue shift in the transverse peak position is expected during dimer formation; however, the anibonding mode due to the transverse coupling is too weak to be observed (Schemes 3.4B).
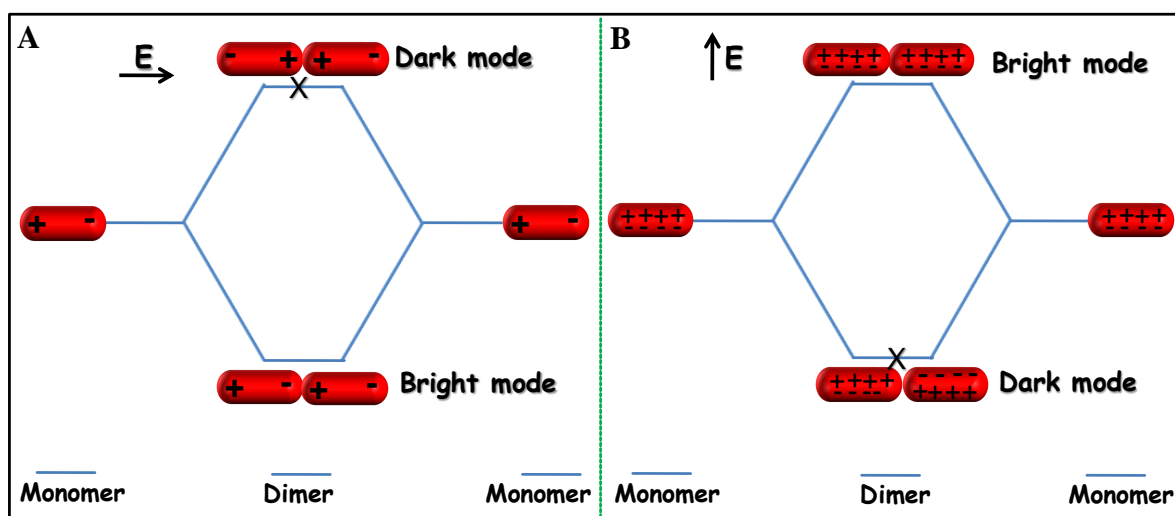
Scheme 3.4. *Schematic illustration of the plasmon hybridization model of longitudinally assembled Au nanorod dimers during (A) longitudinal and (B) lateral polarizations.*

As the number of nanorods in an assembly increases, the longitudinal bonding mode further stabilizes, resulting in higher bathochromic shifts in peak positions. The pronounced shift in the longitudinal plasmon band with increase in aspect ratio can be explained based on stronger dipolar coupling as illustrated in Scheme 3.5 using the plasmon hybridization model.
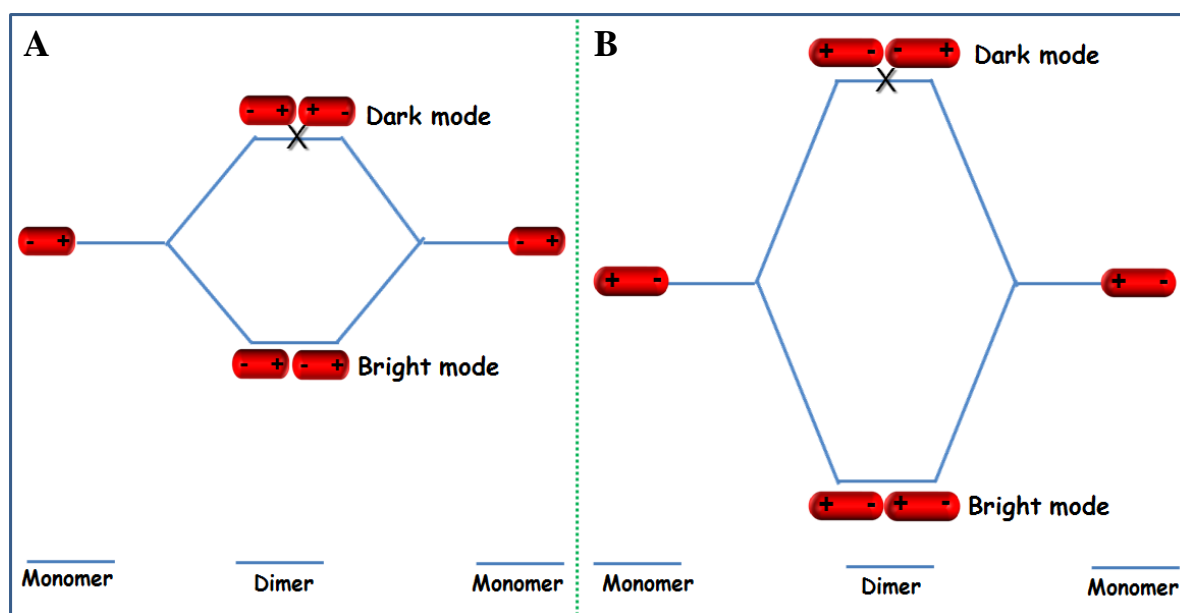
Scheme 3.5. *Schematic illustration of the plasmon hybridization model during longitudinal polarization of linearly assembled Au nanorod dimers having (A) lower aspect ratio and (B) higher aspect ratio.*

3.3.5. Effect of higher concentration of linker

To find the effect of higher concentrations of the linker molecule on the SERS intensity, excess of **bz-DT** (4 µM) was added to the nanorod solution after the oligomerization step and absorption and Raman spectral changes were monitored as a function of time. The changes in absorption and Raman peak intensities with higher concentrations of the linker molecule are shown in Figure 3.11. Absorption spectral changes corresponding to dimerization and oligomerization were observed with 1 µM of **bz-DT** and

no further red shift in the longitudinal band (a small dampening of the higher wavelength band is observed due to the precipitation of the nanorod assemblies from solution at the final stages) was observed on addition of higher amounts of the linker molecule (Figure 3.11A), indicating the completion of the plasmon coupling process. Raman spectrum showed no further increase in intensity from the oligomerization stage (blue trace in Figure 3.11B), on addition of higher concentration of **bz-DT** (red trace in Figure 3.11B) and this may be attributed to the saturation of the active sites present on the nanorod surface that can produce significant enhancement in signal intensity.
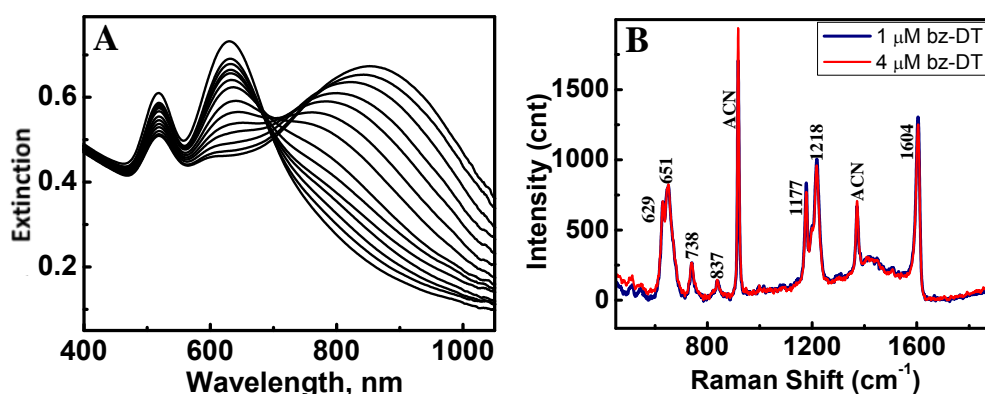
Figure 3.11. *(A) Extinction spectral changes on addition of higher concentration (4.0 μM) of **bz-DT** to Au nanorods in a mixture (1:4) of water and acetonitrile. (B) The corresponding Raman spectral changes on addition of 1.0 μM (blue trace) and 4.0 μM (red trace) of **bz-DT**.*

3.3.6. Calculation of Enhancement Factor (EF)

Enhancement in signal intensity at the various stages of nanochain formation was further quantified by estimating the signal enhancement factor (EF) [Li 2009 and Ru 2007]. One of the factors which influence the calculation of EF is the orientation of molecules on the surface of nanomaterials. It is difficult to identify the exact orientation of molecules on the surface of nanorods during the incubation, dimerization and oligomerization stages of plasmon coupling process. For example, the molecules at the junctions of Au nanorod

dimers may be more rigid compared to that attached to isolated nanorods (Scheme 3.3), however, quantification of these aspects are difficult. It was earlier reported that the totally symmetric in-plane vibrations of 2,2'-bipyridine are strongly enhanced upon adsorption to SERS active Au(111) surface and the out-of-plane vibrations (at 407 and 814 cm^{-1}) did not appear [Brolo 2003]. The absence of out-of-plane vibrational modes indicates that the 2,2'-bipyridine molecules are adsorbed perpendicular to the surface. In the present study, we do not observe any out-of-plane vibrations corresponding to **bipy-DT** (or **bipy-MT**) molecules linked on to Au nanorods, clearly indicating the perpendicular adsorption of molecules (Figure 3.7A and 3.7B). The distance between the rods in nanorod dimer matches well with the molecular chain length (Figure 3.7C and 3.7D) further confirming the perpendicular orientation of molecules at the junctions. Hence for calculating the EF we have taken an approximation that the orientation of the molecules does not undergo any significant variation during the nanochain formation. The enhancement factor (EF) at the various stages of chain formation on addition of dithiols were estimated using the equation (1)

$$EF = (I_{SERS} \times N_{bulk}) / (I_{bulk} \times N_{ads}) \tag{1}$$

where I_{bulk} and I_{SERS} are the intensities of the ring deformation band of dithiols in the absence of Au nanorods (90 mM for **bipy-DT** and 50 mM for **bz-DT** in acetonitrile) and in the presence on Au nanorods containing various concentrations of dithiols respectively. N_{bulk} and N_{ads} are the number of molecules probed in acetonitrile solution in the absence and presence of Au nanorods respectively. The details regarding the calculation of enhancement factor are provided in the experimental section. The EF of monothiol and dithiol derivatives of bipyridine at lower concentrations (0.5 µM) are more or less same (2.5 x 10^4 for **bipy-MT** and 2.4 x 10^4 for **bipy-DT**) indicating that these molecules are bound on the edges of

isolated Au nanorods with similar orientation. Molecules experience a high electric field when placed at the junctions in between the rods and a higher EF value was observed (1.4×10^5 for dimers and 1.5×10^5 for oligomers). EF values for the phenyl derivatives (**bz-MT** and **bz-DT)** also showed similar results: EF values estimated (i) at lower concentrations (0.5 μM) of **bz-MT** and **bz-DT** are 6.8×10^4 and 4.3×10^4, respectively and (ii) when **bz-DT** is placed between Au rods are 1.5×10^5 for dimers and 1.9×10^5 for oligomers. In both cases, we observe an order of magnitude increase in the enhancement factor values on moving form monomers (edge effect) to the dimers and oligomers (hybridized plasmons).

3.4. Conclusions

In summary, the anisotropic features of gold nanorods have been successfully utilized for the fabrication of SERS substrates capable of producing enhanced Raman signals. The variation in the Raman intensity of molecules when placed at the edges of an isolated Au nanorod and junctions of Au nanorod dimers were compared. The enhancement in signal of molecules in the former case is due to specific interaction and localization of monothiol molecules at the edges of Au nanorods, which are domains of high electric field. The enhancement in the Raman signal intensity during the various stages of nanochain formation was investigated in detail. A large enhancement in the signal intensity observed during the dimerization step was due to the presence of hot spots. The enhancement factor is an order of magnitude higher when molecules are placed at the junctions ($\sim 10^5$) compared to the edges ($\sim 10^4$). The methodology presented in this chapter can be further extended to the detection of analytes, of significance in environmental health and safety.
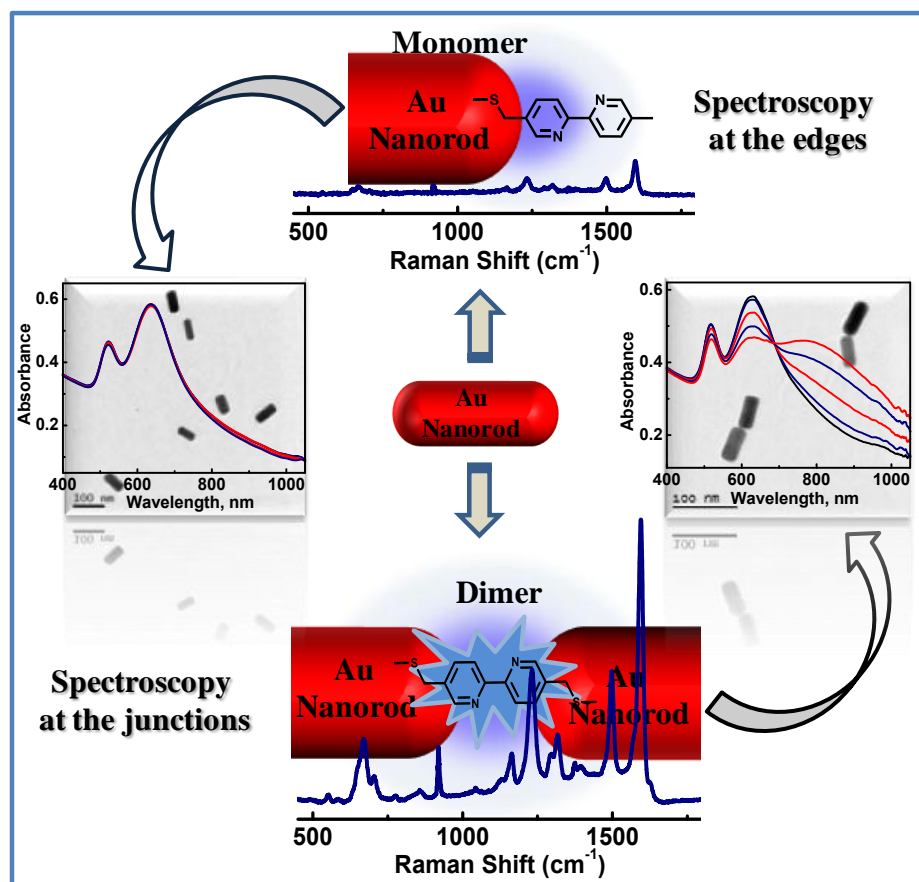
Scheme 3.6. *Schematic representation and TEM images of Au nanorod monomers and dimers with the corresponding extinction and Raman spectral changes during the dimerization process.*

3.5. Experimental Section

3.5.1. Materials and Instrumental Methods

Solvents and reagents used were purified and dried by standard methods. Photophysical studies were carried out using spectroscopic grade solvents. The absorption spectral changes, upon the addition of aromatic dithiols, were recorded in a UV-Visible diode array spectrophotometer (Agilent 8453). Stock solutions of the monothiols and dithiols were prepared in acetonitrile. ^{1}H and ^{13}C NMR spectra were measured on a 300 or 500 MHz Bruker advanced DPX spectrometer. For HRTEM studies, samples were prepared by drop casting dilute solution from the cuvette on a carbon coated Cu grid and the solvent

was allowed to evaporate and specimens were examined on a FEI-Tecnai 30G^{2}S-Twin or

with a 300 kV (JEOL 3010) transmission electron microscope operated at an accelerating

voltage of 300 kV. Raman and SERS spectra were recorded using a HR800 LabRAM

confocal Raman spectrometer operating at 20 mW laser power using a peltier cooled CCD

detector. Raman spectra were collected in a quartz cuvette using a He-Ne laser source

having an excitation wavelength of 633 nm and with an acquisition time of 10 seconds using

a 5x objective. All the studies were carried out in a mixture (4:1) of acetonitrile and water.

The baseline was corrected and the spectra were presented after subtracting the gold nanorod

spectra from the original ones. No noticeable absorption spectral changes were observed for

the nanorod solution during the measurements, confirming that the nanorods remain stable in

solution even after exposure to laser beam.

3.5.2. Synthesis of linker molecules

Synthesis of monothiol derivative, bipy-MT
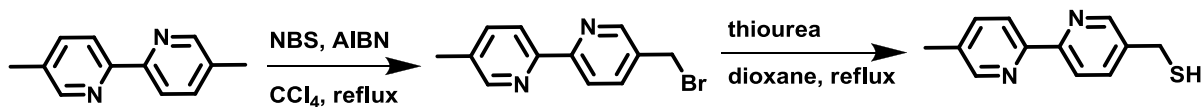
Synthesis of 5-Bromomethyl-5'-methyl-2,2'-bipyridine: 5,5'-Dimethyl-2,2'-dipyridyl

(1.47 g, 8.0 mmol) was dissolved in 30 mL of dry CCl$_4$ and N-bromosuccinimide   (1.42 g,

8.0 mmol) and catalytic amount of AIBN were added. The reaction was heated under reflux

for 2.5 h. The crude product was filtered, when it was hot, to remove the precipitated

succinimide. CCl$_4$ was removed by rotary evaporation and the residue was diluted with

dichloromethane, chromatographed over silica using a mixture (1:19) of ethyl acetate and

dichloromethane to yield the mono-brominated product in 40% yield. ^{1}H NMR (500 MHz,

CDCl$_3$): δ (ppm) 8.66 (d, 1H), 8.50 (d, 1H), 8.36 (d, 1H), 8.29 (d, 1H), 7.84 (s, 1H), 7.63 (s, 1H), 4.53 (s, 2H), 2.40 (s, 3H).

Synthesis of 5-mercaptomethyl-5'-methyl-2,2'-bipyridine: A solution of 5-Bromomethyl-5'-methyl-2,2'-dipyridyl (250 mg, 0.95 mmol) and thiourea (90 mg, 1.18 mmol) in 20 mL dry dioxane was refluxed under N$_2$ for 3 h. To the above solution, NaOH (80 mg, 2 mmol) dissolved in 10 mL of degassed water was added, and the mixture was heated to reflux for another 3 h. The solvent was removed by rotary evaporation, pH adjusted to ~ 4 using HCl, and extracted with CH$_2$Cl$_2$. The organic phase was collected, and the solvent was removed. The residue was column chromatographed over silica using a mixture of (1:48) ethyl acetate and dichloromethane to yield the product as yellow solid in 42% yield. ^{1}H NMR (500 MHz, CDCl$_3$): δ (ppm) 8.59 (d, 1H), 8.49 (d, 1H), 8.33 (d, 1H), 8.27 (d, 1H), 7.99 (s, 1H), 7.63 (s, 1H), 3.80 (s, 2H), 2.42 (s, 3H), 1.82 (t, 1H).

Synthesis of dithiol derivative, bipy-DT
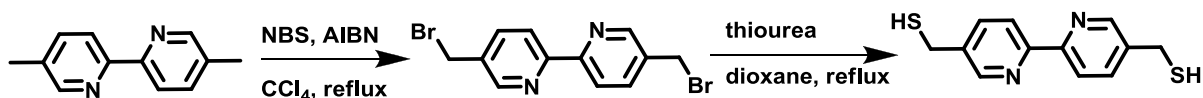
Synthesis of 5,5'-Bis(bromomethyl)-2,2'-bipyridine: (**bipy-DBr**): 5,5'-Dimethyl-2,2'-dipyridyl (500 mg, 2.7 mmol) was dissolved in 30 mL of dry CCl$_4$ and N-bromosuccinimide (1.2 g, 6.7 mmol) and catalytic amount of AIBN were added. The reaction was heated under reflux for 6 h. The crude product was filtered when it was hot to remove the precipitated succinimide. CCl$_4$ was removed by rotary evaporation and the residue was diluted with dichloromethane. The crude product was recrystallized from CH$_2$Cl$_2$ to give the dibrominated product as a white powder in 45% yield. ^{1}H NMR (500 MHz, CDCl$_3$): δ (ppm) 8.59 (s, 2H), 8.32 (d, 2H), 7.78 (d, 2H), 3.80 (s, 2H), 3.7 (s, 3H).

Synthesis of 5,5'-Bis(mercaptomethyl)-2,2'-bipyridine (bipy-DT): A solution of 5,5'-bisbromomethyl-2,2'-bipyridine (200 mg, 0.58 mmol) and thiourea (123 mg, 1.61 mmol) in 20 mL dry dioxane was refluxed under N_2 for 3 h. To the above solution, NaOH (80 mg, 2 mmol) dissolved in 10 mL of degassed water was added, and the mixture was heated to reflux for another 3 h. The solvent was removed by rotary evaporation, pH adjusted to ~4 using HCl and extracted with CH_2Cl_2. The organic phase was collected, and the solvent was removed. The crude product was recrystallized from CH_2Cl_2 to give the product as a white powder in 75% yield. ^{1}H NMR (500 MHz, $CDCl_3$): δ (ppm) 8.61 (s, 2H), 8.35 (d, 2H), 7.81 (d, 2H), 3.81 (s, 2H), 3.7 (s, 2H), 1.83 (t, 2H).

3.5.3. Calculation of Enhancement Factor (EF)

$$EF = [I_{SERS}]/[I_{Raman}] \ x \ [N_{bulk}]/[N_{ads}]$$

I_{bulk} and I_{SERS} correspond to the intensities of the ring deformation band of monothiols/dithiols in the absence and presence on Au nanorod, containing various concentrations of monothiols/dithiols. N_{bulk} and N_{ads} are the number of molecules probed in acetonitrile solution in the absence and presence of Au nanorods.

Au nanorods possess a capsule shape having two hemispherical caps at the two ends of a cylinder and various calculations are carried by following the procedure given in reference 9.

Total surface area of Au nanorod (length = 50.9 nm and diameter =20.1 nm) = ~4700 nm^2

Lateral surface area of nanorod = ~2610 nm^2

Surface area of both edges together = ~2090 nm^2

Footprint of thiol on Au surface = 0.214 nm^2

Maximum number of thiol moieties that can be accommodated on the each edge of a Au nanorod = ~4880

Volume of sample probed   (for depth of focus 1.01 mm) = 168 pL

Concentration of Au nanorod = 0.12 nM

Number of nanorods in 3 mL of the solution = ~2.16 x 10^{11}

Number of nanorods in the probed volume = ~1.2 x 10^4

I. Enhancement Factor using **bipy-DT** as linker

<u>In the absence of nanorods</u>

Number of molecules in the probed volume (90 mM in ACN), N_{bulk} = 9.63 x 10^{11}

Intensity of the ring deformation band of dithiols, **bipy-DT** (90 mM in ACN), I_{bulk} = 740

Intensity of the ring deformation band of monothiol, **bipy-MT** (90 mM in ACN), I_{bulk} = 760

<u>In the presence of nanorods</u>

Number of thiol molecules at each edge during incubation step = ~2100 (based on rod to molecular ratio)

Number of thiols in the probed volume (adsorbed on nanorods) during incubation step (0.5 µM), N_{ads} = ~50,400 (value corresponding to 1.2 x 10^4 rods)

No. of thiol molecules at each edge during dimerization and oligomerization step = ~3300 (based on rod to molecular ratio)

Number of thiols in the probed volume (adsorbed on nanorods) during dimerization and oligomerization step (0.8 µM), N_{ads} = ~7.9 x 10^7 (value corresponding to 1.2 x 10^4 rods)

Intensity of the ring deformation band of dithiols (**bipy-DT**) during incubation step (0.5 µM), I_{SERS} = 946

Intensity of the ring deformation band of dithiols (**bipy-DT**) during the dimerization step (0.8 µM), I_{SERS} = 8586

Intensity of the ring deformation band of dithiols (**bipy-DT**) during the oligomerization step (0.8 µM), I_{SERS} = 9258

EF (incubation) = [I_{SERS}]/ [I_{Raman}] X [N_{bulk}]/ [N_{ads}]

$$= 946 \text{ x } 9.63 \text{ x } 10^{11} / 740 \text{ x } 5.0 \text{ x } 10^7 = \mathbf{2.44 \text{ x } 10^4}$$

EF (dimerization) = $8586 \text{ x } 9.63 \text{ x } 10^{11} / 740 \text{ x } 7.9 \text{ x } 10^7 = \mathbf{1.41 \text{ x } 10^5}$

EF (oligomerization) = $9258 \text{ x } 9.63 \text{ x } 10^{11} / 740 \text{ x } 7.9 \text{ x } 10^7 = \mathbf{1.52 \text{ x } 10^5}$

Intensity of the ring deformation band of dithiols for monothiol **bipy-MT** (0.5 μM),

I_{SERS} = 1018

EF (monothiol, 0.5 μM) = $1018 \text{ x } 9.63 \text{ x } 10^{11} / 760 \text{ x } 5.0 \text{ x } 10^7 = \mathbf{2.56 \text{ x } 10^4}$

II. Enhancement Factor using **bz-DT** as linker

In the absence of nanorods

Number of molecules in the probed volume (50 mM in ACN), $N_{bulk} = 5.05 \text{ x } 10^{12}$

Intensity of the ring deformation band of dithiols, **bz-DT** (50 mM in ACN), I_{bulk} = 351

Intensity of the ring deformation band of monothiol, **bz-MT** (50 mM in ACN), I_{bulk} = 421

In the presence of nanorods

No. of thiol molecules at each edge during incubation step = ~2100 (based on rod to

molecular ratio)

Number of thiols in the probed volume (adsorbed on nanorods) during incubation step (0.5

μM), N_{ads} = ~5.0 x 10^7 (value corresponding to 1.2 x 10^4 rods)

No. of thiol molecules at each edge during dimerization and oligomerization step = ~4100

(based on rod to molecular ratio)

Number of thiols in the probed volume (adsorbed on nanorods) during dimerization and

oligomerization step (1.0 μM), N_{ads} = ~9.8 x 10^7 (value corresponding to 1.2 x 10^4 rods)

Intensity of the ring deformation band of dithiols (**bz-DT**) during incubation step (0.5 μM),

I_{SERS} = 151

Intensity of the ring deformation band of dithiols (**bz-DT**) during the dimerization step (1.0 µM), $I_{SERS} = 1041$

Intensity of the ring deformation band of dithiols (**bz-DT**) during the oligomerization step (1.0 µM), $I_{SERS} = 1310$

EF (incubation) $= [I_{SERS}]/ [I_{Raman}]$ x $[N_{bulk}]/ [N_{ads}]$

$$= 151 \text{ x } 5.05 \text{ x } 10^{12} / 351 \text{ x } 5.0 \text{ x } 10^7 = \textbf{4.31 x 10}^{\textbf{4}}$$

EF (dimerization) $= 1041 \text{ x } 5.05 \text{ x } 10^{12} / 351 \text{ x } 9.8 \text{ x } 10^7 = \textbf{1.52 x 10}^{\textbf{5}}$

EF (oligomerization) $= 1310 \text{ x } 5.05 \text{ x } 10^{12} / 351 \text{ x } 9.8 \text{ x } 10^7 = \textbf{1.91 x 10}^{\textbf{5}}$

Intensity of the ring deformation band of monothiol **bz-MT** (0.5 µM), $I_{SERS} = 288$

EF (monothiol, 0.5 µM) $= 288 \text{ x } 5.05 \text{ x } 10^{12} / 421 \text{ x } 5.0 \text{ x } 10^7 = \textbf{6.85 x 10}^{\textbf{4}}$

Lateral Assembly of Gold Nanorods and Creation of Quartets for Raman Signal Enhancement
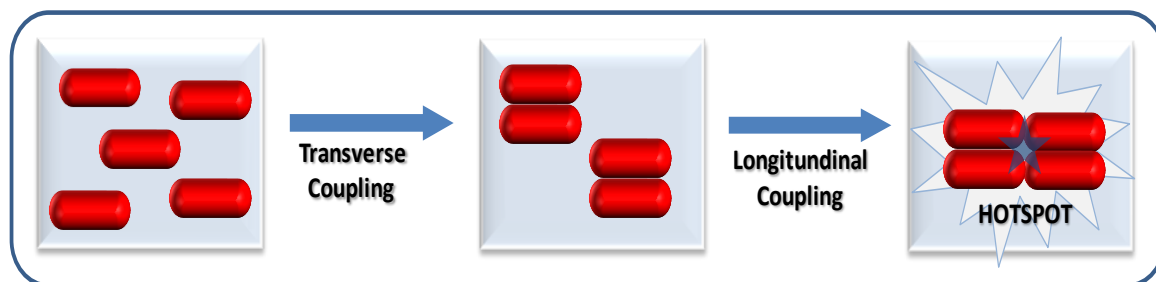
4.1. Abstract

A new methodology has been developed for the controlled lateral assembly of gold nanorods using a linker which possesses hydrophobic and hydrophilic moieties. The extinction spectral changes during the assembly were monitored as a function of time and aspect ratio of Au nanorods. It was observed that the lateral assembly proceeds through dimers, trimers and tetramers to larger assembly and the number of nanorods assembled can be controlled by varying the concentration of the linker molecule. It was also found that the extent of lateral coupling increases with the increase in aspect ratio of Au nanorods. Quartets of Au nanorods were fabricated by combining the methodologies of lateral and longitudinal assembly. The molecules placed at this quartet junction showed higher Raman signal enhancement compared to the dimeric junctions. When four nanorods are brought close to form the quartet junction, their plasmons couple with each other, forming a region of enhanced electric field and molecules placed at these quartet junctions showed substantial enhancement in Raman signal intensity.

4.2. Introduction

Stepwise integration of nanomaterials into higher-order assemblies and tuning their optoelectronic properties is one of the main objectives of research in the area of nanaoscience and nanotechnology [Shipway 2000, Kamat 2002, Shenhar 2003 and Thomas 2003]. More recent efforts are focused on the integration of various nanoscale building blocks such as nanoparticles, nanorods and nanotubes into organized assemblies. [Nikoobakht 2000 and Dujardin 2001]. Various theoretical methods have been utilized for investigating electromagnetic interactions in arrays of spherical nanoparticles by varying their particle size, array spacing and array symmetry [Zhao 2003 and Zhong 2004]. These aspects were experimentally verified by linking nanoparticles into nanochains [Yoshikawa 2004 and Lin 2005]. Such closely packed metal nanoparticles and nanorods can, in principle, function as waveguides of electromagnetic radiation [Maier 2002 and Maier 2003] allowing miniaturization of devices below the diffraction limit [Gittins 2000, Huang 2001 Kovtyukhova 2001 and Mokari 2004]. The isotropic nature of spherical nanoparticles prevents the selective binding of molecules onto their surface through chemical functionalization methods, leading to random aggregation [Thomas 2003 and Jackson 2004]. However, the anisotropic features of gold nanorods were successfully utilized for their one dimensional organization [Gluodenis 2002 and Joseph 2006] and these aspects are discussed below.

Various strategies have been adopted for the linear assembly of Au nanorods in an end-to-end fashion. This includes the (i) linear organization of gold nanorods using biotin-streptavidin connectors [Caswell 2003], (ii) longitudinal assembly through cooperative intermolecular hydrogen bonding/electrostatic interaction by using molecules such as 3-

mercaptopropionic acid [Thomas 2004], cysteine and glutathione [Sudeep 2004], (iii) linear organization of Au nanorods using covalent interactions with dithiols as linkers [Joseph 2006], (iv) end-to-end electrostatic assembly of Au nanorods on multiwall carbon nanotubes [Correa-Duarte 2005] and (v) linear assembly of Au nanorods induced by 4-mercaptopyridine [He 2011]. However, there are only a few reports in the literature on the side by side assembly of Au nanorods. In most cases, these organizations lead to the uncontrolled aggregation. The lateral self-assembly of Au nanorods driven by DNA [Pan 2007], citrate [McLintock 2011], EDTA [Sreeprasad 2011], lipids [Nakashima 2008] and biotin-streptavidin [Gole 2005 and Wang 2007] as connectors has been demonstrated earlier. Most of the chemical methods utilize the electrostatic interaction of negatively charged molecules with positively charged CTAB present on the nanorod surface leading to side-by-side aggregation of nanorods. Lateral assembly of gold nanorods in solution using citrate as the aggregating agent was demonstrated by Wark and co-workers [McLintock 2011]. A Raman reporter dye namely, diethylthiatricarbocyanine iodide (DTTCI) was inserted into nanorod assembly and these clusters were further stabilized by coating with a polymer layer. It was found that these clusters act as efficient substrates in SERS (Scheme 4.1).
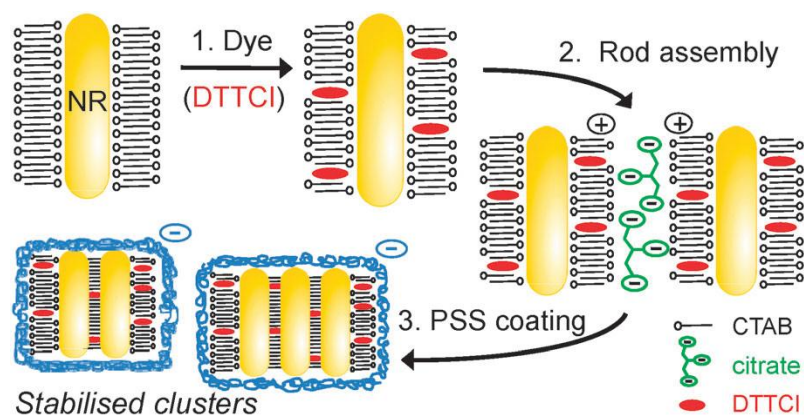
Scheme 4.1: *Schematic representation illustrating the preparation and stabilisation of self-assembled gold nanorod-dye clusters [McLintock 2011].*

UV light induced ladder-like arrangement of poly(vinylpyrrolidone) (PVP) stabilized Au nanorods using N-methyl-2-pyrrolidone (NMP) as solvent, has been demonstrated by Liz-Marzan and co-workers [Grzelczak 2012]. UV irradiation induces formation of radicals in solvent molecules, which then promote cross-linking of PVP chains on the surface of adjacent particles leading to the formation of ladder-like assemblies of Au nanorods (Figure 4.1A). The ladder-like arrangement of Au nanorods was followed by monitoring the extinction spectral changes (Figure 4.1B) and the TEM images (Figure 4.1C).
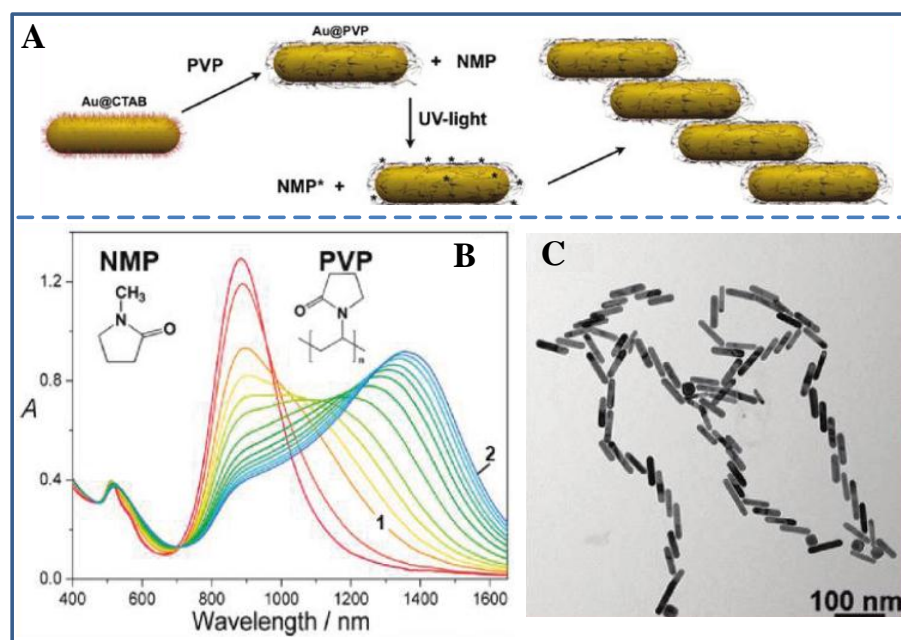
Figure 4.1. *(A) Schematic representation of UV-light induced gold nanorod assembly. (B) Extinction spectra showing the changes in the longitudinal surface plasmon resonance band with time (the chemical structures of PVP and NMP are shown in the inset). (C) TEM images demonstrating the formation of ladder-like assemblies [Grzelczak 2012].*

The lateral as well as linear assembly of Au nanorods have been utilized for the detection of amino acids, peptides, proteins and biomolecules. Both linear as well as lateral assembly of the Au nanorods were utilized by Kotov and co-workers for the detection of environmental toxin, namely microcystin-LR (MC-LR) in nanomolar quantities [Wang

2010]. The sides and ends of nanorods were modified and the assembly was achieved by using complimentary antibody-antigen interaction. The type of assembly depends on the modification of nanorod surface with MC-LR antibodies. One type of nanorod carried the antibodies preferentially on the sides, while the other type carried antibodies at the ends. Attachment of antibodies at the sides was primarily achieved through the electrostatic binding due to the larger area of contact at the lateral faces. Covalent attachment of antibodies at the ends is mediated by a bifinctional linker, thioctic acid, through the formation of S-Au bond. The high reactivity and better accessibility of thiols towards the ends of nanorods facilitates the conjugation of antibodies preferentially at the ends of the nanorods. Similar strategy was adopted for the modification of nanorods with MC-LR OVA antigen. On mixing the nanorod solutions, side-by-side (Scheme 4.2A) and end-to-end (Scheme 4.2B) assembled nanostructures were obtained depending on the type of modification on nanorods.
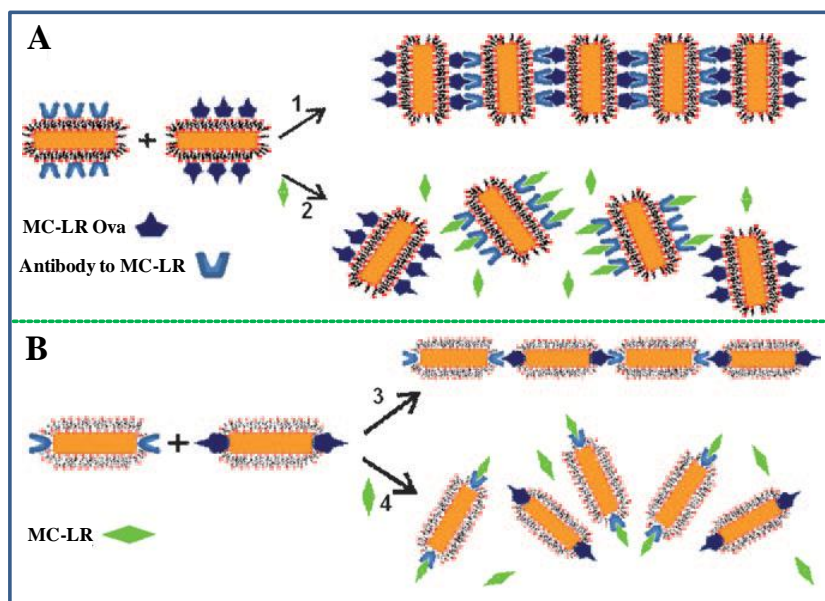
Scheme 4.2. *Toxin detection method with (A) side-by-side and (B) end-to-end nanorod assemblies. The numbers 1–4 denote routes for nanorod assembly [Wang 2010].*

Theoretical aspects dealing with the electrodynamic responses of assembled nanoparticles of various size and shape, have been discussed in detail by Schatz and coworkers [Hao 2004]. Using Au nanorods as specific examples, Gluodenis and Foss have proposed the effect of mutual orientation of nanorod-nanorod on the plasmon resonance spectra at different distances by involving a simple quasistatic treatment [Gluodenis 2002]. Longitudinal plasmon band of Au nanorods are influenced by the way in which they interact: linear assembly result in a red shifted band and lateral assembly result in the formation of a blue shifted band (Figure 4.2A). The lateral assembly yields more pronounced spectral changes as the aspect ratio of nanorods increases (Figures 4.2B, 4.2C and 4.2D).
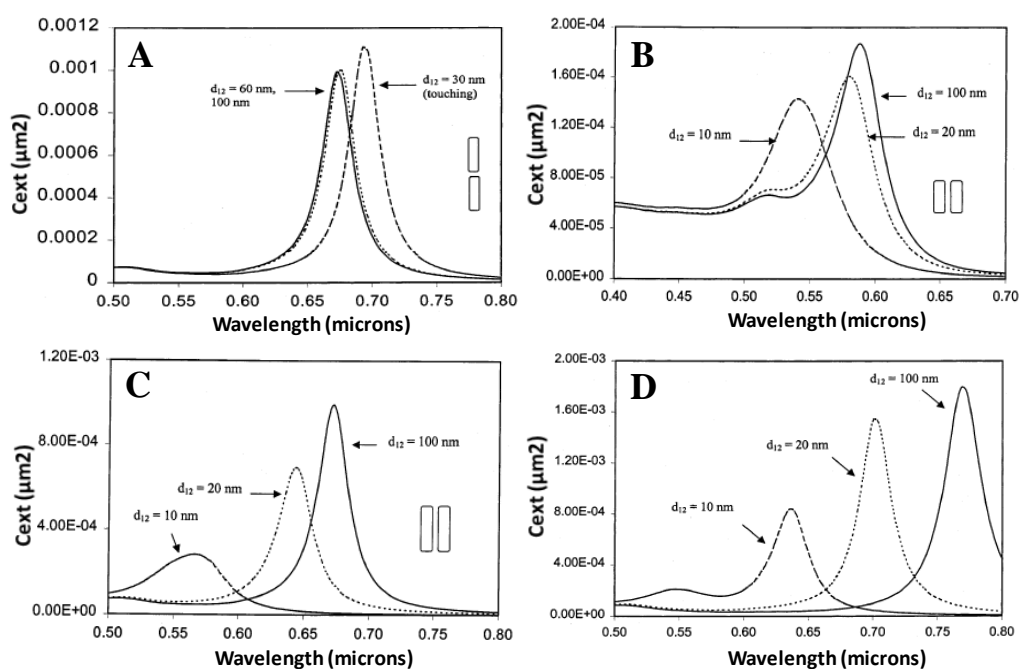
Figure 4.2. *(A) Calculated spectra of two medium length rods (a = 15 nm, b = 5 nm) interacting end-to-end at d_{12} 30 nm (touching), 60 nm, and 100 nm (isolated). Calculated spectra of two rods interacting side-to-side at varying d_{12} lengths of 10, 20 and 100 nm with different lengths: (B) short rods (a = 10 nm, b = 5 nm); (C) medium rods (a = 15 nm, b = 5 nm); (D) long rods (a = 20 nm, b = 5 nm).(Note: a – length of the rod, b – width of the rod, $d_{1,2}$ – distance between the centers of two rods) [Gluodenis 2002].*

As discussed in the previous chapters, both the variation of optical signal arising from plasmon resonance and enhanced spectroscopic signals resulting from the electric field on the surface of nanoparticle can be utilized for the selective detection of various analyte molecules. In comparison with spherical nanoparticles having their field uniformly distributed around the surface, Au nanorods possess enhanced electric field at the edges. These aspects have been theoretically demonstrated by Wang and co-workers by comparing the field intensity distribution in nanoparticles, nanorods and nanobipyramids [Kou 2007]. The high electric field at the edges has been utilized for obtaining enhanced Raman signal intensities from molecules placed at the edges of isolated Au nanorods and dimer junctions. These aspects are presented in chapter 3.

Significant progress has been achieved in this decade on the design and fabrication of wide variety of substrates for SERS. Major research in this field is focused on the design of reproducible nanoparticle assemblies capable of producing large Raman signal enhancement. Herein, we report the controlled lateral organization of Au nanorods and investigated the variation in their plasmon resonance. Nanorod quartets were designed by the controlled lateral and longitudinal assembly of Au nanorods and their use as SERS substrates have been investigated.

4.3. Results and Discussion

Gold nanorods were synthesized by following a photochemical method and excess capping agents were removed by two repeated centrifugations at 5000 rpm for 15 min [Kim 2002]. Au nanorods having aspect ratio of 3.0 were suspended in a mixture (1:4) of water and acetonitrile and used for investigating the lateral assembly. Au nanorods remain stable for several hours in water and mixtures of water and acetonitrile containing more than 70%

acetonitrile. This is due to the large zeta potential (ζ) of Au nanorods: in water ζ value was found to be 28.5 mV and in a mixture (1:4) of water and acetonitrile ζ value was reported as -28.8 mV [Pramod 2008]. Au nanorods, having an aspect ratio of ~3.0, possess two distinct surface plasmon absorption bands (Figure 4.3). The short wavelength band at 520 nm corresponds to the transverse mode of plasmon oscillation and the long wavelength band at 700 nm corresponds to the longitudinal mode of oscillation.

4.3.1. Lateral assembly of Au nanorods

There are a few reports in the literature dealing with the lateral assembly of Au nanorods. These studies have shown that the linker molecules play an important role in bringing the nanorods in a lateral fashion [Pan 2007, McLintock 2011, Sreeprasad 2011, Nakashima 2008, Gole 2005 and Wang 2007]. Gao and coworkers utilized the electrostatic interactions between negatively charged DNA molecules and positively charged Au nanorod surface for the lateral assembly of Au nanorods [Pan 2007], whereas, Murphy and co-workers could assemble nanorods in a side-by-side fashion by varying the pH of the medium [Orendorff 2005]. The main objective of the present investigation is to develop newer methods for organizing nanorods in a lateral fashion. To achieve effective lateral organization, the linker molecules should be compatible with the surface capping agent and they should bind on to the lateral surface. Zeta potential (ζ) studies have provided a better understanding on the organization of surface capping agent on the surface of Au nanorod in various solvent systems. Au nanorods are covered with a bilayer of CTAB in water which reorganizes to monolayer in acetonitrile rich solvents. Charge reversal from positive to negative ζ was observed on increasing the CH_3CN content. The reorganization of capping agent results in the reversal of ζ and a schematic representation is shown below (Scheme

4.3B). The linker molecule used in the present study possesses both hydrophilic and hydrophobic moiety having a thiol group attached on the hydrophobic end (Scheme 4.3A). The selection of the linker molecule is based on the fact that the alkyl group penetrates into the hydrophobic pocket of CTAB layer and bind onto the surface of nanorod whereas the ethylene glycol chain is exposed to polar solvent.
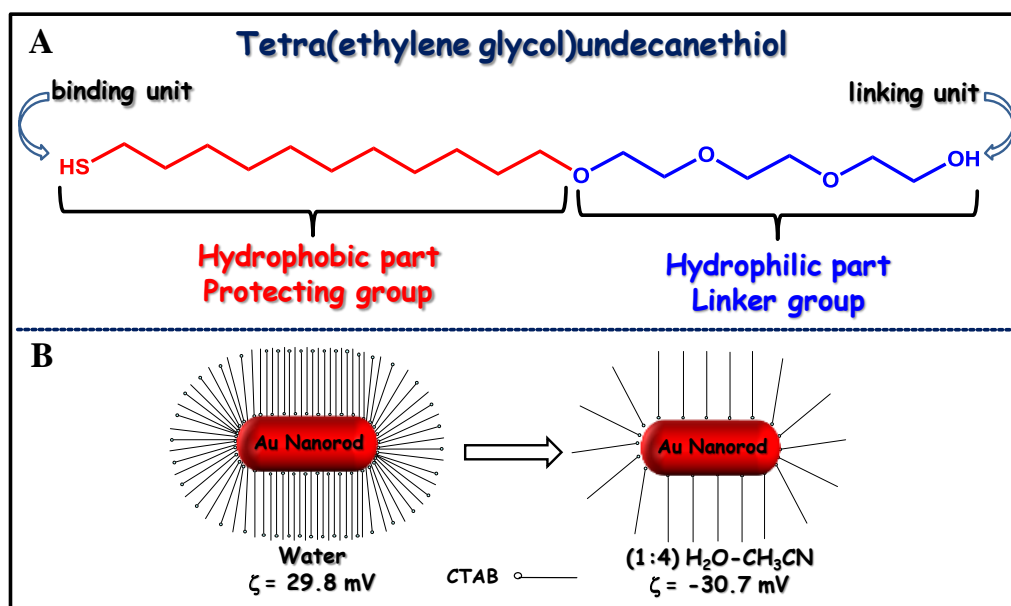
Scheme 4.3. *(A) Molecular structure of the linker molecule, tetra(ethylene glycol)undecanethiol (**TEGU**) possessing both hydrophobic and hydrophilic parts. The thiol group binds to the surface of Au nanorods and the hydroxyl group acts as the linking moiety, bring two nanorods close together in a lateral fashion through multiple hydrogen bonding. (B) Schematic representation showing the presence of CTAB bilayer on the surface of Au nanorods in water which collapses to monolayer on changing the solvent composition to a mixture (1:4) of water and acetonitrile.*

We have investigated the effect of addition of linker molecule tetra(ethylene glycol)undecanethiol (**TEGU**) on the extinction spectrum of Au nanorods. Microliter quantities of ligands were added to Au nanorods in a mixture (1:4) of water and acetonitrile. Solutions were kept for 5 min and the extinction spectral changes were recorded as a

function of time. Both the longitudinal as well as the transverse plasmon band of Au nanorods remain unaffected on addition of lower concentrations of linker molecule (<5 µM). Interestingly, both the plasmon bands underwent dramatic changes on increasing in the concentration of the ligand to 10 µM. The longitudinal plasmon band of Au nanorod underwent a hypsochromic shift with a decrease in intensity and the transverse plasmon band underwent a bathochromic shift with an increase in intensity. The spectral changes of Au nanorods, recorded at various time intervals, are presented in Figure 4.3. It was found that the extinction spectral changes were pronounced and spontaneous on further increasing the concentration of linker molecules (20 µM).
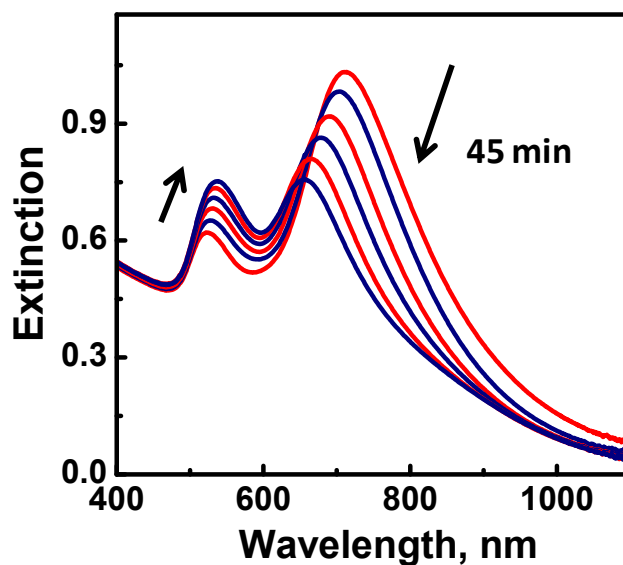
*Figure 4.3. Extinction spectral changes of Au nanorods upon addition of 10 µM of the linker molecule (**TEGU**) in a mixture (1:4) of water and acetonitrile.*

It is well established that the plasmon oscillations of Au nanoparticle, when brought in close contact, undergo spectral changes and these aspects were explained using plasmon hybridization model [Prodan 2003]. As discussed earlier, nanorods possess transverse as well as longitudinal plasmon oscillations [Joseph 2006]. Each of these modes, in principle,

can couple with plasmon oscillations of the neighbouring rods. In the present investigation, we observe a coupling of the transverse as well as longitudinal plasmon bands. Recently, El-Sayed and co-workers have theoretically calculated the optical spectra of the assemblies of Au nanorods (dimers and trimers) using the discrete dipole approximation (DDA) method [Jain 2006]. Optical spectra calculated for the lateral assembly of nanorods showed a blue shift of the longitudinal plasmon band and a red shift of the transverse plasmon band. In another report, Mulvaney and co-workers used both experimental and theoretical methods to determine the scattering spectra of individual gold nanorod dimers arranged in lateral as well as longitudinal fashion [Funston 2009]. The scattering spectra of the linearly assembled rods are dominated by an intense peak which is red-shifted compared to individual nanorods. In contrast, the spectra of rod dimers aligned in a lateral configuration displayed a single peak with scattering intensity comparable to that for a single rod. In order to gain further insight on the way in which nanorods interact, we have investigated the time dependent extinction spectral changes of Au nanorods on addition of linker molecule and investigated their morphological changes using TEM.

4.3.2. Lateral assembly as a function of time

The extinction spectral changes of Au nanorods on addition of 10 μM of linker molecule and the corresponding TEM images of nanorods at various stages are presented in Figure 4.4. TEM grids containing Au nanorods were prepared by drop casting 75 μL of the solution used for spectroscopic investigation onto a carbon coated copper grid. It is observed that immediately after the addition of the ligand, extinction spectral changes were not observed and Au nanorods were found to be randomly distributed on the grid (Figure 4.4A and 4.4E). After 15 minutes, longitudinal band underwent a hypsochromic shift of 18 nm

and a bathochromic shift of 6 nm in the transverse band was observed (Figure 4.4B). Interestingly, TEM analysis at this stage showed the presence of laterally arranged dimers which are uniformly distributed throughout the grid (Figure 4.4F). TEM images after 30 min showed the formation of trimers with a small amount of tetramers (Figure 4.4G). A hypsochromic shift of 30 nm in the longitudinal plasmon band and a bathochromic shift of 12 nm in the transverse plasmon band (Figure 4.4C) were observed at this stage. Arrays of gold nanorod which are laterally assembled could be seen throughout the grid after 45 min of addition of the linker molecule (Figure 4.4H) and the spectral shifts become more prominent: hypsochromic shift of 40 nm in the longitudinal band and bathochromic shift of 20 nm in the transverse band (Figure 4.4D).
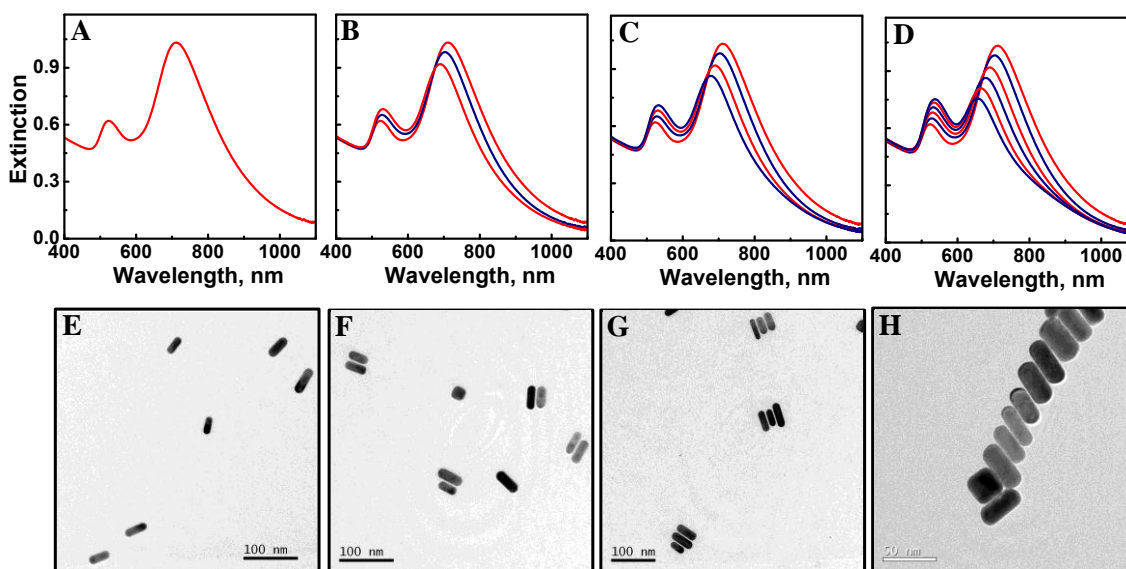
Figure 4.4.*Extinction spectral changes (A-D) and the corresponding TEM images (E-H) of Au nanorods recorded at various time intervals after the addition of **TEGU** (A,E) 0 min, (B,F) 15 min, (C,G) 30 min and (D,H) 45 min.*

The time dependent studies shows that the lateral assembly of nanorods is relatively slow compared to longitudinal assembly. Morphological investigations at various stages

indicate that the lateral assembly proceeds through the formation of dimers, which subsequently assemble to trimers and tetramers and finally to arrays of nanorods assembled in lateral fashion. The TEM images of nanorod assemblies at various time intervals are presented in Figure 4.5. The lateral assembly of nanorods can also be controlled by varying the concentration of the linker molecule. Thus, we have developed a simple and convenient method for the lateral assembly Au nanorods in a stepwise fashion, by using a linker molecule which possesses both hydrophobic and hydrophilic moieties.
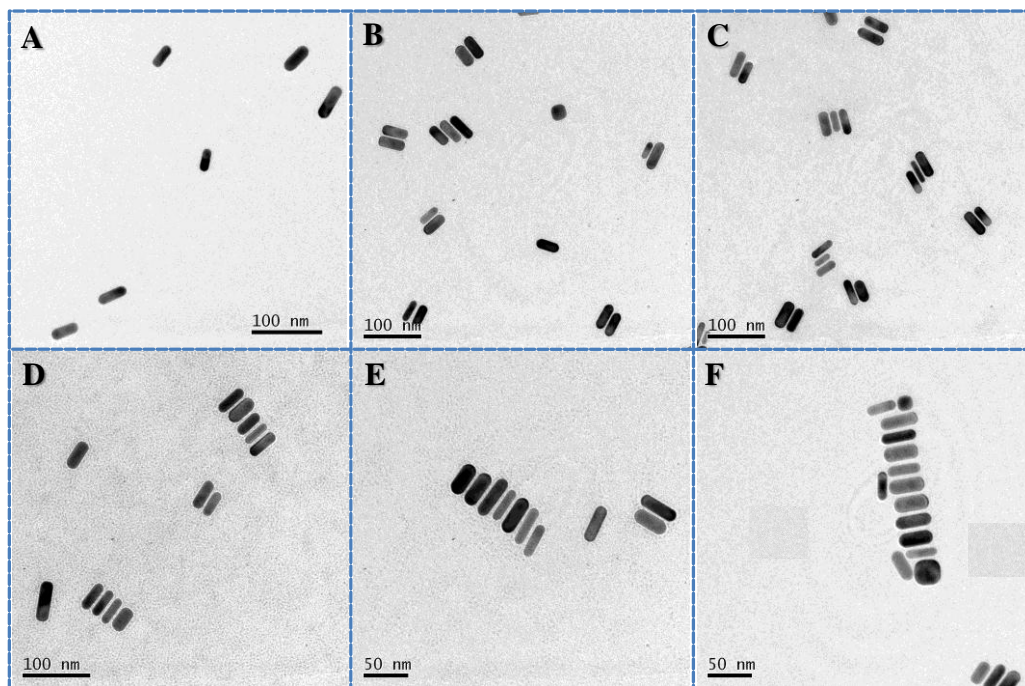
Figure 4.5. *TEM images of gold nanorods recorded at various time intervals after the addition of 10 μM **TEGU**. (A) 0 min, (B) 10 min, (C) 20 min, (D) 30 min, (E) 40 min and (F) 50 min.*

The linker molecule used in the present study possesses several functions. The thiol group at one end binds to the nanorod surface which is covered by a monolayer of CTAB. The hydrophobic interactions between the alkyl chains of linker molecules and the CTAB molecules can further impart stability. The tetraethylene glycol moiety of the linker

molecule, which is hydrophilic in nature, can impart solubility to nanorods (Scheme 4.3A). Multiple hydrogen bonding is primarily responsible for the lateral organization of nanorods. The terminal hydroxyl groups of the linker molecules bound onto the nanorods can undergo hydrogen bonding with the oxygen atom on the ethylene glycol units present on the adjacent nanorod (Scheme 4.6).

The spectral changes observed in the present study can be explained on the basis of plasmon hybridization model developed by Nordlander and coworkers [Prodan 2003, Nordlander 2004] later applied to nanorods by Mulvaney and co-workers [Funston 2009]. The plasmon hybridization model provides detailed understanding on the energies and the extinction cross sections of the plasmons in a nanorod dimer. The model has been utilized by different groups to study the coupling between various nanostructures such as spherical nanoparticles, core-shell nanoparticles and nanorods. The dimer plasmons can be treated as bonding and antibonding plasmons resulting from the linear combinations of individual nanorod plasmons. In the case of nanorods aligned in a lateral fashion, the individual monomer plasmons hybridize giving rise to two modes, one of which remains as dark mode. For longitudinal polarization, the higher energy mode is active (bright mode) and the lower energy mode remains as the dark mode (Scheme 4.4A), whereas for polarization along the transverse axis, the lower energy mode is active (bright mode) and the higher energy mode remains as the dark mode (Scheme 4.4B). Hence, we observe a blue shift in the longitudinal plasmon band and a red shift in the transverse plasmon band during the side-by-side assembly of Au nanorods.
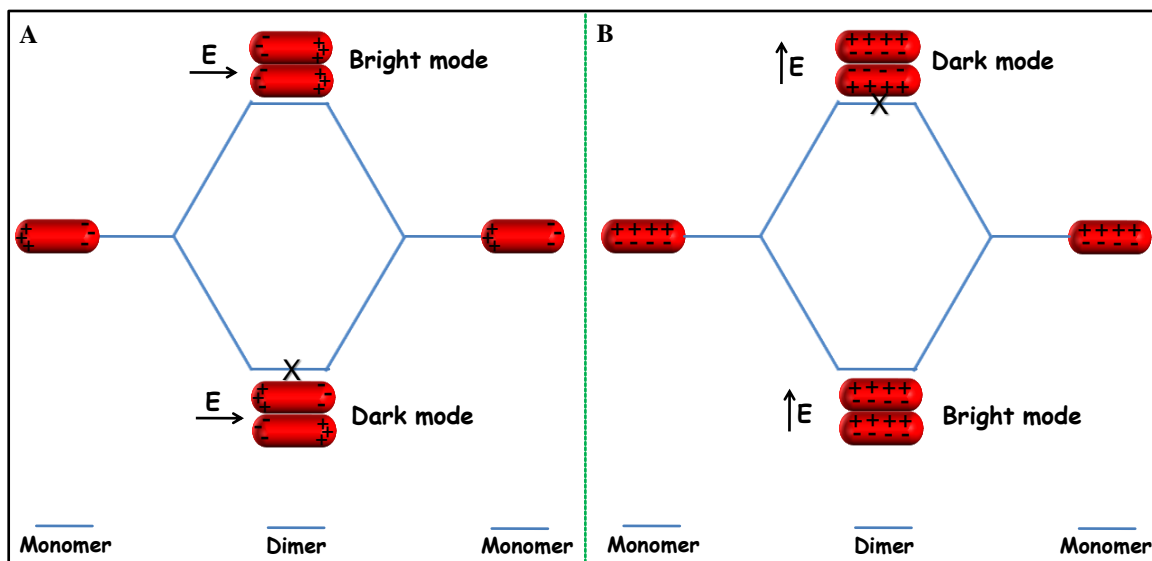
Scheme 4.4. *Schematic illustration of the plasmon hybridization model of laterally assembled Au nanorod dimers during (A) longitudinal and (B) lateral polarizations.*

4.3.3. Dependence on aspect ratio

Further we have investigated the effect of aspect ratio of the nanorods on the plasmon coupling during their lateral organization and the results are presented in Figure 4.6. In an earlier report, Foss and coworkers have theoretically proposed that the lateral orientation of nanorods results in more pronounced spectral changes with increasing aspect ratio of the nanorod. In the present study, we have observed that the longitudinal plasmon band underwent a hypsochromic shift of 20 nm on addition of 10 µM of the ligand in case of Au nanorods having aspect ratio of 2.3. However, under similar conditions, the shift was more pronounced (60 nm) for nanorods having aspect ratio of 3.2. The lateral interaction of the nanorods substantially increases with increase in aspect ratio of the nanorod. The pronounced shift in the longitudinal plasmon band can be explained based on stronger dipolar coupling as illustrated in Scheme 4.5 using the plasmon hybridization model.
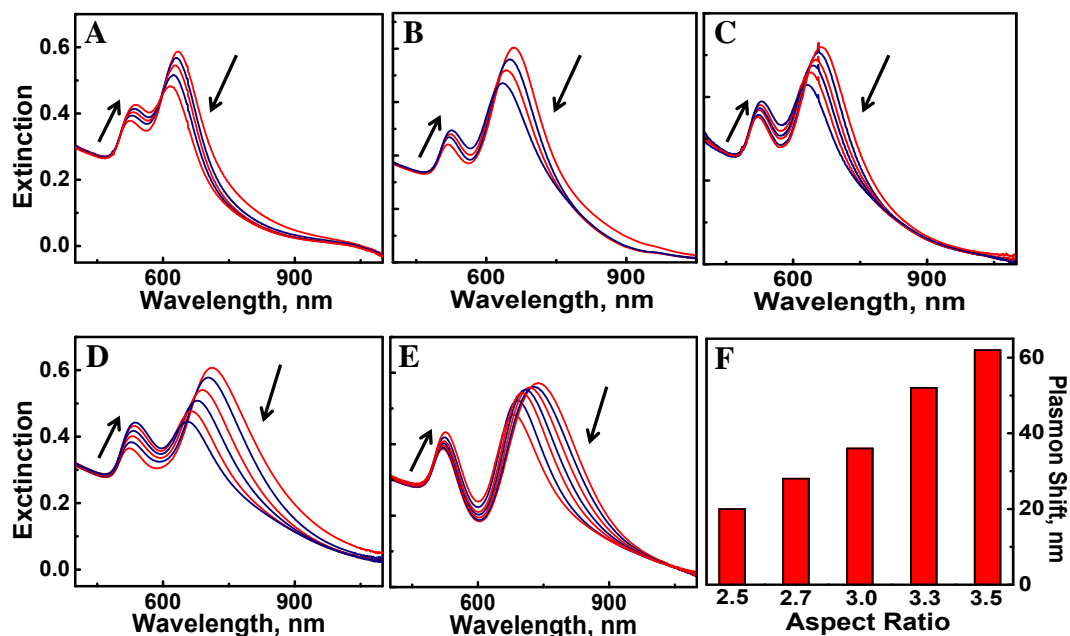
Figure 4.6. *Extiction spectral changes of Au nanorods on addition of 10 μM **TEGU** to Au nanorods with aspect ratio (A) 2.2, (B) 2.5, (C) 2.7, (D) 3.0, (E) 3.3 in a mixture (1:4) of water and acetonitrile. (F) Blue shift in longitudinal plasmon band plotted as a function of aspect ratio of the nanorod.*
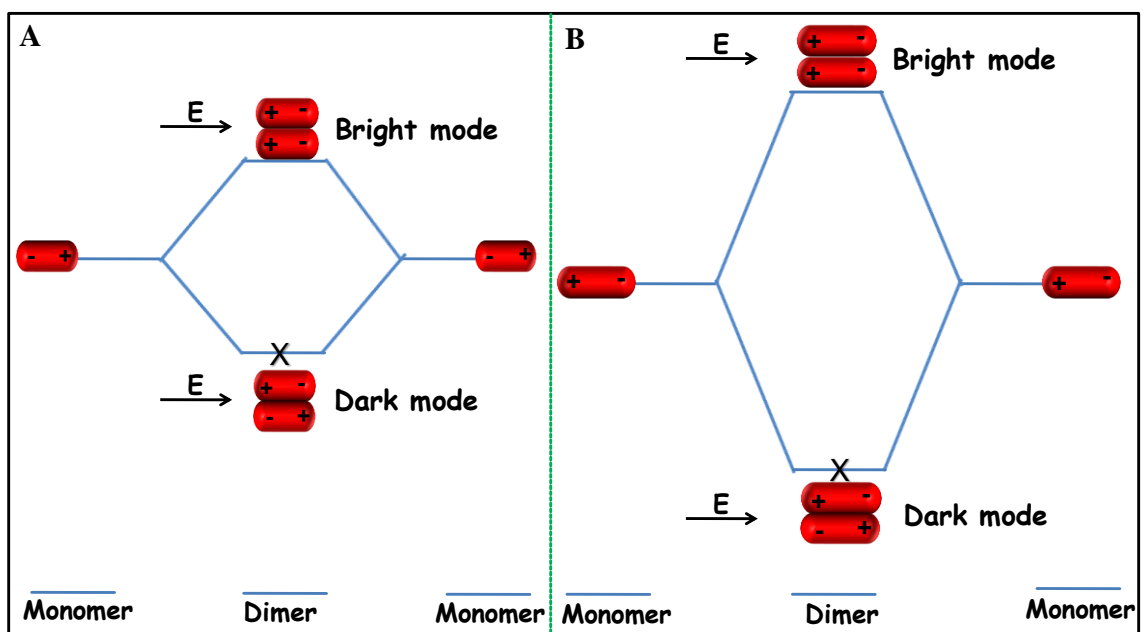
Scheme 4.5. *Illustration of the plasmon hybridization model during longitudinal polarization of laterally assembled Au nanorod dimers of (A) lower aspect ratio and (B) higher aspect ratio.*

4.3.4. Design of quartets

The strong electric fields prevailing on the surfaces of higher order plasmonic assemblies can substantially enhance Raman spectroscopic signals of analyte molecules. Attempts were made to design such two dimensional plasmonic nanostructures (for e.g., quartets) through step wise organization of nanorods by following two approaches. In the first case, nanorods were organized in the lateral fashion and further the longitudinal assembly of laterally arranged dimers was achieved through the addition of an aromatic dithiol, namely 5,5'-bis(mercaptomethyl)-2,2'-bipyridine (**bipy-DT**). The linker molecules (**TEGU**; 8 µM) were first added to Au nanorod solution for assembling them in lateral fashion and extinction spectral changes were followed (Figure 4.7B). To the above solution, 0.6 µM of **bipy-DT** was added at a stage were spectral changes corresponds to formation of lateral dimers (confirmed independently using TEM analysis; Figure 4.7E). Spontaneous decrease in the intensity of the longitudinal surface plasmon band with concomitant formation of a new red shifted band in the near-infrared (NIR) region, marked through a clear isosbestic point, was observed (Figure 4.7C). The extinction spectral changes clearly indicate that the lateral dimers are further brought together in an end-to-end fashion through dithiol linkage. The TEM images showed the formation of nanorod quartets distributed at various locations of the grid (Figures 4.7F and 4.8). The solution is dilute and hence, after assembly, it is difficult to locate more than one quartet in a frame.
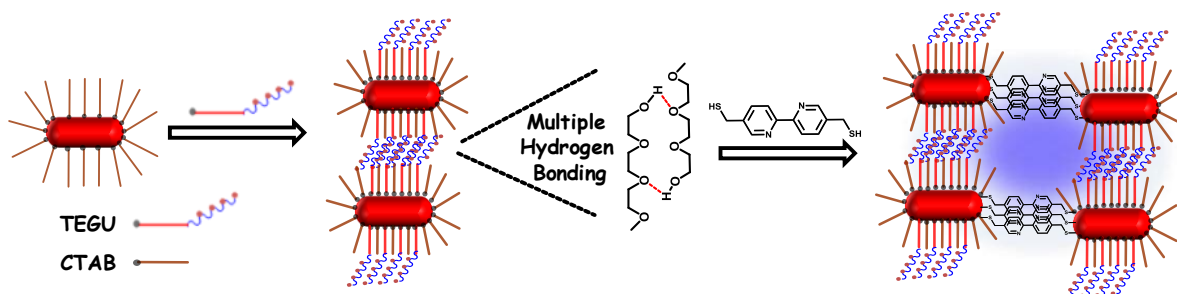
Scheme 4.6. *Schematic representation of quartet formation through the combination of lateral and longitudinal assembly processes.*
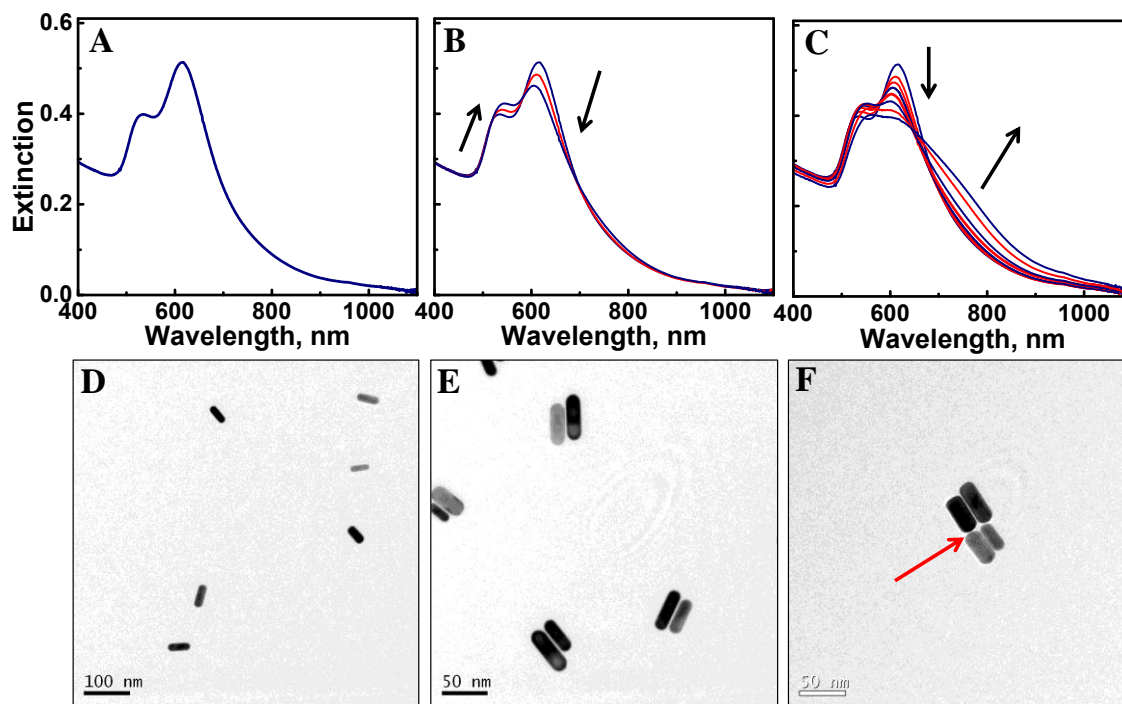
Figure 4.7. *Extinction spectral changes (A,B,C) and TEM images (D,E,F) of Au nanorod at various stages of quartet formation. (A,D) monomers, (B,E) lateral dimers formed on addition of* ***TEGU*** *(8 μM) and (C,F) quartets formed through the addition of 0.6 μM of* ***bipy-DT*** *(when the spectral changes corresponds to the formation of lateral dimers). All studies were carried out in a mixture (1:4) of water and acetonitrile.*
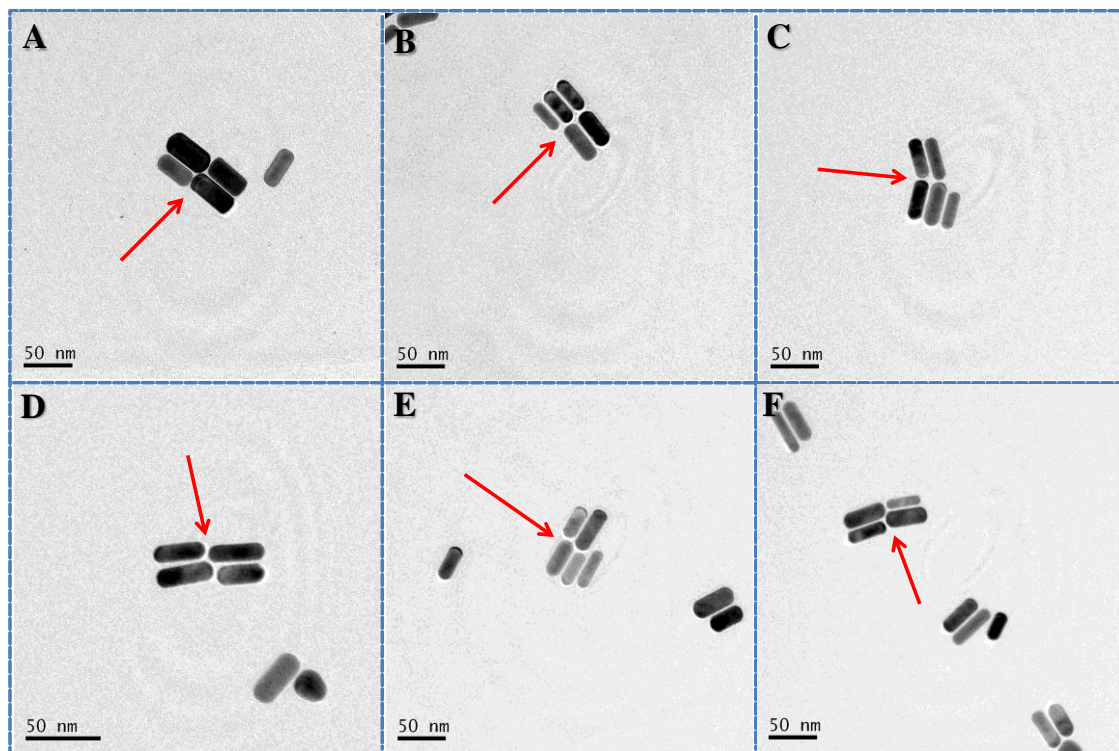
Figure 4.8. *TEM images of Au nanorod quartets formed by the combination of lateral and longitudinal assembly processes. Images are from various locations of the grid (note: solution is dilute and hence it is difficult to locate more than one quartet in a frame after assembly).*

In the second approach, the quartet formation was achieved in a reverse order: linear dimers were first prepared and further organized laterally. The extinction spectral changes and the TEM images at various stages of quartet formation are shown in Figure 4.9. Initially, the nanorods were assembled in linear fashion by adding **bipy-DT** (0.6 μM) as the linker. The decrease in the intensity of longitudinal plasmon band with the concomitant formation of a new red shifted band, through a clear isosbestic point, confirms the formation of linear dimers (Figure 4.9B). Extinction spectral changes corresponding to the lateral assembly of nanorods were observed on addition of **TEGU** (8 μM): blue shift in the longitudinal plasmon band and red shift in the transverse plasmon band (Figure 4.9C). Thus the addition

115

of **TEGU** resulted in the formation of quartets. Stepwise formation of dimers to quartets was confirmed using TEM studies (Figure 4.9 D-F).
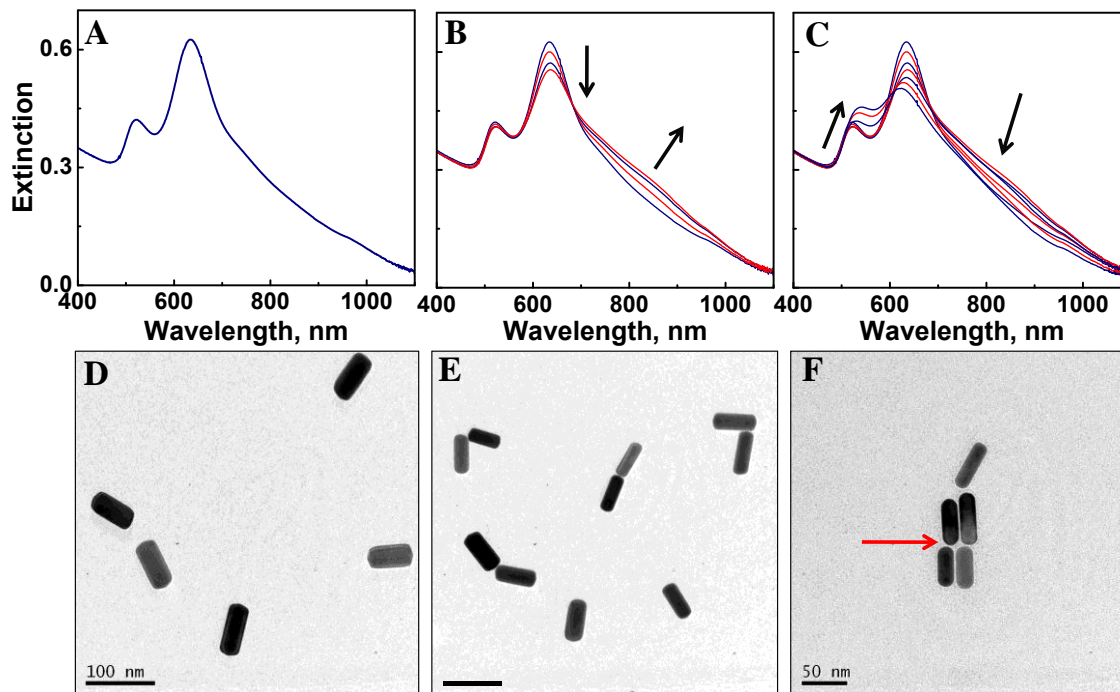
Figure 4.9. *Extinction spectral changes (A,B,C) and TEM images (D,E,F) of Au nanorod at various stages of quartet formation. (A,D) monomers, (B,E) dimers formed using **bipy-DT** (0.6 μM) as the linker and (C,F) quartets formed through the addition of 8 μM of **TEGU** (when the spectral changes corresponds to the formation of longitudinal dimers). All studies were carried out in a mixture (1:4) of water and acetonitrile.*

Morphological studies indicate that the percentage formation of quartets is much more when former procedure is followed, mainly due to kinetic reasons. The longitudinal assembly is a faster process and nanorod dimers quickly undergo oligomerization and precipitation. In contrast, the lateral assembly of nanorods is a slow process. A better control of the longitudinal assembly of laterally arranged dimers can be achieved through the addition of dithiol, **bipy-DT**. Attempts were made to assemble trimers and tetramers in an

end to end fashion, however various types of assemblies were observed in the TEM grid and hence these studies were not further perused.

4.3.5. SERS at the quartet junctions

Various methodologies have been developed for the creation of hot spots with spherical nanoparticles as substrates; however there are only few reports on the use of Au nanorods as SERS substrates. As mentioned in previous section, anisotropic features of nanorods allow the organization of nanorods as linear and lateral assemblies and as quartets by following chemical functionalization methods. Quartets of Au nanorods were prepared by the combination of the lateral and longitudinal coupling processes and their junction can act as hot spots in SERS due to the intense electric field prevailing. Raman spectra were recorded using a confocal Raman spectrometer using a He-Ne laser source having an excitation wavelength of 633 nm and an acquisition time of 10 s. CTAB-capped Au nanorods suspended in a mixture (1:4) of water and acetonitrile showed Raman signals corresponding to the solvent molecules; however, no spectroscopic signals corresponding to the CTAB molecules were observed. The Raman intensity of bipyridine molecule placed at the edges of isolated nanorods, junctions of longitudinal dimer and quartets of Au nanorods were compared (Figure 4.10). Longitudinal dimers and quartets containing bipyridines at their junctions were prepared by following the procedure mentioned in the above section. The intensity of molecular peaks at the edges of isolated nanorods was found to be low (Figure 4.10a). A large enhancement was observed when the molecules are placed at the longitudinal dimer junctions (Figure 4.10b). Interestingly the intensity of the peaks was almost doubled for molecules at the quartet junctions of nanorods (Figure 4.10c).
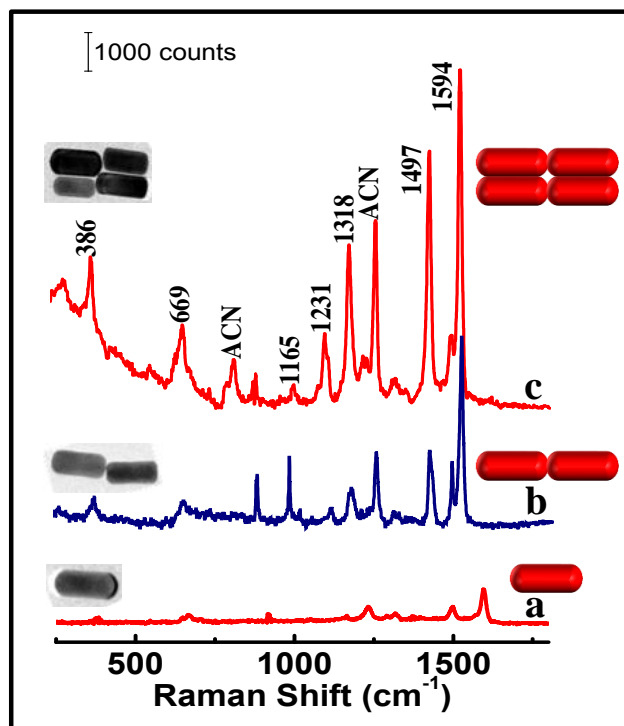
*Figure 4.10. SERS spectrum of **bipy-DT** molecule placed (a) at the edges of isolated nanorods, (b) at the junctions of nanorod dimers formed through their longitudinal assembly and (c) at the junctions of nanorod quartet assemblies formed through a combination of longitudinal and lateral organization.*

Enhancement in signal intensity at the monomer, dimer and quartet stages were further quantified by estimating the enhancement factors (EF). The EF at the different stages were estimated using eq 1

$$EF = (I_{SERS} \times N_{bulk}) / (I_{bulk} \times N_{ads}) \qquad (1)$$

where I_{bulk} and I_{SERS} are the intensities of the ring deformation band of dithiols in the absence of Au nanorods (80 mM for **bipyDT** in acetonitrile) and in the presence of Au nanorods containing various concentrations of dithiols. N_{bulk} and N_{ads} are the number of molecules probed in acetonitrile solution in the absence and presence of Au nanorods, and the details are provided in the experimental section. The EF at the monomeric, dimeric and

118

quartet stages was calculated to be 2.5 x 10^4, 1.1 x 10^5 and 2.3 x 10^5 respectively. The value of enhancement factor for the quartets is almost two times in comparison with linear dimers and the enhancement in signal intensity at the quartet junctions may be attributed to the plasmon coupling of four nanorods. When four nanorods are brought close together to form the quartet junctions, their plasmons couple each other, to form a region of enhanced electric field and molecules placed at the junction experiences high electric field giving rise to enhanced Raman signal intensity. The quartet junctions are found to be efficient substrates in SERS that can be used for the detection and identification of chemically and biologically important molecules.

4.4. Conclusions

In summary, controlled lateral assembly of Au nanorods was achieved using a linker molecule namely tetra(ethylene glycol)undecanethiol, which possesses hydrophobic and hydrophilic moieties. The thiol group on the linker binds onto the lateral surface of the nanorods. The terminal hydroxyl groups undergo multiple hydrogen bonding with the oxygen atoms on the ethylene glycol chain on adjacent nanorods, thereby bringing the two nanorods close together in a lateral fashion. It was observed that the lateral assembly proceeds slowly through dimers, trimers and tetramers to larger assemblies and the extent of lateral coupling increases with increase in the aspect ratio of nanorods. Fabrication of nanorod quartets was achieved through lateral and longitudinal assembly. A molecule when placed at the quartet junction gave rise to huge Raman signal enhancement due to the high electric field prevailing at the junction.
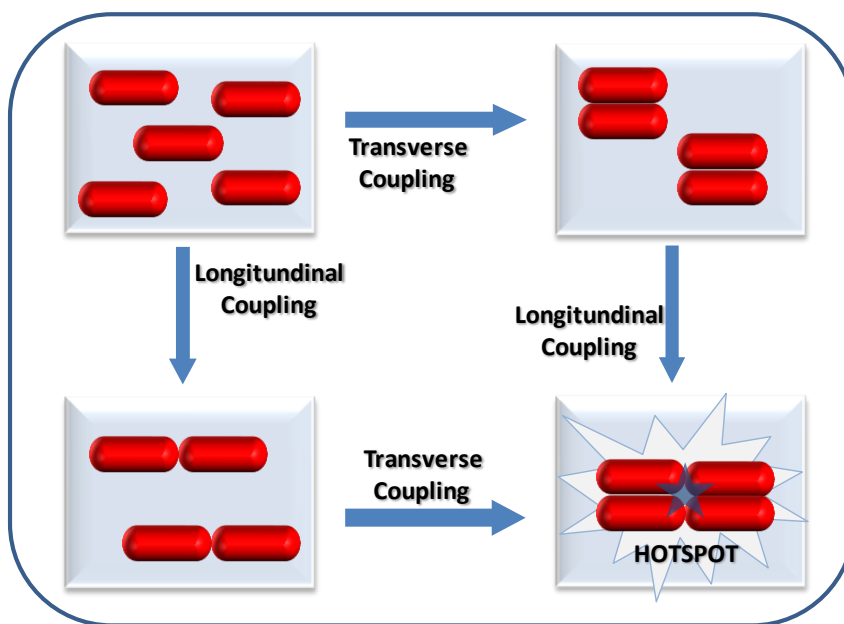
Scheme 4.7. *Schematic representation of gold nanorod dimers formation through longitudinal and transverse coupling and the quartets formed through the combination of both coupling modes.*

4.5. Experimental Section

4.5.1. Materials and Instrumental Methods

Solvents and reagents used were purified and dried by standard methods. Photophysical studies were carried out using spectroscopic grade solvents. The absorption spectral changes, upon the addition of aromatic dithiols, were recorded in a UV-Visible diode array spectrophotometer (Agilent 8453). Stock solutions of the linker molecules were prepared in acetonitrile. For HRTEM studies, samples were prepared by drop casting dilute solution from the cuvette on a carbon coated Cu grid and the solvent was allowed to evaporate and specimens were examined on a FEI-Tecnai 30G^{2}S-Twin or with a 300 kV (JEOL 3010) transmission electron microscope operated at an accelerating voltage of 300 kV. Raman and SERS spectra were recorded using a HR800 LabRAM confocal Raman

spectrometer operating at 20 mW laser power using a peltier cooled CCD detector. Raman spectra were collected in a quartz cuvette using a He-Ne laser source having an excitation wavelength of 633 nm and with an acquisition time of 10 seconds using a 5x objective. All the studies were carried out in a mixture (4:1) of acetonitrile and water. The baseline was corrected and the spectra were presented after subtracting the gold nanorod spectra from the original ones. No noticeable absorption spectral changes were observed for the nanorod solution during the measurements, confirming that the nanorods remain stable in solution even after exposure to laser beam.

4.5.2. Calculation of Enhancement Factor (EF)

$$EF = [I_{SERS}]/[I_{Raman}] \; x \; [N_{bulk}]/[N_{ads}]$$

I_{bulk} and I_{SERS} correspond to the intensities of the ring deformation band of monothiols/dithiols in the absence and presence of Au nanorod respectively, containing various concentrations of monothiols/dithiols. N_{bulk} and N_{ads} are the number of molecules probed in acetonitrile solution in the absence and presence of Au nanorods respectively.

Au nanorods possess a capsule shape having two hemispherical caps at the two ends of a cylinder and various calculations are carried by following the procedure given in our earlier reference (Joseph 2006).

Total surface area of Au nanorod (length = 54.2 nm and diameter = 18.5 nm) = ~4070 nm^2

Lateral surface area of nanorod = ~2470 nm^2

Surface area of both edges together = ~1600 nm^2

Footprint of thiol on Au surface = 0.214 nm^2

Maximum number of thiol moieties that can be accommodated on the each edge of a Au nanorod = ~3740

Volume of sample probed   (for depth of focus 1.01 mm) = 168 pL

Concentration of Au nanorod = 0.12 nM

Number of nanorods in 3 mL of the solution = ~2.16 x 10^{11}

Number of nanorods in the probed volume = ~1.2 x 10^4

I) Enhancement Factor using **bipy-DT** as linker

In the absence of nanorods

Number of molecules in the probed volume (80 mM in ACN), N_{bulk} = 8.08 x 10^{11}

Intensity of the ring deformation band of dithiols, bipy-DT (80 mM in ACN), I_{bulk} = 550

In the presence of nanorods

Maximum number of thiol molecules that can be accommodated at each edge of nanorod =
~3740

No. of thiol molecules at each edge during incubation = ~1250 (based on rod to molecular
ratio)

No. of thiol molecules at each edge during dimerization and quartet formation = ~2500
(based on rod to molecular ratio)

Number of thiols in the probed volume (adsorbed on nanorods) during incubation (0.3 µM),
N_{ads} = ~3 x 10^7 (value corresponding to 1.2 x 10^4 rods)

Number of thiols in the probed volume (adsorbed on nanorods) during dimerization and
quartet formation (0.6 µM), N_{ads} = ~6 x 10^7 (value corresponding to 1.2 x 10^4 rods)

Intensity of the ring deformation band of dithiols (**bipy-DT)** at the edges of isolated
nanorods (0.3 µM), I_{SERS} = 525

Intensity of the ring deformation band of dithiols (**bipy-DT)** during the dimerization step
(0.6 µM), I_{SERS} = 4528

Intensity of the ring deformation band of dithiols (**bipy-DT**) during the quartet formation

(0.6 µM), $I_{SERS} = 9247$

EF (monomers) = $[I_{SERS}]/ [I_{Raman}] \times [N_{bulk}]/ [N_{ads}]$

$$= 525 \times 8.08 \times 10^{11} / 550 \times 3 \times 10^{7} = \mathbf{2.57 \times 10^{4}}$$

EF (dimers) = $4528 \times 8.08 \times 10^{11} / 550 \times 6 \times 10^{7} = \mathbf{1.1 \times 10^{5}}$

EF (quartets) = $9447 \times 8.08 \times 10^{11} / 550 \times 6 \times 10^{7} = \mathbf{2.31 \times 10^{5}}$

Single Particle Optical Investigations of Gold Nanorod Assemblies

5.1. Abstract

The main objective of the present investigation was to align Au nanorods in (i) linear fashion utilizing the covalent interaction of dithiols and (ii) lateral fashion through electrostatic interaction. The scattering properties of the various assemblies were investigated at the single particle level by combining the dark-field spectroscopy and high resolution scanning electron microscopy techniques. Single particle investigations on Au nanorod assemblies were carried out by organizing them in the longitudinal and transverse fashion. Au nanorods assembled in a longitudinal fashion showed a gradual bathochromic shift in the longitudinally coupled plasmon band with increase in the number of rods in a chain. The coupled plasmon band showed maximum intensity for polarization along the nanorod axis; a gradual decrease in intensity was observed on changing the axis of polarizer from parallel to perpendicular direction. Similar studies on laterally assembled Au nanorods showed a gradual hypsochromic shift in the longitudinally coupled plasmon band and bathochromic shift in the transverse coupled band. The effect of orientation on the optical properties of linearly assembled Au nanorod dimers was investigated. It is observed that the position and intensity of the coupled plasmon resonance largely depends on the angle between the dimers. The energy levels involved in various modes of excitation were deduced from the polarization dependent scattering studies and explained using plasmon hybridization model.

5.2. Introduction

The functional properties of noble metal nanomaterials can be fine-tuned by integrating them in a stepwise manner to higher order assemblies [Daniel 2004 and Girard 2006]. Such metal nanoparticle based assemblies can propagate light below their diffraction limit and have potential application in the miniaturization of devices. The plasmon coupling in noble metal nanoparticles is usually accompanied by variation in their extinction or scattering spectrum. Such variations are often used for the development of sensors for chemical and biological systems [Min 2008 and Yoosaf 2007]. Among various nanoscale building blocks, Au nanorods have gained much attention due to their anisotropic nature allowing their organization in different orientations (for e.g., in end-to-end and side-by-side fashion) [Thomas 2004, Sudeep 2005, Pan 2007 and McLintock 2011]. These aspects are discussed in the Chapters 3 and 4. Various strategies have also been adopted for the design of nanorod assemblies by following electrostatic, hydrogen bonding and covalent bonding interaction [Joseph 2006, Caswell 2003, Murphy 2005 and Wang 2007]. The optical properties of the assembled structures are dependent on the way in which they orient and can be further tuned by varying (i) the number of rods and (ii) aspect ratio.

The extinction spectral properties of nanorod assemblies in solution have been investigated by following various experimental and theoretical methods. However, the major disadvantage of solution based investigations is that, it provides an average of the ensemble properties of nanoassemblies. Hence, it is difficult to deduce any structural-optical property relationships based on these studies. The exact optical properties of the nanostructures can be obtained by collecting the spectrum from single particle assemblies after identifying them by microscopic techniques. Different groups have developed methods for collecting the

single particle properties of nanomaterials by correlating various microscopic and spectroscopic techniques. Among these, a combined scanning electron microscopy (SEM) and dark-field microscopy (DFM) technique has gained much attention [Hu 2008 and Novo 2007].

The precise structural information of single nanorod assemblies can be obtained by combining SEM imaging and dark-field spectroscopy. The image pattern of a single particle recorded using dark-field and scanning electron microscopic methods are presented in Figure 5.1.The identification marks are made on the substrate during imaging, by etching the surface using focused ion beam (FIB). The marks on the substrates near to the particle help in identifying the nanoparticles when viewed under dark-field microscope. The close correspondence between the patterns in the two images allows us to correlate the structural and spectroscopic measurements. Further details on the FIB SEM-DFM correlation method is provided in the experimental section (Section 5.5.2)
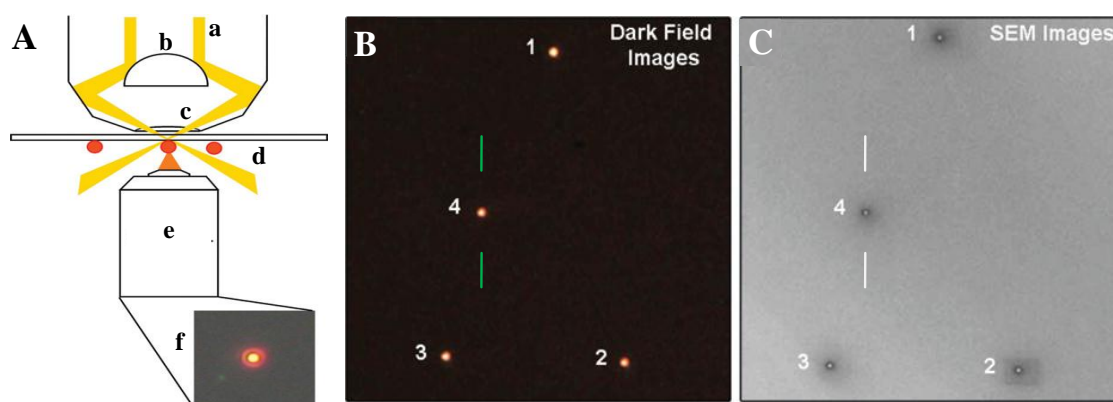
Figure 5.1. *(A) Schematic representation of the set up for dark-field microscopic investigations of metal nanoparticles. (a) light source, (b) dark field patch stop, (c) condenser lens, (d) sample, (e) objective lens and (f) dark field image [Hu 2008]. (B) Optical image of a particle pattern recorded by dark-field microscopy and (C) the SEM image of the same particle pattern [Hu 2007].*

5.2.1. Single particle investigations of nanoparticle assembly

Recently few groups have reported the single particle investigations on spherical Au nanosphere and their linear assemblies [Nehl 2004, Henry 2011 and You 2012]. Light scattering properties of linear assembly of Au nanoparticles by varying the number of particles in a chain from one to six, having an interparticle spacing of 1 nm, were reported by Mulvaney and coworkers [Barrow 2011]. The CTAB stabilized Au nanoparticles, having an average diameter of 64 nm, were assembled using thiolated single stranded oligonucleotides. It was found that their surface plasmon resonance underwent a bathochromic shift with increasing chain length (Figure 5.2). The observed bathochromic shift decreases progressively with chain length and levels off. An exponential model applied to the experimental data allowed the determination of an asymptotic maximum resonance at a chain length of 10-12 particles. This resonance is identified as a longitudinal coupling mode along the length of the nanoparticle chain. Polarization studies on linear tetramer gave maximum intensity for polarization of light along the axis of the nanoparticle chain.
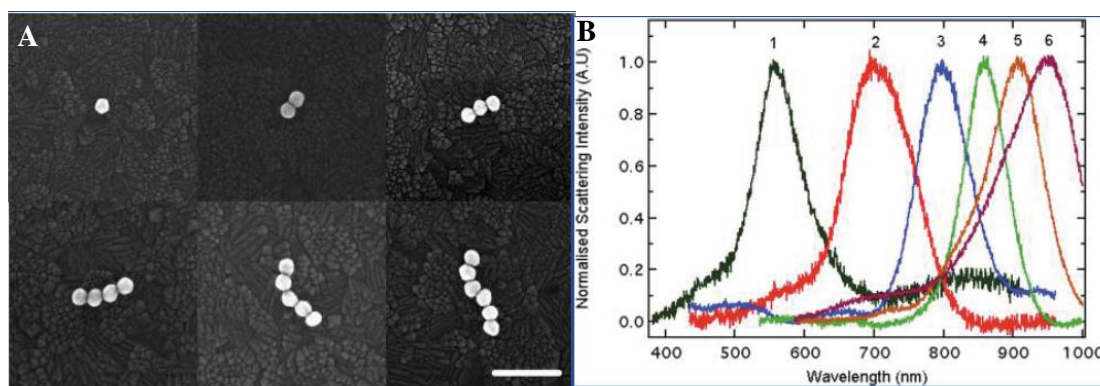
Figure 5.2. *(A) SEM images of self-assembled nanoparticle chains (mean diameter of gold particles = 64 nm; interparticle spacing = 1 nm); Scale bar = 250 nm. (B) Normalized spectra of the nanoparticle chains in Figure 5.2 A. Spectra were collected in air on an ITO coated glass substrate. Spectra are numerically labeled according to chain length [Barrow 2011].*

Even though there have been few studies on the single particle investigations on spherical nanoparticles, there are only three to four reports on single particle investigations of nanorods and their assembled nanostructures (Slaughter 2010, Lombardi 2012 and Shah 2012). Scattering spectra of gold nanorod dimers arranged in side-by-side, end-to-end and various other orientations were reported through the combination of SEM and dark field microscopy by Funston et al. [Funston 2009]. The optical properties of the dimers were found to be dependent on the orientation of nanorods in the dimer (Figure 5.3). Depending on the orientation, both bathochromic and hypsochromic shift in surface plasmon resonances were observed and these results are in consistent with the plasmon hybridization model. However, the plasmon coupling constant for gold dimers with less than a few nanometers separation between the particles does not obey the exponential dependence predicted by the Universal Plasmon Ruler equation. The experimentally determined spectra are compared with electrodynamic calculations and the interactions between the individual rod plasmons in different dimer orientations were explained using hybridization model.
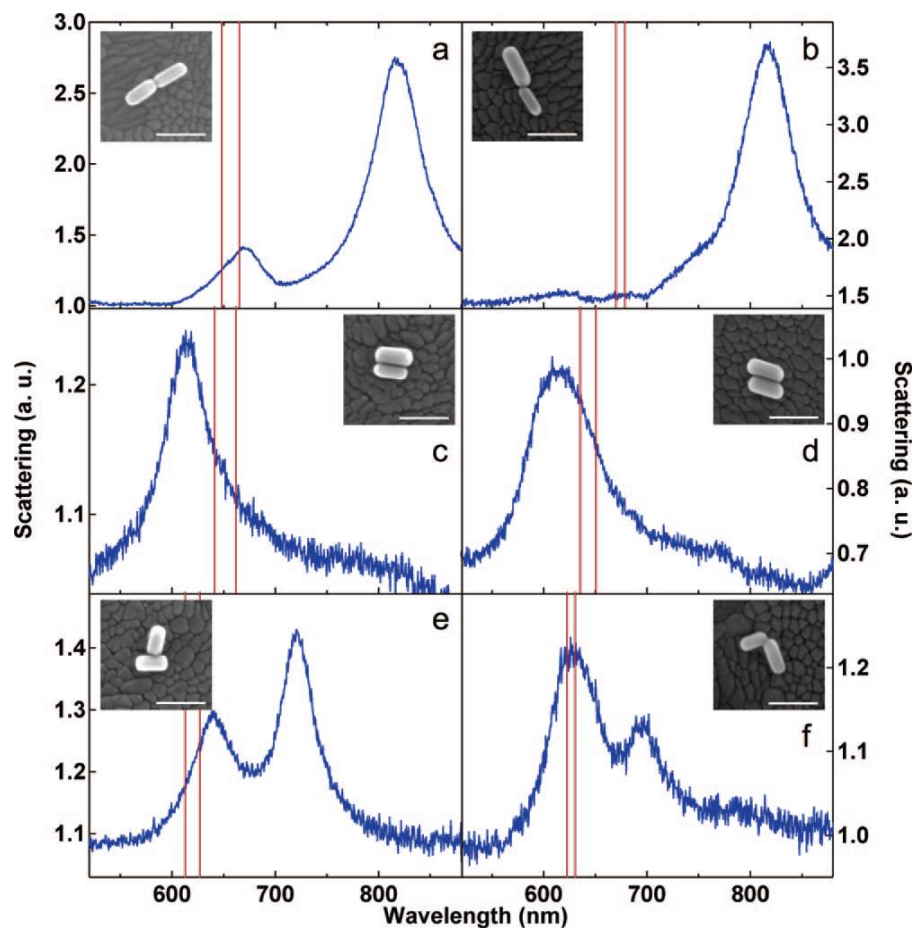
Figure 5.3. *Scattering spectrum of nanorod dimers aligned (a,b) end-to-end, (c,d) side-to-side, (e) as T configuration, and (f) as L configuration (on the surface of ITO and in air). Insets show the SEM images of the corresponding dimers. Scale bar = 100 nm [Funston 2009].*

Surface plasmon excitation in noble metal nanoparticles can lead to strong enhancement in their absorption, scattering, and local electric field [Evanoff 2004 and Jain 2006]. It is desirable to have nanomaterials with a high absorption cross-section for sensing and other diagnostic applications, whereas, for imaging applications nanoparticles having strong optical scattering is useful [Huang 2006 and Jain 2006]. It is important to understand and tune the contributions of scattering by varying the dimensions and the mode of assembly. Au nanorods possessing two distinct surface plasmon absorption bands (associated with the

transverse and longitudinal oscillations of electrons) can function as powerful candidates for such studies. Herein, we report the scattering spectrum of Au nanorod assemblies by increasing the number of rods, organized laterally and longitudinally in a chain and correlating their optical properties with their structure. The anisotropic features of Au nanorods were utilized to assemble them (i) in a linear fashion by using covalent interactions of dithiol molecules at the edges of Au nanorods and (ii) in a lateral fashion, utilizing the electrostatic interaction between the oppositely charged nanorod surface and citrate molecules.

5.3. Results and Discussion

5.3.1. Single Particle Investigations on Longitudinal Assemblies of Au Nanorods

Gold nanorods used for single particle studies were synthesized by following the seed mediated method developed by Nikoobakht et al. [[b]Nikoobakht 2003]. Thicker nanorods can scatter light efficiently; compared to photochemical methods, it is easy to increase the width of the nanorods through seed mediated method. The excess capping agents such as CTAB present in the solution were removed by repeated centrifugation. They were found to be stable in water as well as in mixtures of water and acetonitrile, containing more than 70% of acetonitrile. Au nanorods possess a large positive zeta potential in water (ζ = 28.5 mV), and a reversal in ζ was observed on increasing acetonitrile content [Pramod 2008]. In the present investigations, we have used a solvent mixture (1:4) of water and acetonitrile (ζ = -28.8 mV) and experiments were carried out with two sets of nanorods having average aspect ratios 1.7 and 2.0. In the latter one, the longitudinal plasmon band resonates at 618 nm, whereas the band resonates at 595 nm in the case of former one. In both the cases, the transverse mode of electron oscillation was observed at 520 nm. The nanorods

were assembled linearly by following the procedure reported in Chapter 3 using an aromatic dithiol, namely 5,5'-bis(mercaptomethyl)-2,2'-bipyridine (1 μM). The edges of Au nanorods are less saturated with CTAB. The thiol derivatives preferentially bind onto the edges leading to the localization of molecules which results in dimerization and subsequent oligomerization of nanorods.

ITO coated glass slides functionalized with (3-mercaptopropyl)trimethoxysilane (MPS) were prepared by following a reported procedure [Ali 2008]. Freshly prepared glass slides, coated with MPS, were dipped in Au nanorod solution at different stages of oligomerization (for 10 s) and dried using a flow of nitrogen. Two sets of Au nanorods having average dimensions of (i) 58 nm in length and 30 nm in width (Figure 5.4B) and (ii) 52 nm in length and 30 nm in width (Figures 5.4D) were used in the present study. These slides were imaged under SEM and found that the extent of chain formation is time dependent. Monomers and dimers were observed at the initial stages (after 5 min), whereas trimers, tetramers and higher aggregates were found on the slide after 15 min. Nanorod assemblies of interest (having varying number of nanorods, i.e., one to four nanorods) were selected by SEM imaging and ITO substrates were marked using a focused ion beam (FIB). Marking of ITO substrate allows pattern matching when viewed under a dark field microscope. From the SEM images, we estimate that the spacing between two nanorods in a chain is ~1 nm, which is matching with the chain length of the linker molecule. The scattering spectra obtained for two sets of nanorod assemblies with their corresponding SEM images are shown in Figure 5.4. In both set of experiments, the wavelength of plasmon resonance underwent bathochromic shift as the number of nanorods in the chain increases from one to four. The observed bathochromic shift in the plasmon wavelength progressively

decreases with increase in chain length. As the number of nanorods in a chain increases, the assembly deviates slightly from linearity due to several possible orientations existing between the nanorods in a chain.
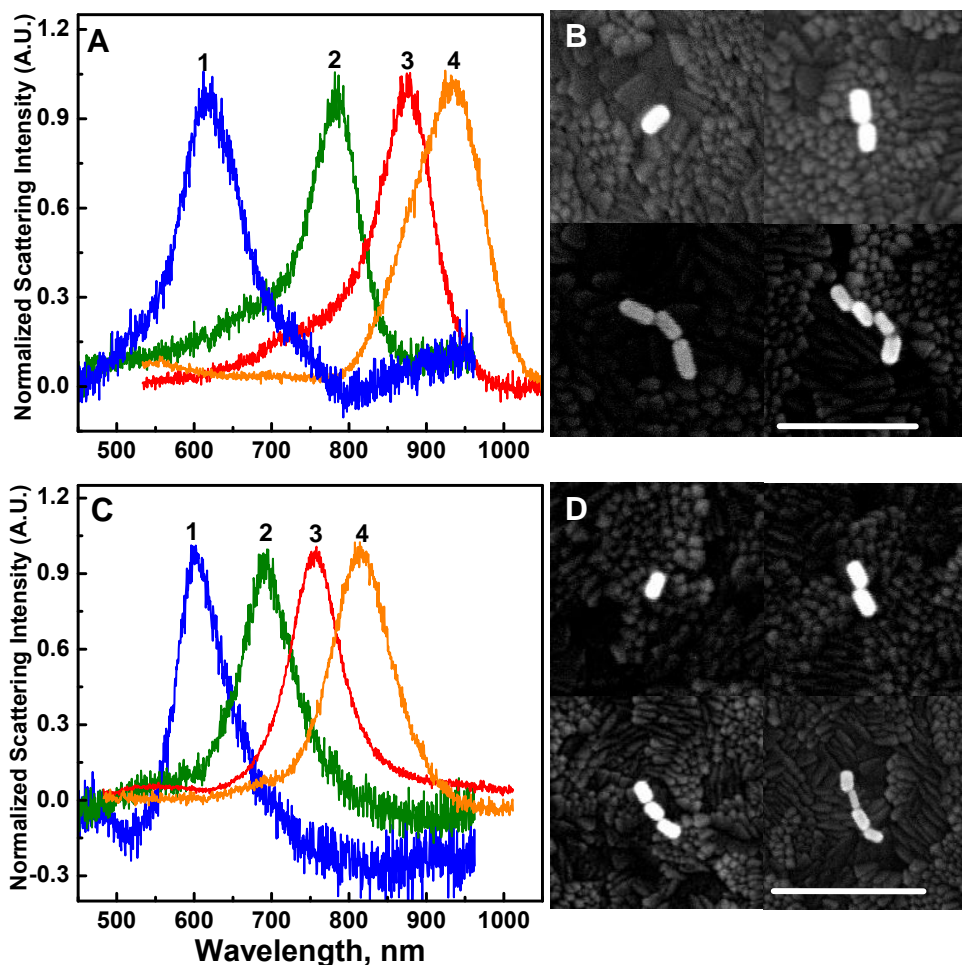
Figure 5.4. *Normalized scattering spectra of the Au nanorod chains (A) with aspect ratio 2.0 and (C) aspect ratio 1.7. Spectra were collected in air on an ITO coated glass substrate. Spectra are numerically labeled according to chain length. SEM images of self-assembled nanorod chains having (C) aspect ratio 2.0 and (D) aspect ratio 1.7. Scale bar = 250 nm.*

In both sets of nanorods, the observed bathochromic shift in the plasmon wavelength decreases with increase in number of nanorods in a chain. The coupled longitudinal plasmon mode was fitted exponentially as a function of nanoparticle chain length and the results are

presented in Figure 5.5. Based on the exponential fit, it is concluded that the bathochromic shift levels off at approximately (i) 6-8 nanorods for shorter rods (aspect ratio = 1.7) and (ii) 10-12 nanorods for longer rods (aspect ratio = 2.0). These trends are in accordance with the previous studies based on linear chains of Au nanoparticles, reported by Mulvaney and coworkers. Even though the nature of plots is similar for nanorods of different aspect ratios, the extent of shift varies significantly with change in aspect ratio. Compared to that of monomer of Au nanorod, having an aspect ratio of 2.0, the coupled longitudinal plasmon band dimer is bathochromically shifted by 165 nm. Under similar condition, Au nanorod having an aspect ratio of 1.7 is shifted only by 95 nm towards red region. Similar trend were observed for trimers and tetramers also and the details are presented in Table 5.1. These studies indicate that the coupled plasmon oscillations of Au nanorods are highly dependent on the aspect ratio of the nanorods.
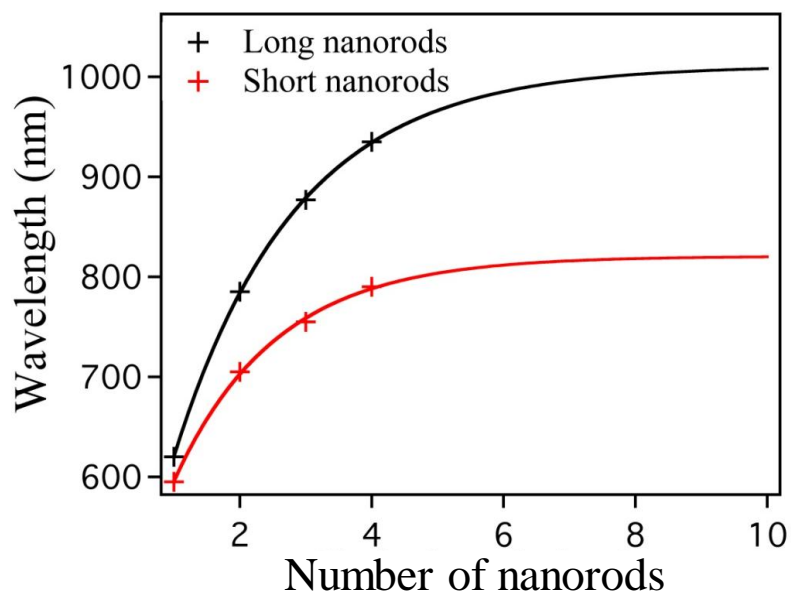
Figure 5.5. Maximum wavelength of coupled longitudinal plasmon band plotted against number of nanorods in a nanochain. Nanorods having an aspect ratio of 1.7 and 2.0 were represented by red trace and black trace, respectively. The maximum wavelength was taken from Figure 5.4 and the curves were obtained using an exponential fit.

Table 5.1: Coupled longitudinal plasmon band for linear assemblies of Au nanorods.

Nanorod Assembly	Aspect Ratio 2.0 (nm)	Aspect Ratio 1.7 (nm)
Monomer	618	597
Dimer	785	695
Trimer	880	760
Tetramer	930	795

The polarization studies of assembled nanorods were carried out to confirm that the long wavelength band originates from the coupling of the longitudinal plasmon mode along the length of the rod. The polarized scattering spectra were collected by placing a polarizer in the incident light path. The scattering spectra of the linear nanorods dimer, when exposed to excitation light of varying polarizations (0 to 90 degrees) are shown in Figure 5.6A. In principle, transverse mode should be observed at polarization perpendicular to the axis of the assembled nanorods. However, this mode could not be observed in the case of Au nanorod assembly, may be due to its low intensity. Spectra were taken at increments of 10 degree and a plot of plasmon band intensity *versus* polarizer angle is shown in Figure 5.6B. The spectra showed a gradual decrease in intensity on changing the axis of polarizer from parallel to perpendicular direction, along the length of assembled nanorods. The polarizer angle of zero degree is represented by the arrow mark (inset of Figure 5.6A) along the length of the dimer. It is expected that, for a perfectly linear assembly, longitudinal plasmon mode should not be observed, when the incident light is polarized perpendicular to the chain. However, the residual intensity observed may be due to the deviation of dimer from linearity and background counts.
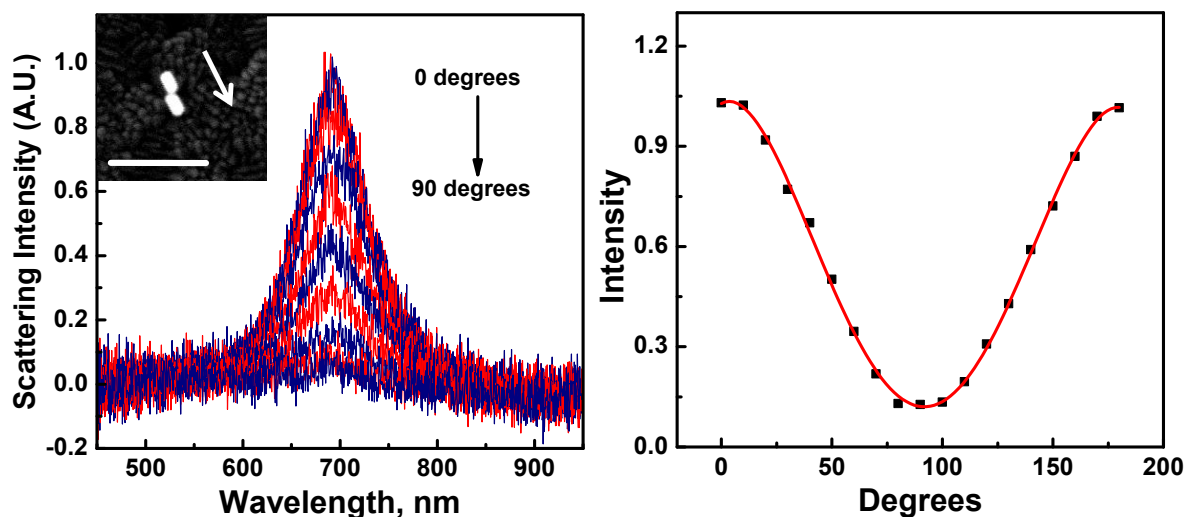
Figure 5.6. *(A) Scattering spectra of nanorod dimer (aspect ratio of Au nanorod is 1.7) at different polarizations. Inset shows the SEM image of the dimer and the polarizer angle compared to the position of the dimer is located by using the FIB marks on the substrate as reference. The polarization angle of zero degree is indicated by the arrow mark on the SEM micrograph. The spectra were collected on an ITO coated glass substrate in air. The scale bar in the inset is 250 nm. (B) A plot of scattering intensity of the coupled longitudinal plasmon band (at 695 nm) of a nanorod dimer resonance versus polarizer angle.*

We have also collected the scattering spectra of various linear assemblies (dimers to tetramer) of nanorods having aspect ratio of 2, at different angles of polarizations (Figures 5.7). The spectral features were similar to that reported in Figure 5.6A for linear dimers linked together by Au nanorods of aspect ratio 1.7. Scattering spectra showed maximum intensity for polarization along the nanorod axis and the intensity decreases gradually on rotation of the polarizer. The peak almost vanishes for polarization perpendicular to the nanorod axis. In the case of linear trimer and tetramer (Figures 5.7B and 5.7C), a weak band at the shorter wavelength is observed, for polarization perpendicular to the nanorod axis. This may be attributed to the coupling modes arising from the deviation of the chain from linearity.
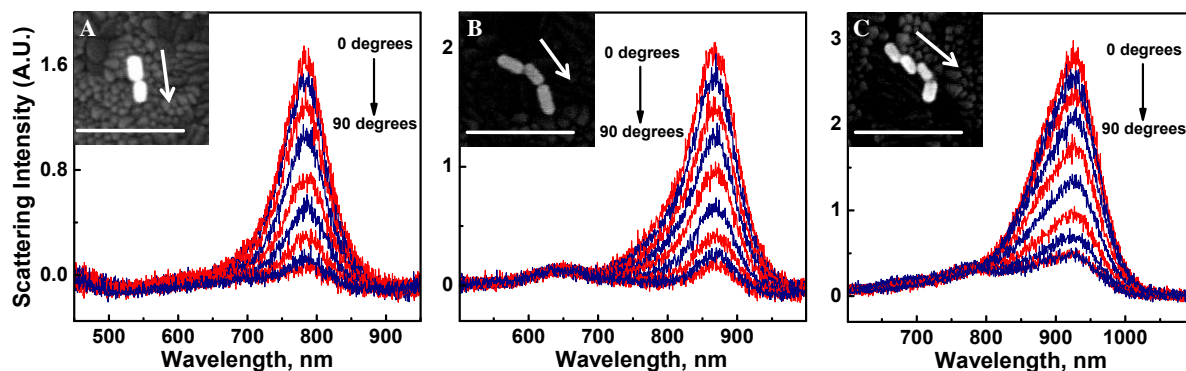
Figure 5.7. *Scattering spectra at different polarizations of linear assemblies of Au nanorods (A) dimer, (B) trimer and (C) tetramer (aspect ratio of Au nanorods is 2.0). Inset shows an SEM image of the corresponding nanostructures. The polarizer angle compared to the position of the dimer is located by using the FIB marks on the substrate as reference. The polarization angle of zero degree is indicated by the arrow mark on the SEM micrograph. The spectra were collected on an ITO coated glass substrate in air. The scale bar in the inset is 250 nm.*

5.3.2. Orientation dependent plasmon coupling in Au nanorod dimers

We have further carried out systematic investigation on the coupling of plasmon modes in Au nanorod dimers as a function of the relative orientation of nanorods. This is achieved by recording the scattering spectra by varying the angle between the nanorods in the dimer. Au nanorods having an average aspect ratio of 2.0 with the longitudinal plasmon band at 620 nm was selected for this purpose. The angle between the dimers plays a crucial role in plasmon coupling, which can be modulated by varying the nature of the linker group. The nanorods were linked through the dithiol molecules. It is reported from our group that the orientation between the nanorod dimers is dependent on the nature of linker molecules [Pramod 2008]. Aromatic dithiols give rise to more linear dimers, whereas bent dimers can be obtained using aliphatic dithiols. In the present case, 5,5'-bis(mercaptomethyl)-2,2'-bipyridine was used as aromatic dithiol and 1,6-hexanedithioldithiol as aliphatic dithiol

molecules. We have selected six Au nanorod dimers from ITO plate, having an angle of 0, 45, 90, 120,150 and 180 degrees, between the nanorods, by imaging them using scanning electron microscopy (SEM). The scattering properties of the Au nanorod dimers were measured by using dark-field microscopy (DFM). The scattering spectra and corresponding SEM images of six representative nanorod dimers having varying angles between the nanorods are presented in Figure 5.8. When the angle between the two nanorods in the dimer is 0° and 180°, only one scattering peak is observed (Figures 5.8A and 5.8F), whereas two peaks were observed in the scattering spectrum in all the other cases. Interestingly, the lower energy peak was found to be more intense for Au nanorod dimers with an angle of 120º and 150º (Figures 5.8B and 5.8C). With decrease in angle between the dimers (45º and 90º), the intensity of lower energy peak decreases and the higher energy peak becomes more prominent (Figures 5.8D and 5.8E). Thus, the extent of dipolar overlap between the dimers was found to be highly dependent on the angle between the dimers. For linear nanorod dimer with an angle of 180°, coupled plasmon peak was found to resonate at 785 nm. A gradual hypsochromic shift in the peak position was observed with decrease in the angle between the dimers. For example, Au nanorod dimer with an angle of 150º possess a coupled plasmon band at 662 nm which is shifted to 655 nm, 648 nm and 620 nm for dimers with angles 120º, 90º and 45º respectively. A hypsochromic shift of 18 nm from the monomer peak was observed for Au dimer assembled laterally (Figure 5.8F), and the resultant peak position was observed at 602 nm. Thus, the peak position and intensity of the coupled plasmon band is highly dependent on the orientation between the dimers.
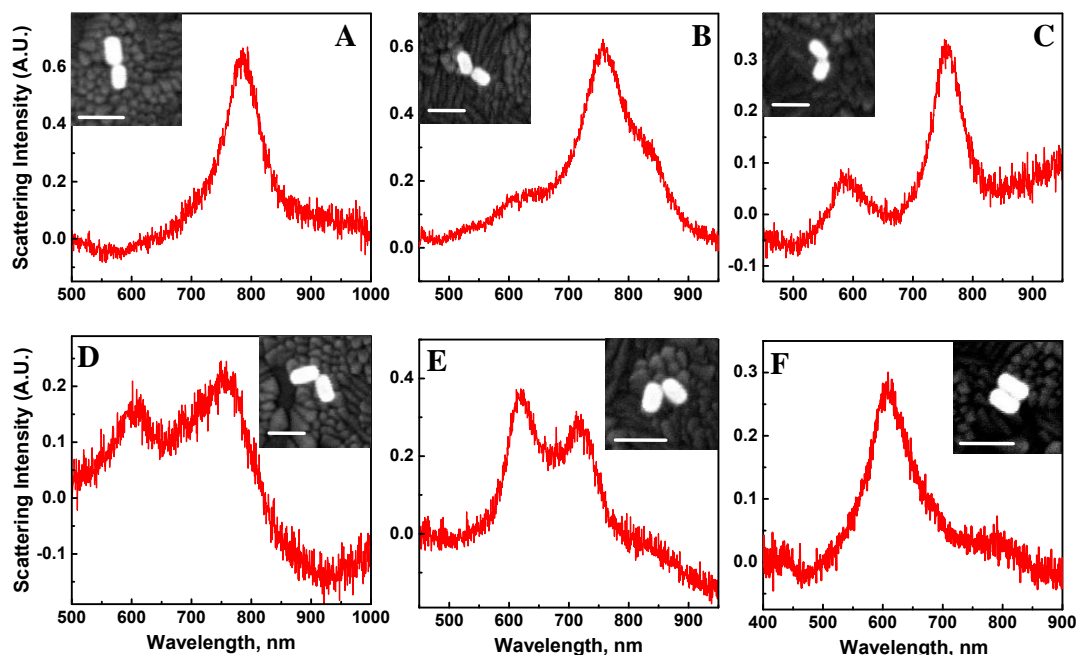
Figure 5.8. *Scattering spectra of linearly assembled Au nanorod dimers with varying angles in between the dimers (A = 180º, B = 150º, C = 120º, D = 90º, E = 45º and F = 0º). The SEM images of the corresponding dimers are shown in the inset. Scale bar = 100 nm.*

Further insight on orientation dependent plasmon coupling in four different nanorod dimers, with varying angles (45º, 90º, 150º and 180º), were obtained through polarization dependent studies. The scattering spectra of these nanorod dimers were collected by changing the angle of polarization and the results are presented in Figure 5.9. For the linear nanorod dimers, maximum intensity of the coupled longitudinal plasmon was observed when the polarization was along the nanorod axis (Figure 5.9A). A decrease in intensity of this band was observed on varying the angle of polarization and it reaches a minimum when the angle is at 90º. Interestingly, nanorod dimers having varying angles of 45º, 90º and 150º showed both longitudinal and transverse plasmon modes. The intensity of these modes underwent variation by changing the angle of polarization. For nanorods with an angle of 150º, the lower energy peak, due to the coupled longitudinal plasmon, is more pronounced and the higher energy peak due to the transverse mode was found to be less intense. The

138

intensity of coupled longitudinal plasmon band decreased on decreasing the angle of polarization (Figure 5.9B) and the higher energy peak becomes more prominent. For example, in the case of nanorod dimer having an angle of 45°, we observed a single peak at lower energy during longitudinal polarization which switched to the higher energy mode during lateral polarization (Figure 5.9D). Polarization dependent investigations of laterally organized nanorod dimers (angle of 0°) are discussed in detail in Section 5.3.3. Thus, nanorod dimers, with varying angles, show strong polarization dependence.
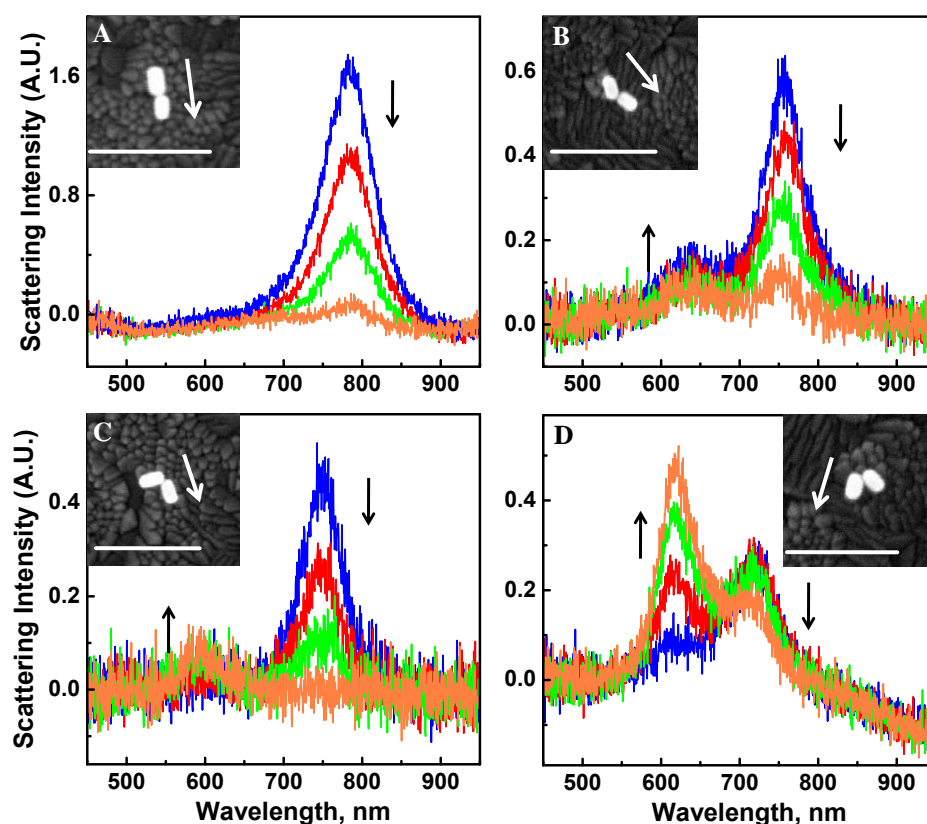
Figure 5.9. *Polarization dependent spectra of nanorod dimers* *with varying angles (A = 180°, B = 150°, C = 90° and D = 45°) and the inset shows the SEM image of the dimers. The spectra were collected at different polarization angles (blue - 0°, red - 30°, green - 60° and orange - 90°). The polarizer angle compared to the position of the dimer is located by using the FIB marks on the substrate as reference. The polarization angle of zero degree is indicated by the arrow mark on the SEM micrograph. The spectra were collected on an ITO coated glass substrate in air. Scale bar = 250 nm.*

A better understanding on the origin of various peaks in nanorod dimers can be obtained from the plasmon hybridization model. According to the plasmon hybridization model, organization of Au dimeric nanorods in the lateral as well as longitudinal fashion can have four hybridized plasmon modes designated as bonding and antibonding modes (Scheme 5.1). Two of the modes are optically active (bright modes; dipoles add up), and the other two are optically inactive (dark modes; dipoles cancel each other). At 180°, the transverse antibonding and longitudinal bonding modes are optically active, however, the former is very weak and hence only one peak (at 885 nm for nanorods of aspect ratio 2.0) corresponding to longitudinal bonding mode is observed in the scattering spectrum (Schemes 5.1b and 5.1d). For lateral dimers having an angle of 0°, the scattering peaks arising from the optically active longitudinal antibonding and transverse bonding modes are close to each other since their energy levels are close (Schemes 5.1a and 5.1c). As a result, only one scattering peak at 605 nm is observed. For nanorods with angles between 180° and 0°, two scattering peaks were observed. The polarization studies on these nanorod dimers showed that, the lower-energy mode is excited when the excitation polarization is along the nanorod axis, while the higher-energy mode is excited when the excitation polarization is perpendicular to the nanorod axis (Figure 5.9). Since the nanorods are in an angle, dipoles cannot completely cancel each other as in the case of longitudinal and transverse dimers. The new plasmon peaks may be originating through the mixing of bonding and antibonding modes and hence, only two hybridized plasmon modes are observed.
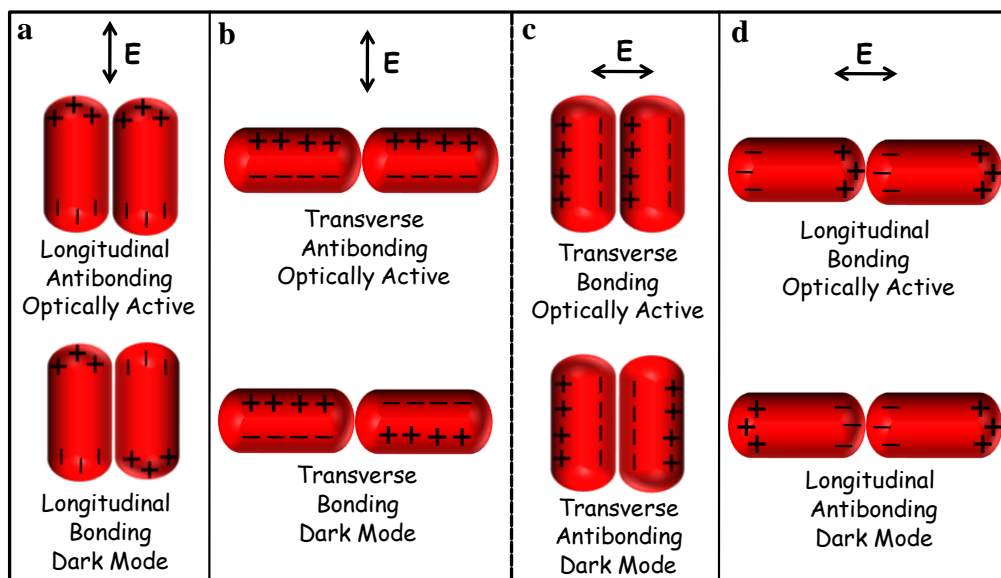
Scheme 5.1. Schematic representation of the different coupled plasmon modes involved in the longitudinal and lateral assembly of Au nanorod dimers.

5.3.3. Single Particle Investigations on Lateral Assemblies of Au Nanorods

The surface of Au nanorod is covered by a bilayer of CTAB surfactant which give rise to a high positive zeta potential ($\zeta = 30$ mV). Au nanorods possess high stability in water which is attributed to the large positive ζ value. The lateral assembly of nanorods is achieved by the addition of citrate anions. The thick coverage of CTAB bilayer and the larger surface area on the lateral faces are responsible for the assembly of nanorods in the lateral fashion. The electrostatic interaction between the positive charged nanorods and the citrate anions drives the assembly of nanorods in the lateral fashion (Scheme 5.2). In solution, the longitudinal plasmon resonance band underwent hypsochromic shift from 655 nm to 615 nm, on addition of citrate ions, accompanied by a decrease in intensity. Interestingly, the transverse band underwent bathochromic shift from 515 nm to 525 nm. The number of Au nanorods in lateral assembly (dimer, trimer, tetramer to oligomers) can be controlled by varying the ratio of citrate to nanorods in the solution.
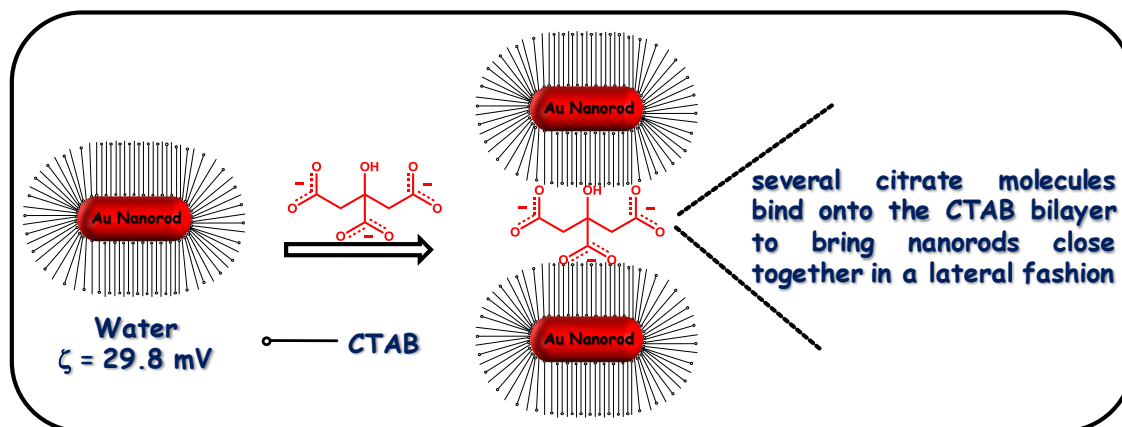
Scheme 5.2. *Schematic illustration of the binding of negatively charged citrate molecule onto the positively charged CTAB bilayer bringing two nanorods close together in a lateral fashion.*

The ITO coated glass slides were further functionalized with (3-mercaptopropyl) trimethoxysilane (MPS) by following a reported procedure [Ali 2008]. The assembly of nanorods in lateral fashion was achieved by adding sodium citrate (3 µM) to Au nanorod (0.012 nM) solution in water. It may be noted that the lower concentration of citrate ion allowed slow assembly of nanorods. The lateral assembly was monitored by following the extinction spectra of nanorods in solution and the ITO glass plates, coated with MPS, were dip coated at different stages of assembly. Glass slides were dipped in Au nanorod solution for 10 s and dried using a flow of nitrogen. It was found that the ITO glass sides dip-coated after 10 min were covered with dimers and trimers (and small amount of monomers). When dip-coated after 20 min, we could observe tetramers and pentamers of nanorods on the ITO glass sides. Higher order clusters were not observed since the nanorods underwent uncontrolled aggregation at the final stages leading to precipitation. Lateral assemblies having varying number of nanorods were selected by SEM imaging and ITO substrates were marked using a Focused Ion Beam (FIB). The marked samples were viewed under a dark-field microscope and the scattering spectra were collected.

The scattering spectra and the corresponding SEM images of the nanorod assembly are presented in Figure 5.10. The plasmon coupling in the nanorod assemblies depends on the aspect ratio as well as the number of nanorods in the assembly. In the present case, individual gold nanorods possess an average length of 54 nm and width of 23 nm (aspect ratio of 2.3). The monomers and nanorod assemblies consisting of two to five rods, arranged laterally, were selected for the present studies. From the SEM images, it is observed that the spacing between the nanorods in the assembly is ~1 nm. The CTAB molecules possess a length of ~2.2 nm in its extended configuration; however, the nanorods are closely spaced (~1 nm) in the present case due to the conformational changes in the alkyl chain and interdigitation. The scattering spectra of the dimeric and trimeric assembly of Au nanorod in the lateral fashion possess a single peak corresponding to longitudinal plasmon oscillation. Compared to that of isolated Au nanorods, the longitudinal plasmon band of the dimer and trimer underwent a hypsochromic shift of 18 nm and 28 nm respectively. The longitudinal plasmon resonance continually underwent blue shifts as the number of nanorods in the lateral assembly increases. The shift progressively decreased and leveled off with increase in the number of rods. Interestingly for higher order assemblies such as tetramers and pentamers, a new band was observed at the longer wavelength region (at 684 nm for tetramer and 704 nm for pentamer) along with the blue shifted longitudinal resonance. The new band at lower energy region was found to be more intense for the pentamer.
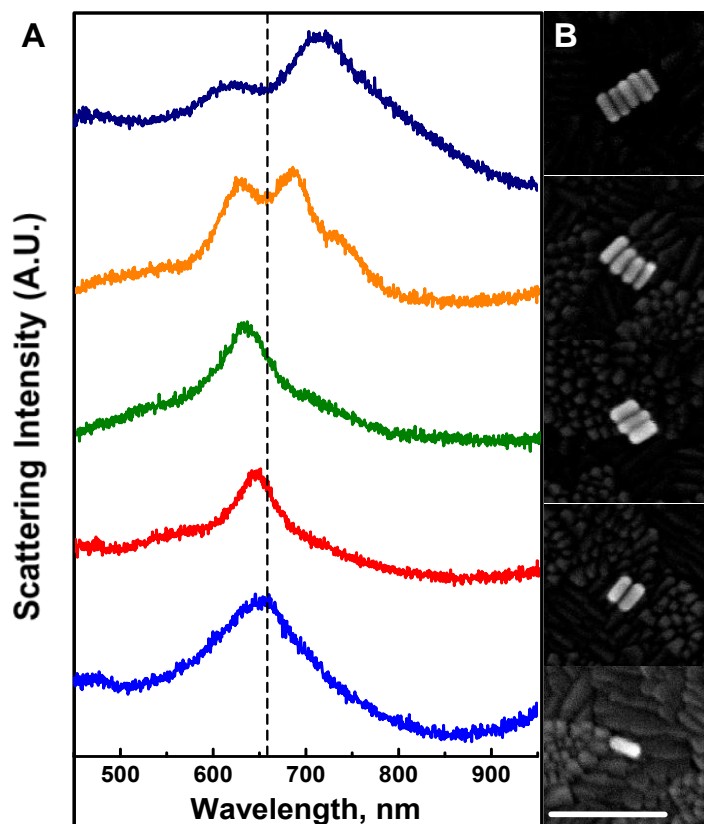
Figure 5.10. *(A) Scattering spectra of laterally assembled Au nanorods (aspect ratio 2.3). Spectra were collected in air on an ITO coated glass substrate. (B) SEM images of laterally arranged Au nanorods. Scale bar = 200 nm.*

Simulations using Finite Element Method (FEM) were carried out to understand the dependence of the plasmonic properties of lateral assembly of Au nanorods. The hypsochromic shift in the longitudinal plasmon band observed on increasing the number of nanorods in the assembly is in agreement with the results obtained from simulation studies using FEM. The wavelength maximum of the longitudinal plasmon band, obtained through experimental and theoretical methods, were plotted against the number of rods in the assembly and fitted exponentially. The results are presented in Figure 5.11. In both the cases, the extent of the shift decreases with increase in number of rods and is leveled off at about 7-8 rods in an assembly. The difference in plasmon band positions observed in the

experimental and theoretical calculations may be attributed to the slight variations in size of the nanorods and the difficulty in accurately determining the spacing between the nanorods in an assembly.
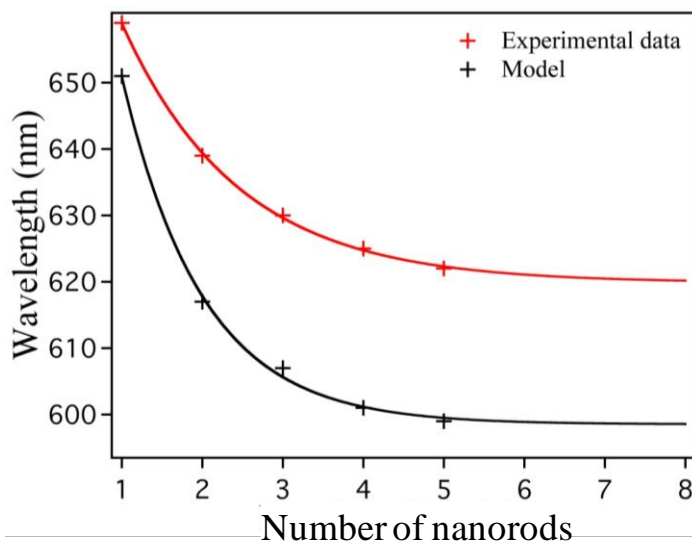
Figure 5.11. *Plot of the wavelength maximum of the longitudinal plasmon band, obtained through experimental (red trace) and theoretical methods (black trace), against the number of rods in the assembly. Curves were obtained using an exponential fit to the data points.*

Polarization studies were carried out on dimeric to pentameric Au nanorod assemblies to obtain further insight on the origin of the new band observed at the lower energy region. The experimental and theoretical results obtained when these assemblies are subjected to longitudinal and transverse polarization are presented in Figure 5.12. For longitudinal polarization, only one peak was observable at the higher energy region of the spectrum which corresponds to the longitudinal plasmon band. This band underwent a hypsochromic shift with increase in the number of nanorods in the assembly. Interestingly, a gradual bathochromic shift in the peak position of transverse band was observed, in both simulated and experimental spectra, on moving to tetramer and pentamer. The band becomes more pronounced and got further shifted with increase in number of nanorods in an assembly.

145
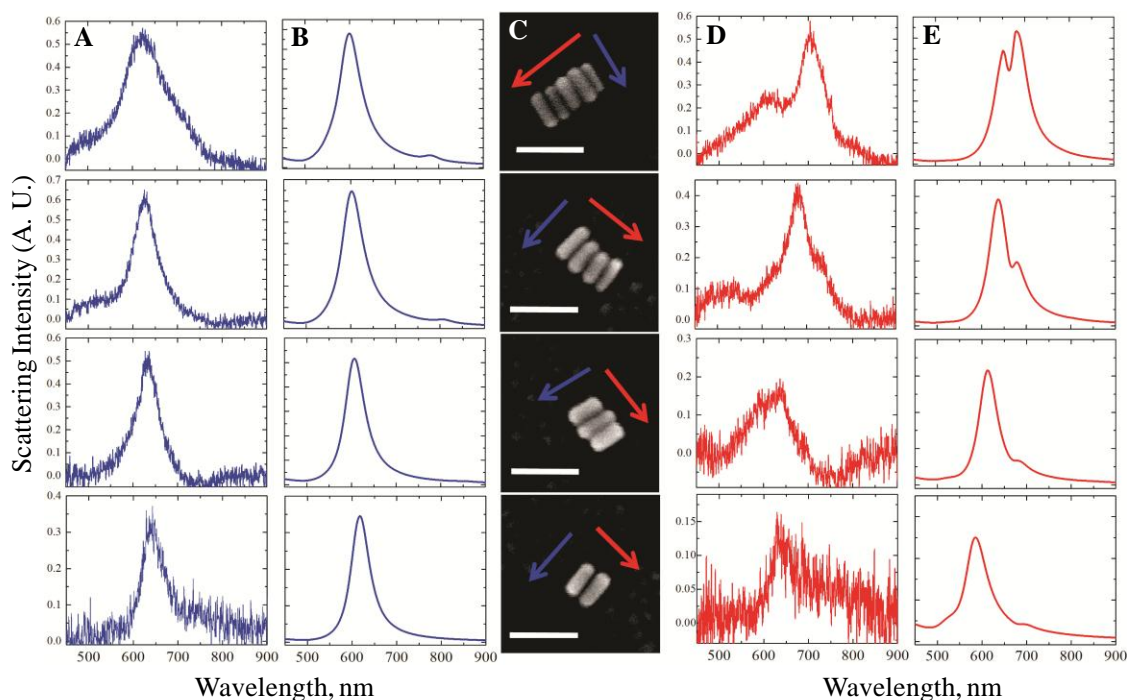
Figure 5.12. *(A,D) Experimental and (B,E) the corresponding theoretical scattering spectra of lateral nanorod assemblies, obtained during (A,B) longitudinal and (D,E) lateral polarizations. (C) SEM images of the corresponding laterally assembled nanorods from dimers to pentamers. The polarizer angle compared to the position nanorod assemblies were known by using the FIB marks on the substrate as a reference. The longitudinal and the lateral polarizations directions have been indicated on the inset SEM micrograph using blue and red arrows respectively. The spectra corresponding to these polarizations are plotted in the respective colors. All spectra were collected on an ITO coated glass substrate in air. Scale bar in the inset = 200 nm.*

The observed shifts in band positions during the longitudinal and transverse polarization of laterally assembled nanorods can be explained based on the plasmon hybridization model [Prodan 2003 and Nordlander 2008]. In plasmon hybridization, the linear combinations of individual nanorod plasmons give rise to coupled bonding and antibonding plasmons. In the case of nanorod dimer aligned in a lateral fashion, the individual monomer plasmons hybridize giving rise to two modes, one of which remains as

dark mode. For longitudinal polarization, the higher energy mode is active (bright mode) and the lower energy mode remains as the dark mode (Scheme 4.4A). Hence, we observe a blue shift in the band position during longitudinal polarization. In contrast, for polarization along the transverse axis, the lower energy mode is active (bright mode) and the higher energy mode remains as the dark mode giving rise to bathochromic shift in the peak position (Scheme 4.4B). The shifts in peak positions increases with increase in number of nanorods in an assembly, due to higher splitting between the bonding and antibonding modes. During the transverse polarization studies of Au nanorods, a new peak was observed in the long wavelength region of the simulated spectrum. The intensity of this peak increases and becomes pronounced for the pentameric assembly. The peak was found to be of low intensity in the experimental spectrum. These peaks may be originating either from (a) the multipolar resonance in these rectangular type assemblies of Au nanorods or (b) from the higher energy bright modes in larger assemblies (for example, new modes for trimeric assembly in Scheme 5.3).
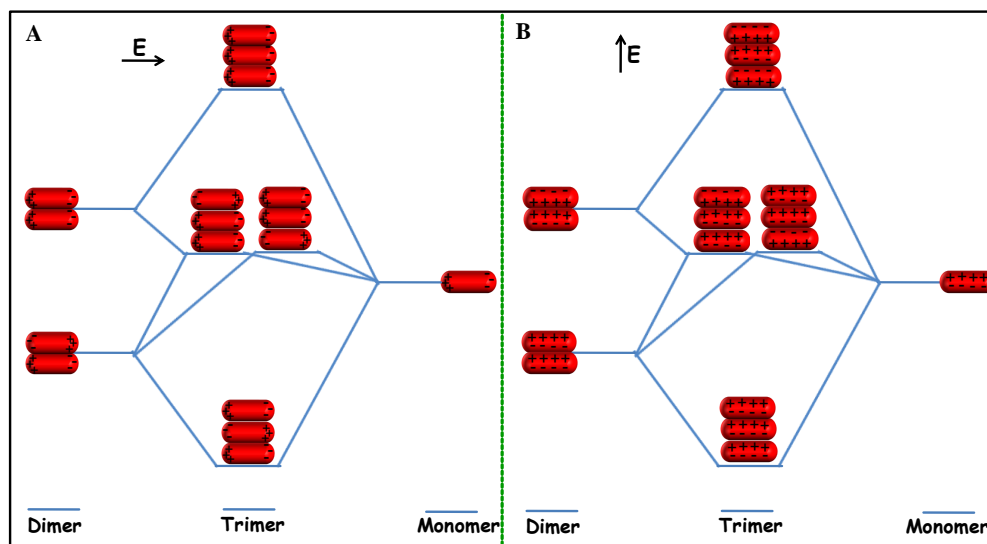
Scheme 5.3. *Illustration of the plasmon hybridization model of laterally assembled Au nanorod trimer during (A) longitudinal and (B) lateral polarizations.*

Thicker Au nanorods can give better scattering and nanorods having an average length of 54 nm and thickness 30 nm (aspect ratio of 1.8) were further used for scattering spectral studies. As observed in the earlier case, on moving from monomers to tetramers, a gradual hypsochromic shift in the longitudinal coupled plasmon band and a bathochromic shift in the transverse coupled plasmon band was observed (Figure 5.13). During the transverse polarization studies, additional bands were observed in the long wavelength region for larger assemblies of these Au nanorods.
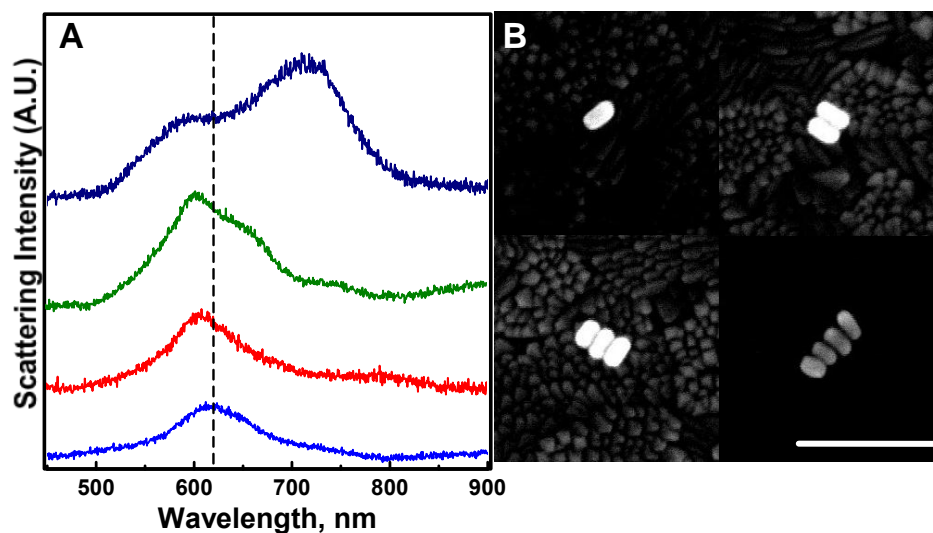
Figure 5.13. *(A) Scattering spectra of laterally assembled Au nanorods having an average aspect ratio of 1.8. Spectra were collected in air on an ITO coated glass substrate. (B) The corresponding SEM images of laterally arranged Au nanorods. Scale bar = 250 nm.*

The polarization studies on laterally assembled nanorods clearly confirm the contribution of the longitudinal and transverse modes. Experimental and simulated polarization data of lateral assemblies of Au nanorods are presented in Figure 5.14. As observed in the previous case, the polarization studies show a gradual hypsochromic shift in the longitudinally coupled plasmon band and bathochromic shift in the transverse coupled band. The magnitude of bathochromic shift was more pronounced for thicker rods during

transverse polarization. Thus, the transverse to longitudinal intensity ratio can be tuned by varying the thickness of Au nanorods.
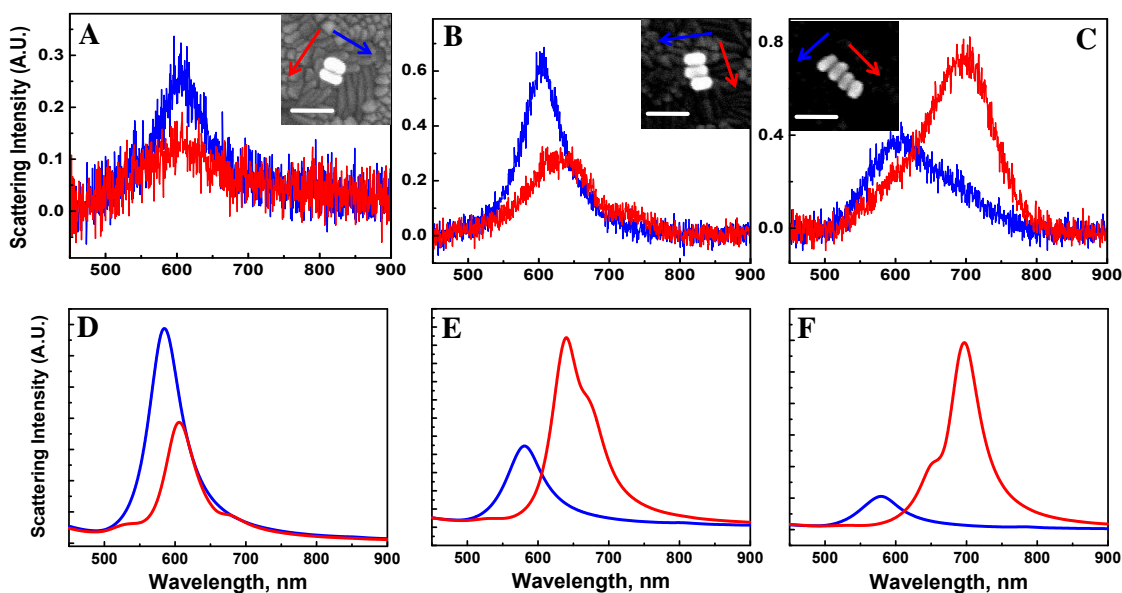
Figure 5.14. *(A-C)Experimental and (D-F) the theoretical scattering spectra of laterally assembled nanorod assemblies (aspect ratio = 1.8) obtained during longitudinal and lateral polarizations. Inset shows the SEM images of Au nanorod assemblies. The polarizer angle compared to the position of nanorod assemblies were known by using the FIB marks on the substrate as a reference. The longitudinal and the lateral polarization directions have been indicated on the inset SEM micrograph using blue and red arrows respectively. The spectra corresponding to these polarizations are plotted in the respective colors. All spectra were collected on an ITO coated glass substrate in air. The scale bar in the inset is 100 nm.*

5.4. Conclusions

In summary, we have investigated the single particle scattering properties of various Au nanorod assemblies by aligning them both linearly and laterally. The nanorods under investigation were identified using a pattern matching technique involving a combination of scanning electron microscopy and dark-field microscopy. The scattering wavelength and intensity of the peaks were highly dependent on the number of nanorods and their orientation

in the assembly. Linearly assembled Au nanorods showed a bathochromic shift in the longitudinal coupled plasmon band, which leveled off with increase in the number of rods in a chain. Lateral assembly of Au nanorods resulted in a hypsochromic shift in the longitudinally coupled plasmon band and a bathochromic shift in the transverse coupled band. All the nanoassemblies exhibit polarization dependent scattering and the energy levels involved in various modes of excitation were calculated from theoretical studies using FEM and plasmon hybridization models.
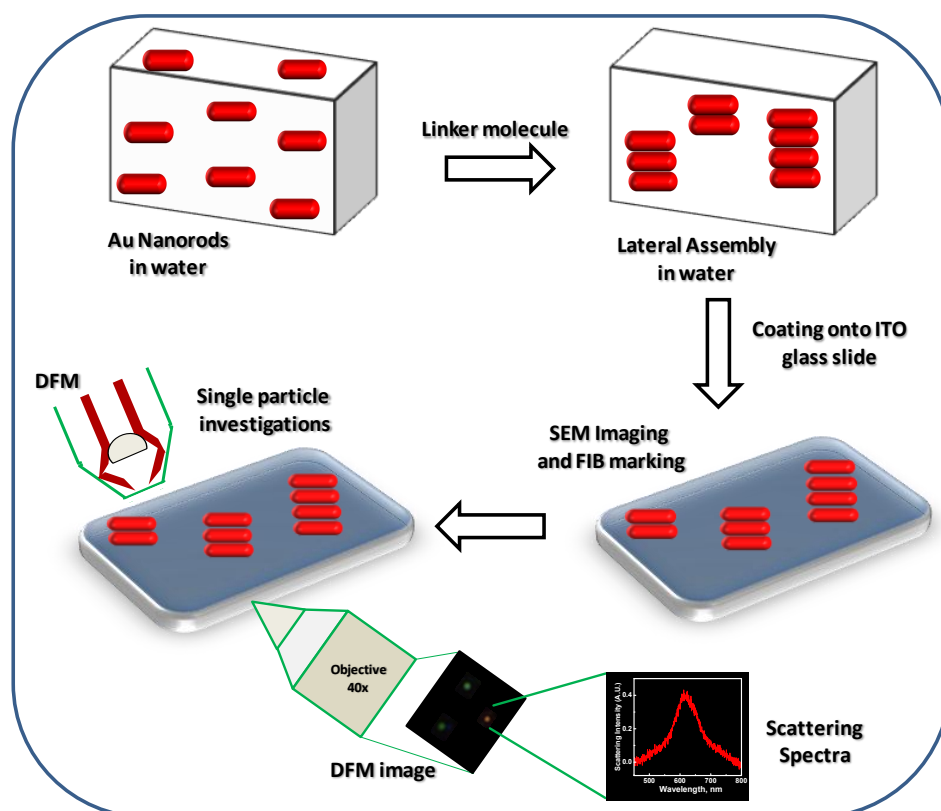
Scheme 5.4. Schematic illustration of single particle investigations of Au nanorod assemblies, taking lateral assembly of Au nanorods as specific example.

5.5. Experimental Section

5.5.1. Materials and Instrumental Methods

Solvents and reagents used were purified and dried by standard methods. Photophysical studies were carried out using spectroscopic grade solvents. The absorption spectral changes, upon the addition of linker molecules (dithiols for longitudinal assembly and sodium citrate for lateral assembly), were recorded in a UV-Visible Diode array spectrophotometer (Agilent 8453). Stock solutions of the dithiols and sodium citrate were prepared in acetonitrile and water respectively. All the studies were carried out by dispersing Au nanorods in water, or in a mixture (1:4) of water and acetonitrile. Nanorod samples were imaged using an xT Nova Nanolab SEM and the substrate was etched using a focused ion beam (FIB) which allows pattern matching when viewed under a dark field microscope. We have utilized a correlated method involving SEM and DFM for collecting the scattering spectra of single nanoparticles and their assemblies, and the details of the technique are provided in Section 5.5.2.

Finite-element method was used to simulate the experimental results and to map the surface plasmon modes. In modeling, the particle clusters of interest were delimited by the perfectly matched layer method (PML), which prevented any unwanted reflections through efficiently absorbing the scattering of the particles. All calculations were performed in an effective embedding medium n=1.28, to match experiment. S-polarized incident light with oblique incident angle 61 degrees to the normal of the cluster plane was chosen to strictly compare with the experiment results. For calculations, the nanorod was assumed as a cylinder of length 30 nm with two hemispherical caps at the ends having a radius of 12 nm each. The diameter of the cylinder was taken to be 23 nm. The gap between the nanorods

was assumed to be ~1 nm. The theoretical results were in good agreement with the experimental data with slight variations in the peak positions. The in-plane plasmon modes of the nanorod assemblies were considered during the calculations by assuming that the excitation light is polarized within the substrate plane either along longitudinal axis or the transverse axis perpendicular to it.

5.5.2. Combined SEM-DFM Technique

We have performed correlated Rayleigh scattering spectroscopy and SEM imaging experiments for investigating the optical properties of single nanoparticle assemblies [Hu 2007, Novo 2007 and Hu 2008]. Nanoparticle samples were imaged using an xT Nova Nanolab SEM and the substrate was etched using a focused ion beam (FIB) which allows pattern matching when viewed under a dark-field microscope. The scattering spectra presented in this chapter were recorded using an inverted optical microscope equipped with a dark-field condenser (Figure 5.1). The dark-field condenser forms a hollow cone of light focused on the sample. Only light that is scattered out of the cone reaches the objective; hence the particles on the substrate appear as bright diffraction-limited spots on a dark background. The particles appear in different colors depending on their scattering wavelength; for example, a particle having a plasmon resonance at approximately 650 nm appears as an orange spot. A Nikon Eclipse TE-2000, with a dry dark-field condenser and a 40x objective, was used in the dark-field microscopic system. The light collected by the objective were directed to an imaging monochromator (Acton Research MicroSpec 2150i) equipped with a liquid nitrogen cooled PIXIS 1024 ACTON Princeton Instruments CCD camera. The experiments were performed by first recording an image of the sample with a mirror in the light path of the spectrometer. After the identification of a suitable particle (or

assembly of particles), the mirror is switched with a grating (150 groves mm-1) to disperse the scattered light. Normalized Rayleigh scattering spectra from individual particles were obtained by subtracting and dividing by a background, taken from a nearby area of the CCD detector (identical pixel width but without particles). The acquisition times for the spectra varied from 10 s to 30 s, depending on the scattering cross section of the sample and sensitivity of the detector. The polarized scattering spectra were collected by placing a polarizer (LPVIS 100, Thorlabs) in the incident light path.

5.5.3. Synthesis of Au nanorods

Au nanorods were synthesized by seed mediated method [[b]Nikoobakht 2003]. For preparation of NRs, seed and growth solutions were made as described below.

Preparation of seed solution: 5 mL of CTAB solution (0.20 M) was mixed with 5.0 mL of $HAuCl_4$ (0.00050 M). To the stirred solution, 0.60 mL of ice-cold $NaBH_4$ (0.010 M) was added which resulted in the formation of a brownish yellow solution. Vigorous stirring of the seed solution was continued for 2 min and the seed solution was stored at 25 °C.

Synthesis of Au nanorods: Varying amounts of 0.0040 M $AgNO_3$ solution (0.050, 0.10, 0.15, 0.20, 0.25 mL) was added to 5 mL of CTAB (0.20 M) solution at 25 °C. To this solution, 5.0 mL of 0.0010 M $HAuCl_4$ was added and gently mixed. A mild reducing agent, ascorbic acid (70 μL, 0.0788 M) was added to this solution resulting in a change in colour of the growth solution from dark yellow to colorless. In the final step, 12 μL of the seed was added to the growth solution at 27-30 °C. The color of the solution gradually changed within 10-20 min; color changes were slow for longer nanorods. Thus, nanorods of different aspect ratio were prepared be changing the concentration of $AgNO_3$.

REFERENCES

Albrecht, M. G.; Creighton, J. A. "Anomalously Intense Raman Spectra of Pyridine at a Silver Electrode" *J. Am. Chem. Soc.* 99, **1977**, 5215–5217.

Ali, M. B.; Bessueille, F.; Chovelon, J. M.; Abdelghani, A.; Jaffrezic-Renault, N.; Maaref, M.A.; Martelet, C. "Use of Ultra-thin Organic Silane Films for the Improvement of Gold Adhesion to the Silicon Dioxide Wafers for (Bio)Sensor Applications*"* *Mater. Sci. Eng. C 28,* **2008**, 628–632.

Alvarez-Puebla, R.; Liz-Marzan, L. M.; Abajo, F. J. G. "Light Concentration at the Nanometer Scale" *J. Phys. Chem. Lett. 1*, **2010**, 2428–2434.

Baier, G.; Costa, C.; Zeller, A.; Baumann, D.; Sayer, C.; Araujo, P. H. H.; Mailänder, V.; Musyanovych, A; Landfester, K. "BSA Adsorption on Differently Charged Polystyrene Nanoparticles using Isothermal Titration Calorimetry and the Influence on Cellular Uptake" *Macromol. Biosci.* 11, **2011**, 628–638.

Ball, D.W. "Theory of Raman Spectroscopy" *Spectroscopy*, *16*, **2001**, 32–34.

Barnes, W. L.; Dereux, A.; Ebbesen, T. W. "Surface Plasmon Subwavelength Optics" *Nature 424*, **2003**, 824–830.

Barrow, S. J.; Funston, A. M.; Gomez, A. M. D.; Davis, T. J.; Mulvaney, P. "Surface Plasmon Resonances in Strongly Coupled Gold Nanosphere Chains from Monomer to Hexamer". *Nano Lett. 11*, **2011**, 4180–4187.

Braun, G.; Pavel, I.; Morrill, A. R.; Seferos, D. S.; Bazan, G. C.; Reich, N. O.; Moskovits, M. "Chemically Patterned Microspheres for Controlled Nanoparticle Assembly

in the Construction of SERS Hot Spots" *J. Am. Chem. Soc. 129*, **2007**, 7760–7761.

Brolo, A. G.; Jiang, Z.; Irish, D. E. "The Orientation of 2,2'- Bipyridine Adsorbed at a SERS-Active Au(111) Electrode Surface" *J. Electroanal. Chem. 547*, **2003**, 163–172.

Brumlik, C. J.; Martin, C. R. "Template synthesis of metal microtubules" *J. Am. Chem. Soc. 113*, **1991**, 3174–3175.

Burda, C.; Chen, X.; Narayanan, R.; El-Sayed, M. A. "Chemistry and Properties of Nanocrystals of Different Shapes" *Chem. Rev. 105*, **2005**, 1025–1102.

Burrows, S. D.; Doyle, M. L.; Murphy, K. P.; Franklin, S. G.; White, J. R.; Brooks, I.; Mc-Nulty, D. E.; Scott, M. O.; Knutson, J. R.; Porter, D.; Young, P. R.; and Hensley, P. "Determination of the Monomer-Dimer Equilibrium of Interleukin-8 Reveals it is a Monomer at Physiological Concentrations" *Biochemistry 33*, **1994**, 12741–12745.

Busbee, B. D.; Obare, S.O.; Murphy, C. J. "An Improved Synthesis of High-Aspect-Ratio Gold Nanorods" *Adv. Mater. 15*, **2003**, 414–416.

Campion, A.; Kambhampati, P. "Surface-Enhanced Raman Scattering" *Chem. Soc. Rev. 27*, **1998**, 241–250.

Campoy, A. V.; Ohtaka, H.; Nezami, A.; Muzammil, S.; Freire, E. "Isothermal Titration Calorimetry" *Current Protocols in Cell Biology*, **2004**, 17.8.1–17.8.24.

Camden, J. P.; Dieringer, J. A.; Wang, Y.; Masiello, D. J.; Marks, L. D.; Schatz, G. C.; Van Duyne, R. P. "Probing the Structure of Single-Molecule Surface-Enhanced Raman Scattering Hot Spots" *J. Am. Chem. Soc. 130*, **2008**, 12616–12617.

Cao, Y. C.; Jin, R.; Mirkin, C. A.; "Nanoparticles with Raman Spectroscopic Fingerprints for DNA and RNA Detection" *Science 297*, **2002**, 1536–1540.

Caswell, K. K.; Wilson, J. N.; Bunz, U. H. F.; Murphy, C. J. "Preferential End-to-End Assembly of Gold Nanorods by Biotin-Streptavidin Connectors" *J. Am. Chem. Soc. 125*, **2003**, 13914–13915.

Cedervall, T.; Lynch, I.; Lindman, S.; Berggård, T.; Thulin, E.; Nilsson, H.; Dawson, K. A.; Linse, S. "Understanding the Nanoparticle–Protein Corona using Methods to Quantify Exchange Rates and Affinities of Proteins for Nanoparticles" *Proc. Natl. Acad. Sci. 104*, **2007**, 2050–2055.

Chang, J.-Y.; Wu, H.; Chen, H.; Ling, Y.-C.; Tan, W. "Oriented Assembly of Au Nanorods Using Biorecognition System" *Chem. Commun. 41,* **2005**, 1092–1094.

Chao, Y.; Zhou, Q.; Li, Y.; Yan, Y.; Wu, Y.; Zheng, J. "Potential Dependent Surface-enhanced Raman Scattering of 4-Mercaptopyridine on Electrochemically Roughened Silver Electrodes" *J. Phys. Chem. C 111*, **2007**, 16990–16995.

Chen, H.; Shao, L.; Woo, C. K.; Ming, T.; Lin, H. Q.; Wang, J. "Shape-Dependent Refractive Index Sensitivities of Gold Nanocrystals with the Same Plasmon Resonance Wavelength" *J. Phys. Chem. C 113*, **2009**, 17691–17697.

[a]Chen, G.; Wang, Y.; Yang, M.; Xu, J.; Goh, S. J.; Pan, P.; Chen, H. "Measuring Ensemble-Averaged Surface-Enhanced Raman Scattering in the Hotspots of

Colloidal Nanoparticle Dimers and Trimers" *J. Am. Chem. Soc. 132*, **2010**, 3644–3645.

[b]Chen, T.; Wang, H.; Chen, G.; Wang, Y.; Feng, Y.; Teo, W. S.; Wu, T.; Chen, H. "Hotspot-Induced Transformation of Surface-Enhanced Raman Scattering Fingerprints" *ACS Nano 4*, **2010**, 3087–3094.

Correa-Duarte, M. A.; Perez-Juste, J.; Sanchez-Iglesias, A.; Giersig, M.; Liz-Marzan, L. M. "Aligning Au Nanorods by Using Carbon Nanotubes as Templates" *Angew. Chem. Int. Ed. 44*, **2005**, 4375–4378.

Colthup, N. B.; Daly, L. H.; Wiberley, S. E. "Introduction to Infrared and Raman Spectroscopy" (Third Edition) *Academic Press*, **1990**.

Compton, A. H. "A Quantum Theory of the Scattering of X-rays by Light Elements" *Phys. Rev. 21*, **1923**, 483–502.

Daniel, M.-C.; Astruc, D. "Gold Nanoparticles: Assembly, Supramolecular Chemistry, Quantum-Size-Related Properties, and Applications toward Biology, Catalysis, and Nanotechnology" *Chem. Rev. 104*, **2004**, 293-346.

De, M.; You, C. C.; Srivastava, S.; Rotello, V. M. "Biomimetic Interactions of Proteins with Functionalized Nanoparticles: A Thermodynamic Study" *J. Am. Chem. Soc. 129*, **2007**, 10747–10753.

Doherty, M. D.; Murphy, A.; McPhillips, J.; Pollard, R. J.; Dawson, P. "Wavelength Dependence of Raman Enhancement from Gold Nanorod Arrays: Quantitative Experiment and Modeling of a Hot Spot Dominated System" *J. Phys. Chem. C 114*, **2010**, 19913–19919.

Dujardin, E.; Hsin, L.-B.; Wang, C. R. C.; Mann, S. "DNA-Driven Self-Assembly of Gold Nanorods" *Chem. Commun. 37*, **2001**, 1264–1265.

El-Sayed, M. A. "Some Interesting Properties of Metals Confined in Time and Nanometer Space of Different Shapes" *Acc. Chem. Res. 34*, **2001**, 257–264.

Evanoff, D. D.; Chumanov, G. "Size-Controlled Synthesis of Nanoparticles. 2. Measurement of Extinction, Scattering, and Absorption Cross Sections" *J. Phys. Chem. B 108*, **2004**, 13957–13962.

Feng, Q.; Yue, W.; Cotton, T. M. "Surface-Enhanced Resonance Raman Scattering from Methyl vlologen at a Silver Electrode: Evidence for Two Distinct Adsorption Interactions" *J. Phys. Chem. 94*, **1990**, 2082–2091.

Fleishmann, M.; Hendra, P.J.; Mcquillan, A. J. "Raman Spectra of Pyridine Adsorbed at a Silver Electrode". *Chem Phys Lett. 26*, **1974**, 163–166.

Funston, A. M.; Novo, C.; Davis, T. J.; Mulvaney, P. "Plasmon Coupling of Gold Nanorods at Short Distances and in Different Geometries" *Nano Lett. 9*, **2009**, 1651–1658.

Gao, J.; Bender, C. M.; Murphy, C. J. "Dependence of the Gold Nanorod Aspect Ratio on the Nature of the Directing Surfactant in Aqueous Solution" *Langmuir 19*, **2003**, 9065-9070.

Ghosh, S. K.; Pal, T. "Interparticle Coupling Effect on the Surface Plasmon Resonance of Gold Nanoparticles: From Theory to Applications". *Chem. Rev. 107*, **2007**, 4797–4862.

Girard, C.; Dujardin, E. "Near-field optical properties of top-down and bottom-up nanostructures" *J. Opt. A: Pure Appl. Opt. 8*, **2006**, S73–S86.

Gittins, D. L.; Bethell, D.; Schiffrin, D. J.; Nichols, R. J. "A Nanometre-Scale Electronic Switch Consisting of a Metal Cluster and Redox-Addressable Groups" *Nature 408*, **2000**, 67–69.

Gluodenis, M.; Foss, C. A. "The Effect of Mutual Orientation on the Spectra of Metal Nanoparticle Rod-Rod and Rod-Sphere Pairs" *J. Phys. Chem. B 106*, **2002**, 9484–9489.

Gole, A.; Murphy, C. J. "Biotin−Streptavidin-Induced Aggregation of Gold Nanorods: Tuning Rod−Rod Orientation" *Langmuir 21*, **2005**, 10756–10762.

Gourishankar, A.; Shukla, S.; Ganesh, K. N.; Sastry, M. "Isothermal Titration Calorimetry Studies on the Binding of DNA Bases and PNA Base Monomers to Gold Nanoparticles" *J. Am. Chem. Soc. 126*, **2004**, 13186–13187.

Grzelczak, M.; Mezzasalma, S. A. Ni, W.; Herasimenka, Y.; Feruglio, L.; Montini, T.; Perez-Juste, J.; Fornasiero, P.; Prato, M.; Liz-Marzan, L. M. "Antibonding Plasmon Modes in Colloidal Gold Nanorod Clusters" *Langmuir 28*, **2012**, 8826–8833.

Hao, E.; Schatz, G. C. "Electromagnetic fields around silver nanoparticles and dimers" *J. Chem. Phys.* 120, **2004**, 357–366.

He, W.; Hou, S.; Mao, X.; Wu, X.; Ji, Y.; Liu, J.; Hu, X.; Zhang, K.; Wang, C.; Yang, Y.; Wang, Q. "Peptide-tailored assembling of Au nanorods" *Chem. Commun. 47*, **2011**, 5482–5484.

Henry, A.; Bingham, J. M.; Ringe, E.; Marks, L. D.; Schatz, G. C.; Duyne, R. P. V. "Correlated Structure and Optical Property Studies of Plasmonic Nanoparticles" *J. Phys. Chem. C 115*, **2011**, 9291–9305.

M. Hu, J. Chen, M. Marquez, Y. Xia and G. V. Hartland, "Correlated Rayleigh Scattering Spectroscopy and Scanning Electron Microscopy Studies of Au−Ag Bimetallic Nanoboxes and Nanocages" *J. Phys. Chem. C*, *111*, **2007**, 12558–12565.

Hu, M.; Novo, C.; Funston, A.; Wang, H.; Staleva, H.; Zou, S.; Mulvaney, P.; Younan Xia, Y.; Hartland, G. V. "Dark-Field Microscopy Studies of Single Metal Nanoparticles: Understanding the Factors that Influence the Linewidth of the Localized Surface Plasmon Resonance" *J. Mater. Chem., 18*, **2008**, 1949–1960.

Huang, Y.; Duan, X. F.; Wei, Q. Q.; Lieber, C. M. "Directed Assembly of One-Dimensional Nanostructures into Functional Networks" *Science 291*, **2001**, 630–633.

Jackson, A. M.; Myerson, J. W.; Stellacci, F. "Spontaneous Assembly of Subnanometre-Ordered Domains in the Ligand Shell of Monolayer-Protected Nanoparticles". *Nat. Mater. 3*, **2004**, 330–336.

Jain, P. K.; Eustis, S.; El-Sayed, M. A. "Plasmon Coupling in Nanorod Assemblies: Optical Absorption, Discrete Dipole Approximation Simulation, and Exciton-Coupling Model" *J. Phys. Chem. B 110*, **2006**, 18243–18253.

Jana, N. R.; Gearheart, L.; Murphy, C. J. "Wet Chemical Synthesis of High Aspect Ratio Cylindrical Gold Nanorods" *J. Phys. Chem. B 105*, **2001**, 4065–4067.

Jeanmaire, D. L.; van Duyne, R. P. "Surface Raman Electrochemistry Part I. Heterocyclic, Aromatic and Aliphatic Amines Adsorbed on the Anodized Silver Electrode". *J. Electroanal. Chem. 84*, **1977**, 1–20.

Johnson, C. J.; Dujardin, E.; Davis, S. A.; Murphy, C. J.; Mann, S. "Growth and form of gold nanorods prepared by seed-mediated, surfactant-directed synthesis" *J. Mater. Chem. 12*, **2002**, 1765–1770.

Joo, S. W.; Han, S. W.; Kim, K. "Adsorption Characteristics of p-Xylene-α,α'-dithiol on Gold and Silver Surfaces: Surface-Enhanced Raman Scattering and Ellipsometry Study" *J. Phys. Chem. B 103*, **1999**, 10831–10837.

Joseph, S. T. S.; Ipe, B. I.; Pramod, P.; Thomas, K. G. "Gold Nanorods to Nanochains: Mechanistic Investigations on Their Longitudinal Assembly Using α,ω-Alkanedithiols and Interplasmon Coupling" *J. Phys. Chem. B 110*, **2006**, 150–157.

Kamat, P. V. "Photophysical, Photochemical and Photocatalytic Aspects of Metal Nanoparticles" *J. Phys. Chem. B 106*, **2002**, 7729–7744.

Katz, E.; Shipway, A. N.; Willner, I. "Nanoscale Materials" *Kluwer Academic Publishers*, Boston, **2003**.

Kelly, K. L.; Coronado, E.; Zhao, L. L.; Schatz, G. C. "The Optical Properties of Metal Nanoparticles: The Influence of Size, Shape, and Dielectric Environment" *J. Phys. Chem. B 107*, **2003**, 668–677.

Kim, F.; Song, J. H.; Yang, P. "Photochemical Synthesis of Gold Nanorods" *J. Am. Chem. Soc. 124*, **2002**, 14316–14317.

Klein, J. "Probing the interactions of proteins and nanoparticles" *Proc. Natl. Acad. Sci. 104*, **2007,** 2029–2030.

Kneipp, K.; Wang, Y.; Kneipp, H.; Perelman, L. T.; Itzkan, I.; Dasari, R. R.; and Feld, M. S. "Single Molecule Detection Using Surface-Enhanced Raman Scattering (SERS)" *Phys. Rev. Lett. 78*, **1997**, 1667–1670.

Kneipp, K.; Kneipp, H.; Itzkan, I.; Dasari, R. R.; Feld, M. S. "Ultrasensitive Chemical Analysis by Raman Spectroscopy" *Chem. Rev. 99*, **1999**, 2957–2975.

Kou, X.; Ni, W.; Tsung, C. K.; Chan, K.; Lin, H. Q.; Stucky, G. D.; Wang. J. "Growth of Gold Bipyramids with Improved Yields and Their Curvature-Directed Oxidation" *Small 3,* **2007**, 2103–2113.

Kovtyukhova, N. I.; Martin, B. R.; Mbindyo, J. K. N.; Smith, P. A.; Razavi, B.; Mayer, T. S.; Mallouk, T. E. "Layer-by-Layer Assembly of Rectifying Junctions in and on Metal Nanowires" *J. Phys. Chem. B 105*, **2001**, 8762–8769.

Krishnan, R.; Gopidas, K. R. "β-Cyclodextrin as an End-to-End Connector" *J. Phys. Chem. Lett. 2*, **2011**, 2094–2098.

Kreibig, U.; Vollmer, M. "Optical Properties of Metal Clusters" *Springer-Verlag*, New York, **1995**.

Lal, S.; Grady, N. K.; Kundu, J.; Levin, C. S.; Lassiterde, J. B.; Halas, N. J. "Tailoring Plasmonic Substrates for Surface Enhanced Spectroscopies" *Chem. Soc. Rev. 37*, **2008**, 898–911.

[a]Landsberg, G. S.; Mandelstam, L. I. "Eine neue Erscheinung bei der Lichtzerstreuung in Krystallen" *Naturw 16*, **1928**, 557–558.

[b]Landsberg, G. S.; Mandelstam, L. I. "U ber die Lichtzerstreuung in Kristallen" *Zeit. f. Phys. 50*, **1928**, 769–780.

Lang, B. "Hybridization Thermodynamics of DNA Bound to Gold Nanoparticles. J. Chem. Thermodynamics" *42*, **2010**, 1435–1440.

Lee, A.; Andrade, G. F. S.; Ahmed, A.; Souza, M. L.; Coombs, N.; Tumarkin, E.; Liu, K.; Gordon, R.; Brolo, A. G.; Kumacheva, E. "Probing Dynamic Generation of Hot-Spots in Self-Assembled Chains of Gold Nanorods by Surface-Enhanced Raman Scattering" *J. Am. Chem. Soc. 133*, **2011**, 7563–7570.

Li, W.; Camargo, P. H. C.; Lu, X.; Xia, Y. "Dimers of Silver Nanospheres: Facile Synthesis and Their Use as Hot Spots for Surface- Enhanced Raman Scattering" *Nano Lett. 9*, **2009**, 485–490.

Li, W.; Camargo, P. H. C.; Au, L.; Zhang, Q.; Rycenga, M.; Xia, Y. "Etching and Dimerization: A Simple and Versatile Route to Dimers of Silver Nanospheres with a Range of Sizes" *Angew. Chem., Int. Ed. 49*, **2010**, 164–168.

Lim, D. K.; Jeon, K. S.; Kim, H. M.; Nam, J. M.; Suh, Y. D. "Nanogap-Engineerable Raman-Active Nanodumbbells for Single-Molecule Detection" *Nat. Mater. 9*, **2010**, 60–67.

Lin, S.; Li, M.; Dujardin, E.; Girard, C.; Mann, S. "One-Dimensional Plasmon Coupling by Facile Self-Assembly of Gold Nanoparticles into Branched Chain Networks" *Adv. Mater. 17*, **2005**, 2553–2559.

Link, S.; Mohamed, M. B.; El-Sayed, M. A. "Simulation of the Optical Absorption Spectra of Gold Nanorods as a Function of Their Aspect Ratio and the Effect of the Medium Dielectric Constant" *J. Phys. Chem. B 103*, **1999**, 3073–3077.

Link, S.; El-Sayed, M. A.; Mohamed, M. B. "Simulation of the Optical Absorption Spectra of Gold Nanorods as a Function of Their Aspect Ratio and the Effect of the Medium Dielectric Constant" *J. Phys. Chem. B 109*, **2005**, 10531–10532.

Liu, K.; Zhao, N.; Kumacheva, E. "Self-assembly of inorganic nanorods" *Chem. Soc. Rev.*, *40*, **2011**, 656–671.

Lombardi, A.; Loumaigne, M.; Crut, A.; Maioli, P.; Fatti, N. D.; Vallée, F. "Surface Plasmon Resonance Properties of Single Elongated Nanoobjects: Gold Nanobipyramids and Nanorods" *Langmuir 28*, **2012**, 9027−9033.

Long, D. A. "The Raman Effect: A Unified Treatment of Raman Scattering by Molecules". *John Wiley & Sons*, New York, **2002**.

Lovatt, M.; Cooper, A.; Camilleri, P. "Energetics of cyclodextrin-induced dissociation of insulin oligomers" *Euro. Biophys. J. 24*, **1996**, 354–357.

Maier, S. A.; Brongersma, M. L.; Kik, P. G.; Atwater, H. A. "Observation of near-field coupling in metal nanoparticle chains using far-field polarization spectroscopy" *Phys. Rev. B 65*, **2002**, 193408–193411.

Maier, S. A.; Kik, P. G.; Atwater, H. A.; Meltzer, S.; Harel, E.; Koel, B. E.; Requicha, A. A. G. "Local detection of electromagnetic energy transport below the diffraction limit in metal nanoparticle plasmon waveguides" *Nat. Mater. 2*, **2003**, 229–232.

Margueritat, J.; Gehan, H.; Grand, J.; Levi, G.; Aubard, J.; Felidj, N.; Bouhelier, A.; Gerard Colas-Des-Francs, G.; Markey, L.; Lucas, C. M. D.; Dereux, A.; Finot, E. "Influence of the Number of Nanoparticles on the Enhancement Properties of Surface-Enhanced Raman Scattering Active Area: Sensitivity versus Repeatability" *ACS Nano 5*, **2011**, 1630–1638.

Martin, C. R. "Membrane-Based Synthesis of Nanomaterials" *Chem. Mater. 8*, **1996**, 1739–1746.

Matulis, D.; Rouzina, I.; Bloomfield, V. A. "Thermodynamics of DNA Binding and Condensation: Isothermal Titration Calorimetry and Electrostatic Mechanism". *J. Mol. Biol. 296*, **2000**, 1053–1063.

McLintock, A.; Hunt, N.; Wark, A. W. "Controlled side-by-side assembly of gold nanorods and dye molecules into polymer-wrapped SERRS-active clusters" *Chem. Commun. 47*, **2011**, 3757–3759.

Min, Y.; Akbulut, M.; Kristiansen, K.; Golan, Y.; and Israelachvili, J. "The role of interparticle and external forces in nanoparticle assembly" *Nat. Mater. 7*, **2008**, 527–538.

Moskovits, M. "Surface-enhanced spectroscopy" *Rev. Mod. Phys. 57*, **1985**, 783–826.

Moskovits, M. "Surface Enhanced Raman Spectroscopy: A Brief Retrospective" *J. Raman Spectrosc. 36*, **2005**, 485–496.

Mokari, T.; Rothenberg, E.; Popov, I.; Costi, R.; Banin, U. "Selective Growth of Metal Tips onto Semiconductor Quantum Rods and Tetrapods" *Science 304*, **2004**, 1787–1790.

Muniz-Mirandaa, M.; Sbrana, G. "SERS-Activation of Smooth Surfaces by Doping with Silver Nanoparticles" *J. Mol. Str. 565*, **2001**, 159–163.

Murphy, C. J.; Sau, T. K.; Gole, A. M.; Orendorff, C. J.; Gao, J.; Gou, L.; Hunyadi, S. E.; Li, T. "Anisotropic Metal Nanoparticles: Synthesis, Assembly, and Optical Applications" *J. Phys. Chem. B 109*, **2005**, 13857–13870.

Nabika, H.; Takase, M.; Nagasawa, F.; Murakoshi, K. "Toward Plasmon-Induced Photoexcitation of Molecules" *J. Phys. Chem. Lett. 1*, **2010**, 2470–2487.

Nair, A. K.; Neelakandan, P. P.; Ramaiah, D. "A supramolecular Cu(II) metallocyclophane probe for guanosine 5'-monophosphate" *Chem. Commun. 42,* **2009**, 6352–6354.

Nakashima, H.; Furukawa, K.; Kashimura, Y.; Torimitsu, K. "Self-Assembly of Gold Nanorods Induced by Intermolecular Interactions of Surface-Anchored Lipids" *Langmuir 24*, **2008**, 5658–5654.

Nehl, C. L.; Grady, N. K.; Goodrich, G. P.; Tam, F.; Halas, N. J.; Hafner, J. H. "Scattering Spectra of Single Gold Nanoshells" *Nano Lett. 4*, **2004**, 2355–2359.

Nie, S.; Emory, S. R. "Probing Single Molecules and Single Nanoparticles by Surface-Enhanced Raman Scattering" *Science 275,* **1997**, 1102–1106.

Nie, S.; Emory, S. R. "Probing Single Molecules and Single Nanoparticles by Surface-Enhanced Raman Scattering" *Science 275*, **2007**, 1102–1106.

Nikoobakth, B.; Wang, Z. L.; El-Sayed, M. A. "Self-Assembly of Gold Nanorods" *J. Phys. Chem. B 104*, **2000**, 8635–8640.

Nikoobakht, B.; El-Sayed, M. A. "Evidence for Bilayer Assembly of Cationic Surfactants on the Surface of Gold Nanorods" *Langmuir 17*, **2001**, 6368–6374.

[a]Nikoobakht, B.; El-Sayed, M. A. "Surface-Enhanced Raman Scattering Studies on Aggregated Gold Nanorods" *J. Phys. Chem. A 107*, **2003**, 3372–3378.

[b]Nikoobakht, B.; El-Sayed, M. A. "Preparation and Growth Mechanism of Gold Nanorods (NRs) Using Seed-Mediated Growth Method" *Chem. Mater. 15*, **2003**, 1957–1962.

Nordlander, P.; Oubre, C.; Prodan, E.; Li, K.; Stockman, M. I. "Plasmon Hybridization in Nanoparticle Dimers" *Nano Lett. 4*, **2004**, 899–903.

Novo, C.; Funston, A. M.; Pastoriza-Santos, I.; Liz-Marz, L. M.; Mulvaney, P. "Spectroscopy and High-Resolution Microscopy of Single Nanocrystals by a Focused Ion Beam Registration Method" *Angew. Chem. Int. Ed. 46*, **2007**, 3517 –3520.

Orendorff, C. J.; Hankins, P. L.; Murphy, C. J. "pH-Triggered Assembly of Gold Nanorods" *Langmuir 21*, **2005**, 2022–2026.

Orendorff, C. J.; Gearheart, L.; Jana, N. R.; Murphy, C. J. "Aspect Ratio Dependence on Surface Enhanced Raman Scattering Using Silver and Gold Nanorod Substrates" *Phys. Chem. Chem. Phys. 8*, **2006**, 165–170.

Otto, A.; Mrozek, I.; Grabhorn, H.; Akemann, W. "Surface-enhanced Raman Scattering" *J. Phys- Condens. Matter. 4*, **1992**, 1143–1212.

Otto, A. "The 'Chemical' (Electronic) Contribution to Surface-Enhanced Raman Scattering" *J. Raman Spectrosc. 36*, **2005,** 497–509.

Pan, B.; Cui, D.; Ozkan, C.; Xu, P.; Huang, T.; Li, Q.; Chen, H.; Liu, F.; Gao, F.; He, R. "DNA-Templated Ordered Array of Gold Nanorods in One and Two Dimensions" *J. Phys. Chem. C 111*, **2007**, 12572–12576.

Pedano, M. L.; Li, S.; Schatz, G. C.; Mirkin, C. A. "Periodic Electric Field Enhancement Along Gold Rods with Nanogaps" *Angew. Chem. Int. Ed. 49*, **2010**, 78–82.

Pérez-Juste, J.; Liz-Marzán, L. M.; Carnie, S.; Chan, D. Y. C.; Mulvaney, P. "Electric-Field-Directed Growth of Gold Nanorods in Aqueous Surfactant Solution" *Adv. Funct. Mater. 14*, **2004**, 571–579.

Pérez-Juste, J.; Pastoriza-Santos, I.; Liz-Marzan, L. M.; Mulvaney, P. "Gold Nanorods: Synthesis, Characterization and Applications" *Coord. Chem. Rev. 249*, **2005**, 1870–1901.

Placzek G. "Rayleigh Streeung und Raman Effekt", *Hdb. der Radiologie 2*, **1934**, 209–212.

Pramod, P.; Joseph, S. T. S.; Thomas, K. G. "Preferential End Functionalization of Au Nanorods through Electrostatic Interactions" *J. Am. Chem. Soc. 129*, **2007**, 6712–6713.

Pramod, P.; Thomas, K. G. "Plasmon Coupling in Dimers of Au Nanorods" *Adv. Mater. 20*, **2008**, 4300–4305.

Prodan, E.; Radloff, C.; N. J. Halas, N. J.; Nordlander, P. "A Hybridization Model for the Plasmon Response of Complex Nanostructures" *Science 302*, **2003**, 419-422.

Qian, X.; Peng, X,-H.; Ansari, D. O.; Yin-Goen, Q.; Chen, G. Z.; Shin, D. M.; Yang, L.; Young, A. N.; Wang, M. D.; Nie, S. "*In vivo* tumor targeting and spectroscopic

detection with surface-enhanced Raman nanoparticle tags" *Nat. Biotech*. *26*, **2008**, 83–90.

Qin, L.; Zou, S.; Xue, C.; Atkinson, A.; Schatz, G. C.; Mirkin, C. A. "Designing, Fabricating, And Imaging Raman Hot Spots" *Proc. Natl. Acad. Sci. 103*, **2006**, 13300–13303.

Raman, C. V.; Krishnan, K. S. "A New Type of Secondary Radiation" *Nature 121*, **1928**, 501–502.

Ru, E. C. L.; Blackie, E.; Meyer, M.; Etchegoin, P. G. "Surface Enhanced Raman Scattering Enhancement Factors: A Comprehensive Study" *J. Phys. Chem. C 111*, **2007**, 13794–13803.

Schatz, G.C. "Theoretical Studies of Surface Enhanced Raman Scattering" *Acc. Chem. Res. 17*, **1984**, 370–376.

Schatz, G. C.; Van Dyune, R. P.; "Handbook of Vibrational Spectroscopy" *Wiley, New York*, **2002**, 759–774.

Shah, R. A.; Guyot-Sionnest, P.; Gray, S. K. "Orientational Interpolation of the Optical Spectra of Nonspherical Nanoparticles" *J. Phys. Chem. C 116*, **2012**, 12712−12724.

Shenhar, R.; Rotello, V. M. "Nanoparticles: Scaffolds and Building Blocks" *Acc. Chem. Res. 36*, **2003**, 549−561.

Shipway, A. N.; Katz, E.; Willner, I. "Nanoparticle Arrays on Surfaces for Electronic, Optical, and Sensor Applications" *ChemPhysChem 1*, **2000**, 18−52.

Slaughter, L. S.; Wu, Y.; Willingham, B. A.; Nordlander, P.; Link, S. "Effects of Symmetry Breaking and Conductive Contact on the Plasmon Coupling in Gold Nanorod Dimers" *ACS Nano 4*, **2010**, 4657–4666.

Smekal, A. "Zur Quantentheorie der Dispersion" *Die Naturw* 11, **1923**, 873−875.

Sreeprasad, T. S.; Pradeep, T. "Reversible Assembly and Disassembly of Gold Nanorods Induced by EDTA and Its Application in SERS Tuning". *Langmuir 27*, **2011**, 3381–3390.

Sudeep, P. K.; Joseph, S. T. S.; Thomas, K. G. "Selective Detection of Cysteine and Glutathione Using Gold Nanorods" *J. Am. Chem. Soc. 127*, **2005**, 6516–6517.

Talley, C. E.; Jackson, J. B.; Oubre, C.; Grady, N. K.; Hollars, C. W.; Lane, S. M.; Huser, T. R.; Nordlander, P.; Halas, N. J. "Surface-Enhanced Raman Scattering from Individual Au Nanoparticles and Nanoparticle Dimer Substrates" *Nano Lett. 5*, **2005**, 1569–1574.

Templeton, A. C.; Pietron, J. J.; Murray, R. W.; Mulvaney, P. "Solvent Refractive Index and Core Charge Influences on the Surface Plasmon Absorbance of Alkanethiolate Monolayer-Protected Gold Clusters" *J. Phys. Chem. B 104*, **2000**, 564-570.

Thomas, K. G.; Kamat, P. V. "Chromophore-Functionalized Gold Nanoparticles" *Acc. Chem. Res. 36*, **2003**, 888- 898.

Thomas, K. G.; Barazzouk, S.; Ipe, B. I.; Joseph, S. T. S.; Kamat, P. V. "Uniaxial Plasmon Coupling through Longitudinal Self-Assembly of Gold Nanorods" *J. Phys. Chem. B 108*, **2004**, 13066–13068.

Thomas, K. G. "Surface Plasmon Resonances in Nanostructured Materials", Nanomaterials Chemistry, *WILEY-VCH Verlag GmbH & Co.* **2007**, 185−218.

Thomas, K. G.; "Tuning functional properties: From nanoscale building blocks to hybrid nanomaterials". *Current Trends in Science* **2009**, 53−66.

Thomas, R.; Kumar, J.; Swathi, R. S.; Thomas, K. G. "Optical effects near metal nanostructures: towards surface-enhanced spectroscopy" *Current Science 102*, **2012**, 1−12.

Tian, Z. Q.; Ren, B.; "Adsorption and Reaction at Electrochemical Interfaces as Probed by Surface-Enhanced Raman Spectroscopy" *Annu. Rev. Phys. Chem. 55*, **2004**, 197−229.

van Duyne, R. P. "Laser Excitation of Raman Scattering from Adsorbed Molecules on Electrode Surfaces" *Chemical and Biochemical Applications of Lasers*, 4:101-185, Academic Press, New York, 1979.

Varghese, N.; Vivekchand, S.R.C.; Govindaraj, A.; Rao, C.N.R. "A calorimetric investigation of the assembly of gold nanorods to form necklaces" *Chem. Phys. Lett. 450*, **2008**, 340–344.

Venkataramanan, M.; Murty, K. V. G. K.; Pradeep, T.; Deepali, W.; Vijayamohanan, K. "Metal Ion Reactivity with 1,4-Benzenedimethanethiol Monolayers on Gold" **2000**, *Langmuir 16*, 7673–7678.

Wang, C.; Chen, Y.; Wang, T.; Ma, Z.; Su, Z. "Biorecognition-Driven Self-Assembly of Gold Nanorods: A Rapid and Sensitive Approach toward Antibody Sensing" *Chem. Mater. 19*, **2007**, 5809–5811.

Wang, L.; Zhu, Y.; Xu, L.; Chen, W.; Kuang, H.; Liu, L.; Agarwal, A.; Xu, C.; Kotov, N. A. "Side-by-Side and End-to-End Gold Nanorod Assemblies for Environmental Toxin Sensing" *Angew. Chem. Int. Ed. 49*, **2010**, 5472–5475.

Wang, Z. L.; Mohamed, M. B.; Link, S.; El-Sayed, M. A. "Crystallographic Facets and Shapes of Gold Nanorods of Different Aspect Ratios" *Surf. Sci. 440*, **1999**, L809–L814.

Wang, Z. L.; Gao, R. P.; Nikoobakht, B.; El-Sayed, M. A. "Surface Reconstruction of the Unstable {110} Surface in Gold Nanorods" *J. Phys. Chem. B 104*, **2000**, 5417–5420.

Weber, A. "Raman Spectroscopy of Gases and Liquids" Topics in Current Physics. *John Springer-Verlag*, Berlin, **1979**.

Woodward, L. A. "General Introduction," Raman Spectroscopy: Theory and Practice" *Plenum Press*, New York, **1967**.

Yang, M.; Chen, T.; Lau, W. S.; Wang, Y.; Tang, Q.; Yang, Y.; Chen, H. "Development of Polymer-Encapsulated Metal Nanoparticles as Surface-Enhanced Raman Scattering Probes" *Small 5*, **2009**, 198–202.

Yoosaf, K.; Ipe, B. I.; Suresh, C. H.; Thomas, K. G. "In Situ Synthesis of Metal Nanoparticles and Selective Naked-Eye Detection of Lead Ions from Aqueous Media" *J. Phys. Chem. C 111*, **2007**, 12839–12847.

Yoshikawa, H.; Matsui, T.; Masuhara, H. "Reversible Assembly of Gold Nanoparticles Confined in an Optical Microcage" *Phys. Rev. E 70*, **2004**, 061406–061411.

You, C. C.; Agasti, S. S.; Rotello, V. M. "Isomeric Control of Protein Recognition with Amino Acid-and Dipeptide-Functionalized Gold Nanoparticles" *Chem. Eur. J. 14*, **2008**, 143–150.

You, E.; Zhou, W.; Suh, J. Y.; Huntington, M. D.; Odom, T. W. "Polarization-Dependent Multipolar Plasmon Resonances in Anisotropic Multiscale Au Particles" *ACS Nano 6*, **2012**, 1786–1794.

Yu, Y.; Chang, S.; Lee, C.; Wang C. R. C. "Gold Nanorods: Electrochemical Synthesis and Optical Properties" *J. Phys. Chem. B 101*, **1997**, 6661–6664.

Zhang, L.; Clark, R. J.; Zhu, L. "A Heteroditopic Fluoroionophoric Platform for Constructing Fluorescent Probes with Large Dynamic Ranges for Zinc Ions" *Chem. Eur. J. 14*, **2008**, 2894–2903.

Zhang, Y.-L.; Zhang, Z.-Y. "Low-Affinity Binding Determined by Titration Calorimetry Using a High-Affinity Coupling Ligand: A Thermodynamic Study of Ligand Binding to Protein Tyrosine Phosphatase" *Anal. Biochem. 261*, **1998**, 139–148.

Zhao, L.; Kelly, K. L.; Schatz, G. C. "The Extinction Spectra of Silver Nanoparticle Arrays: Influence of Array Structure on Plasmon Resonance Wavelength and Width" *J. Phys. Chem. B 107*, **2003**, 7343–7350.

Zheng, J.; Li, X.; Gu, R.; Lu, T. "Comparison of the Surface Properties of the Assembled Silver Nanoparticle Electrode and Roughened Silver Electrode" *J. Phys. Chem. B 106*, **2002**, 1019–1023.

Zhong, Z. Y.; Patskovskyy, S.; Bouvrette, P.; Luong, J. H. T.; Gedanken, A. "The Surface Chemistry of Au Colloids and Their Interactions with Functional Amino Acids" *J. Phys. Chem. B 108*, **2004**, 4046–4052.

Zhu, Z.; Meng, H.; Liu, W.; Liu, X.; Gong, J.; Qiu, X.; Jiang, L.; Wang, D.; Tang, Z. "Superstructures and SERS Properties of Gold Nanocrystals with Different Shapes" *Angew. Chem. Int. Ed. 50*, **2011**, 1–5.

LIST OF PUBLICATIONS

1. Surface Enhanced Raman Spectroscopy: Investigations at the Nanorod Edges and Dimer Junctions.

   Jatish Kumar and K. George Thomas, *J. Phys. Chem. Lett.* **2011**, *2*, 610–615.

2. Optical Effects near Metal Nanostructures: Towards Surface Enhanced Spectroscopy.

   Reshmi Thomas, **Jatish Kumar**, R. S. Swathi and K. George Thomas *Current Science* **2012**, *102*, 1–12.

3. Tunable Photophysical Properties of Phenyleneethynylene Based Bipyridine Ligands.

   P. V. James, K. Yoosaf, **Jatish Kumar**, K. George Thomas, A. Listorti, G. Accorsi and N. Armaroli, *Photochem. Photobiol. Sci.*, **2009**, *8*, 1432–1440.

4. Synthesis, Characterization and Biocompatibility of Surface-Functionalized Gold Nanoparticles.

   V. Raji, **Jatish Kumar**, C.S. Rejiya, M. Vibin, Annie John and Annie Abraham, *J. Exp. Nanosci.,* **2011**, 1–15.

5. Selective Photothermal Efficiency of Citrate Capped Gold Nanoparticles for Destruction of Cancer Cells**.**

   V. Raji, **Jatish Kumar**, C.S. Rejiya, M. Vibin, Vinesh N. Shenoi, Annie Abraham, *Exp. Cell. Res.*, **2011**, *14*, 2052–2058.

6. Laser Immunotherapy with Gold Nanorods Causes Selective Killing of Tumour Cells.

   Rejiya C.S., **Jatish Kumar**, Raji. V, Vibin. M, Annie Abraham, *Pharmacol. Res.* **2012**, *65*, 261–269.

7. Lateral Assembly of Gold Nanorods and the Creation of Hot spots at the Nanorod Quartet Junctions.

   Jatish Kumar and K. George Thomas, *Chem. Commun.* **2012** (Under Submission).

8. Plasmon Coupling in End-to-End Linked Au Nanorods and Nanorod-Nanoparticle Assemblies.

   Jatish Kumar, S. Barrow, W. Xingzhan, Paul Mulvaney and K. George Thomas, *Phys. Chem. Chem. Phys.* **2012** (Under Submission).

175

9. Single Particle Investigations on Laterally Assembled Au Nanorods.

   Jatish Kumar, S. Barrow, W. Xingzhan, Paul Mulvaney and K. George Thomas, *Nano Lett.* **2012** (To be submitted).

10. Gold Nanorods as Substrates in Surface Enhanced Raman Spectroscopy: Investigations on Analyte –Substrate interactions.

    Jatish Kumar and K. George Thomas, *Langmuir* **2012** (To be submitted).

Posters and Oral Presentations at Conferences:

1. Assembly and Spectroscopy of Plasmonic Nanostructures.

   Jatish Kumar, P. Pramod and K. George Thomas

   In *"National Symposium on Nanosensors and Devices"* at Indian Institute of Technology, Delhi, India, December 22-23, 2008.

2. Surface Enhanced Raman Spectroscopy: Investigations at the Nanorod Edges and Dimer Junctions.

   Jatish Kumar and K. George Thomas

   In *"13th CRSI National Symposium in Chemistry",* at National Institute for Science Education and Research, Bhubaneswar, India, February 04-06, 2011.

3. Nanorod Dimer Junctions for Raman Signal Enhancement.

   Jatish Kumar and K. George Thomas

   In *"Seventh International Symposium on Chemistry of Material"* at Cochin, Kerala, India, October 01-03, 2011.

4. Surface Enhanced Raman Spectroscopy at Nanorod Dimer and Quartet Junctions.

   Jatish Kumar and K. George Thomas

   In *"Indo-US bilateral workshop on Nanophotonics and Nanoplasmonics"* at Indian Institute of Science, Bangalore, India, January 09-12, 2012.

Curriculum Vitae:

Jatishkumar was born on December 7, 1982, in Kerala, India. He had his early education at Kendriya Vidyalaya, Calicut and completed his schooling in 2000. He obtained B. Sc. and M. Sc. degrees from the Department of Chemistry, St. Joseph's College, Devagiri, Calicut, affiliated to the University of Calicut, in 2003 and 2006 respectively. He joined as Junior Project Fellow under the guidance of Prof. K. George Thomas at the Photosciences and Photonics Section, CSIR-National Institute for Interdisciplinary Science and Technology, Trivandrum in May 2006. Subsequently he qualified CSIR-JRF examination and joined as Junior Research Fellow in July 2007. Under the guidance of Prof. K. George Thomas, he was involved in the synthesis of various metal nanostructures, their self-assembly and investigations on their photophysical and morphological properties. He visited Prof. Paul Mulvaney's laboratory at the University of Melbourne in 2012, to carry out the single particle investigations of various self-assembled metal nanostructures. These nanoassemblies could be utilized as substrates in surface enhanced Raman spectroscopy for the detection of molecular signals. He worked in the group until July 2012. The results of his research are described in this thesis.